

---

[All ETDs from UAB](#)

[UAB Theses & Dissertations](#)

---

2018

## Bioprocess Development For Novel Anti-Cancer Therapies And High Value Biochemical

Jianfa Ou  
*University of Alabama at Birmingham*

Follow this and additional works at: <https://digitalcommons.library.uab.edu/etd-collection>

---

### Recommended Citation

Ou, Jianfa, "Bioprocess Development For Novel Anti-Cancer Therapies And High Value Biochemical" (2018). *All ETDs from UAB*. 2639.  
<https://digitalcommons.library.uab.edu/etd-collection/2639>

This content has been accepted for inclusion by an authorized administrator of the UAB Digital Commons, and is provided as a free open access item. All inquiries regarding this item or the UAB Digital Commons should be directed to the [UAB Libraries Office of Scholarly Communication](#).

BIOPROCESS DEVELOPMENT FOR NOVEL ANTI-CANCER THERAPIES AND  
HIGH VALUE BIOCHEMICAL

by

JIANFA OU

XIAO GUANG (MARGARET) LIU, CHAIR  
GANGJIAN QIN  
LUFANG ZHOU  
RENATA JASKULA-SZTUL  
WUQIANG ZHU

A DISSERTATION

Submitted to the graduate faculty of The University of Alabama at Birmingham,  
in partial fulfillment of the requirements for the degree of  
Doctor of Philosophy

BIRMINGHAM, ALABAMA

2018

Copyright by  
Jianfa Ou  
2018

# BIOPROCESS DEVELOPMENT FOR NOVEL ANTI-CANCER THERAPIES AND HIGH VALUE BIOCHEMICAL

JIANFA OU

BIOMEDICAL ENGINEERING

ABSTRACT

Cancer treatment is one of the most daunting challenges of human health improvement. Bioprocess development, or biomanufacturing, is an important step in anti-cancer therapy developments. Novel surface receptors were revealed by integrating proteomics data and live-cell characterization, and were used for antibody design with improved specific targeting. A high titer ( $>2$  g/L) of monoclonal antibody (mAb) was produced by Chinese hamster ovary cells from fed-batch cell culture. Live-cell confocal microscopy imaging and flow cytometry analysis demonstrated the strong and specific binding of the produced mAb to cancer cell lines. The cancer treatment effect of mAb was enhanced through the antibody-drug conjugate (ADC) technology. Various conjugation conditions of mAb and drug, including linker selection, ratio of drug and mAb, and conjugation approaches, were investigated to improve the production yield and product quality. High quality human T cell biomanufacturing was investigated to accelerate the cancer cellular therapy development in the next stage. More than 1 billion human T cells were expanded through a 4 day long culture. T cell quality was confirmed by 15 markers using flow cytometry. Finally, an Omics-based mathematical model was established to guide the rational design for process development. A biofuel substitute with high economic value, biobutanol, was used as a model chemical. The model integrated the proteomics, metabolomics, and production kinetics. Rational design strategies were then proposed and confirmed. In-depth

understanding of bioprocess from this study will benefit the novel anti-cancer therapies development in the future.

Keywords: Cancer Therapy, Bioprocess Development, Monoclonal Antibody, Antibody-drug Conjugate, Cellular Therapy, Rational Design

## DEDICATION

This dissertation is dedicated to my encouraging parents and everyone who guided me through the trials of its creation.

## ACKNOWLEDGMENTS

I am indebted to a number of wonderful men and women, without whose help and support this work would not have been possible. First, my advisor, Dr. Liu; her great confidence and sophisticated research skills have guided me through countless challenges in the study. Her modest and cautious attitude will be the North Star of my life and career.

I would like to express my gratitude to my committee members, Dr. Gangjian Qin, Dr. Lufang Zhou, Dr. Renata Jaskula-Sztul, and Dr. Wuqiang Zhu, who never gave me criticism that was not also followed up with encouragement.

I would like to express my appreciation for Dr. Heath Turner at the University of Alabama for his generous help for my adaptation and survival in graduate school. I am thankful to Dr. Ho-Wook Jun for his support in my transition to the University of Alabama at Birmingham.

I would like to thank Dr. Ryan Summers, Dr. Stephen Ritchie, Dr. Yonghyun Kim, and Dr. Janna Fierst at the University of Alabama, Dr. Shang-Tian Yang and Dr. Jingbo Zhao at the Ohio State University, Dr. Herbert Chen, Dr. Hongwei Qin, Dr. Jinda Fan and Dr. Norio Yasui at the University of Alabama at Birmingham, for their support for this research.

I would also like to acknowledge the efforts of my colleagues in making this work a reality. Dr. Chao Ma and Dr. Ningning Xu have built a solid foundation for my work. I am grateful to Yingnan Si, Daniel Flanigan, Patrick Ernst, Dr. Jiajia Song, Dr. Li He, Yun Lu, and Dr. KahYong Goh for their help. I would also like to thank all the previous and

current research assistants in our lab, Ryan Malden, Matthew Miller, Matthew Pate, Donna Xia, Shuyuan Zhang, Yichen Guo, Meredith Bush, Hillary Dimig, Jacob Robinson, Ann Kay Alexander, Alisha Isbell, Abigail Lauterbach, Caroline Huskin, Gabrielle Waller, Liam Finnegan, Christopher Mayhugh, Katherine Beyer, Vaishali Nijampatnam, Brody DeSilva, Nghi Dang, and Seulhee Kim.

Finally, and not least importantly, I am grateful to my wife, Katie, for her patience in the big things and the small things, her sense of humor that never fails to make me laugh, her constant emotional support of me in all things, her delicious cooking that has kept me fed during the past year, and her heart-touching music that never ceases to inspire.

## TABLE OF CONTENTS

	<i>Page</i>
ABSTRACT.....	<i>iii</i>
DEDICATION.....	<i>v</i>
ACKNOWLEDGMENTS .....	<i>vi</i>
LIST OF TABLES.....	<i>x</i>
LIST OF FIGURES .....	<i>xii</i>
CHAPTER	
1. INTRODUCTION .....	<i>1</i>
2. NOVEL THERAPY DEVELOPMENT FOR NEUROENDORINE TUMOR.....	<i>7</i>
3. BIOPROCESS DEVELOPMENT OF ANTIBODY-DRUG CONJUGATE PRODUCTION FOR CANCER TREATMENT.....	<i>27</i>
4. HIGH QUALITY HUMAN T CELL BIOMANUFACTURING IN STIRRED-TANK BIOREACTOR.....	<i>56</i>
5. PROCESS ENGINEERING OF CELLULOSIC N-BUTANOL PRODUCTION FROM CORN-BASED BIOMASS USING <i>CLOSTRIDIUM</i> <i>CELLULOVORANS</i> .....	<i>95</i>
6. INTRACELLULAR METABOLISM ANALYSIS OF <i>CLOSTRIDIUM</i> <i>CELLULOVORANS</i> VIA MODELING INTEGRATING PROTEOMICS, METABOLOMICS AND FERMENTATION.....	<i>129</i>
7. SUMMARY AND CONCLUSION .....	<i>170</i>
GENERAL LIST OF REFERENCES .....	<i>172</i>

APPENDIX

A SUPPLEMENTAL MATERIALS.....	180
B CELL THAWING AND CELL BANKING.....	189
C ANTIBODY TITRATION USING ELISA.....	192
D ANTIBODY PURIFICATION BY LC SYSTEM.....	197
E ANTIBODY BINDING EVALUATION BY FLOW CYTOMETRY .....	200
F BIOCHEMICAL TITRATION BY HPLC .....	202

## LIST OF TABLES

<i>Table</i>	<i>Page</i>
<b>BIOPROCESS DEVELOPMENT OF ANTIBODY-DRUG CONJUGATE PRODUCTION FOR CANCER TREATMENT</b>	
1 Summary of fed-batch cell culture in bioreactor .....	48
2 Summary of ADC cytotoxicity assay .....	49
<b>HIGH QUALITY HUMAN T CELL BIOMANUFACTURING IN STIRRED-TANK BIOREACTOR</b>	
1 Summary of the representative data of the developed novel human T cell biomanufacturing in stirred-tank bioreactor .....	85
2 Evaluation of cell surface markers of human CD4 <sup>+</sup> and CD8 <sup>+</sup> T cells produced in the new biomanufacturing process.....	86
3 Cytokine production summary.....	87
<b>PROCESS ENGINEERING OF CELLULOSIC N-BUTANOL PRODUCTION FROM CORN-BASED BIOMASS USING CLOSTRIDIUM CELLULOVORANS</b>	
1 Effect of the pretreatment of biomass on butanol production by <i>C. cellulovorans- adhE2</i> .....	120
2 Effect of carbon sources on butanol production of <i>C. cellulovorans</i> .....	121

INTRACELLULAR METABOLISM ANALYSIS OF CLOSTRIDIUM  
CELLULOVORANS VIA MODELING INTEGRATING PROTEOMICS,  
METABOLOMICS AND FERMENTATION

1 Summary of cellulosic n-butanol fermentation by wide type and mutant of <i>C. cellulovorans</i> .....	160
2 The cellulolytic enzymes with significant expression identified in proteomics.....	161
3 Expression of enzymes involved in glycolysis and central metabolic pathways .....	162
4 Correlate proteomics with metabolomics via dynamic mathematic modeling.....	163
S1 Biochemical reaction rate equations in dynamic model.....	181
S2 Summary of the representative modeling parameters in the central metabolic pathway.....	182
S3 Mass balance equations used in mathematic models.....	183
S4 Bacterial strains, plasmids, and primers used for the new generation metabolic engineering.....	184
S5 Expression of cellulosic enzymes.....	185
S6 Intracellular metabolite data used for modeling.....	186
S7 Summary of cellulosic n-butanol fermentation by new generation <i>C. cellulovorans mutants</i> .....	187

## LIST OF FIGURES

<i>Figure</i>	<i>Page</i>
NOVEL THERAPY DEVELOPMENT FOR NEUROENDORINE TUMOR	
1 Novel antibody development overview .....	21
2 Specific binding of antibody candidate.....	22
3 <i>In vivo</i> evaluation of antibody specific targeting.....	23
4 ADC <i>in vivo</i> efficacy assay.....	24
5 ELISA ranking of novel antibody from hybridoma.....	25
6 Increased binding and ADC toxicity comparing to commercial antibody .....	26
BIOPROCESS DEVELOPMENT OF ANTIBODY-DRUG CONJUGATE PRODUCTION FOR CANCER TREATMENT	
1 The diagram of ADC construction.....	50
2 Anti-HER2 mAb production and purification .....	51
3 Anti-HER2 mAb production in fed-batch cell culture.....	52
4 Evaluation of mAb purity and surface binding to HER2 receptor.....	53
5 Evaluation of ADCs constructed in different production processes.....	54
6 Surface binding and internalization process of ADC by confocal laser scanning microscopy.....	55

## HIGH QUALITY HUMAN T CELL BIOMANUFACTURING IN STIRRED-TANK BIOREACTOR

1 High quality T cell manufacturing process design .....	88
2 Medium and feeding optimization .....	89
3 Cell growth potential affected by seeding time and stimulation strategy .....	90
4 Human T cell biomanufacturing scale-up.....	91
5 Robustness of the developed scalable human T cell biomanufacturing .....	92
6 CD4 <sup>+</sup> and CD8 <sup>+</sup> cells coculture .....	93
7 T cell quality and status evaluation.....	94

## PROCESS ENGINEERING OF CELLULOSIC N-BUTANOL PRODUCTION FROM CORN-BASED BIOMASS USING CLOSTRIDIUM CELLULOVORANS

1 Metabolic pathway in <i>C. cellulovorans-adhE2</i> .....	122
2 Fermentation kinetics of <i>C. cellulovorans-adhE2</i> using glucose as substrate in ATCC 1345 medium (A) and DSMZ 520 medium (B) in 2-L bioreactor at pH 7.0, temperature 37 °C, and agitation 100 rpm.....	123
3 Effect of pretreatment of corn-based biomass on the cell growth of <i>C. cellulovorans-adhE2</i> .....	124
4 Butanol selectivity (g-butanol/g-total products) and concentration as affected by various carbon substrates at pH 6.5 .....	125
5 SEM analysis for <i>C. cellulovorans-adhE2</i> cells grown on A) cellulose and B) NaOH pretreated cob .....	126
6 Effects of fermentation pH value on butanol selectivity and product concentration using glucose as substrate .....	127
7 Fermentation kinetics for cellulosic n-butanol production from A) cellulose and B) pretreated corncob by <i>C. cellulovorans-adhE2</i> in 2-L bioreactor at pH 6.5, temperature 37 oC, and agitation 100 rpm.....	128

INTRACELLULAR METABOLISM ANALYSIS OF CLOSTRIDIUM  
CELLULOVORANS VIA MODELING INTEGRATING PROTEOMICS,  
METABOLOMICS AND FERMENTATION

1 Fermentation kinetics for cellulosic n-butanol production by A) mutant strain <i>C. cellulovorans adhE2</i> using glucose as substrate, B) <i>C. cellulovorans adhE2</i> using cellulose as substrate, and C) wild type strain (WT) using cellulose as substrate.....	164
2 Global and pairwise analysis of protein expression in <i>C. cellulovorans</i> .....	165
3 Global and pairwise analysis of the function of metabolites in <i>C. cellulovorans</i> .....	166
4 The metabolic flux control coefficient in cellulosic n-butanol production by the mutant of <i>C. cellulovorans</i> using A) glucose and B) cellulose.....	167
5 Metabolic flux analysis of <i>C. cellulovorans</i> using the novel dynamic model developed in this study and the traditional static model. ....	168
6 Fermentation kinetics of new-generation metabolically engineered mutants.....	169

## CHAPTER 1

### INTRODUCTION

#### **Challenges in Cancer treatment**

Cancer is a global public health problem. There were an estimated 8 million deaths and 14 million new cases in 2012 [1], and more than 20 million annual new cases are predicted by 2025 [2]. Chemotherapy and radiotherapy remain the major cancer treatment options for those who cannot be cured by surgery [3, 4]. Because of the severe side effects, the medication is frequently terminated early, resulting in high risk of tumor relapse or recurrence [5]. Tremendous effort has focused on alternative methods to improve the treatment quality while ensuring adequate therapeutic index [6, 7]. The cancer treatment paradigms have changed as knowledge behind tumor biology accumulated. Targeted therapy, in which the cancer abnormalities are targeted accurately and effectively by a toxic reagent, became a promising method to reduce the side effects and increase efficacy. Subsequently, cancer drug resistance becomes a problem for both chemotherapy and molecularly targeted therapy [8]. High-throughput screening from a growing database of anticancer agents provides us another advantage in the race against cancer evolution [9, 10]. Therefore, novel therapies are always in high demand. Rational combination of

existing and new drugs, and progress on identification of new biomarkers, will hopefully bring us more options.

### **Monoclonal antibody and antibody-drug conjugate (ADC)**

The number of emerging targets has grown amazingly in recent years. These targets can potentially block the cancer growth signal, shorten the living time of cancer cells, or destroy the cancer cell directly by inducing apoptosis [11-14]. Some novel targets include growth-related kinase [6, 15], cancer stem cell [16, 17], cancer microenvironment [18], and amino acid metabolism [19]. There are two major “bullets” aiming at cancer cells: small-molecule drugs [20] and monoclonal antibodies (mAb). There are significant hurdles between a target candidate and an effective drug. The knowledge gap in anticancer drug development is known as the “Valley of Death” [21]. Despite the considerable progress made by small molecule therapy, such as epidermal growth factor receptor (EGFR) kinase inhibitors for non-small cell lung cancer [22] and abiraterone for late stage prostate cancer [23], many promising disease targets are extremely difficult to be targeted by small molecules [24]. Monoclonal antibody-based cancer therapy, on the other hand, has proven its success in the last 20 years as the most successful strategy [25]. More than 30 mAb and their derivatives have been approved for use in various disease treatments [26]. Typical mAb streamlines, such as hybridoma and mAb humanization technologies for novel developments, have advanced this strategy to a series of landmark clinical trials [27]. Protein engineering on Fc modification made a fine-tuning of mAb to improve efficacy and reduce side effects [28, 29]. Moreover, many challenges rely on the production process engineering of mAb therapy development.

A trend in next generation cancer therapy development is to integrate two or more current strategies to overcome drug resistance and improve clinical efficacy. Some examples include the combination of surgery, radiation therapy, and chemotherapy; integration of miRNA with chemotherapeutic agent [30]; and empowered mAb with cytotoxic drug. ADC specifically binds to the tumor surface antigen over the blood circulation. ADC is then internalized by endocytosis and degraded in lysosome. The cytotoxic reagent is released and causes cancer cell death [31]. The challenges during an ADC development include 1) target selection and high quality mAb production [32]; 2) generation of linker which has sufficient stability in circulation and quick payload release after endocytosis, 3) a reproducible and efficient preparation process, which should maintain the biological binding activity, with high product stability and reduced heterogeneity [33]. A sophisticated process development method will greatly accelerate new and promising ADC development and commercialization.

### **Cellular therapy**

In recent years there have been enormous advances in the development of cellular therapy. More than 1000 clinical related trials were reported by 2015 [34]. Therapeutic cells, such as stem cell, stem-cell-derived therapeutic cells, and immune cells, bring solutions for currently incurable diseases, including cancer, immune system disorder, cardiovascular disease, and more [35-37]. An efficient manufacturing technique for large scaled cell production is essential to realize such therapies. New technologies are expected to lower the manufacturing cost, shorten the turnaround time, increase or maintain the quality and efficacy of therapeutic cells, and improve the cell product safety. More

importantly, new technologies should produce enough cells, e.g.  $10^9$  cells per patient, for multiple dosages [38, 39]. The manual cell culture technique using the conventional static culture flask cannot even generate enough dosage for a large clinical trial. In addition to cell scale, we need a robust system to integrate the cell isolation, activation/differentiation, proliferation, formulation and packaging, to ensure quality and safety for patient treatment [38, 40]. Different from the manufacturing of vaccine, antibody, and other biologics, where cells are merely biocatalyst to generate the products, therapeutic cell manufacturing requires elaborate knowledge between the physical and nutrient environment and the cell properties. The cell number should be maximized while the byproducts should be controlled under a low level.

### **Process engineering in cancer therapy development**

Though we have accumulated a significant amount of knowledge for cell culture platform design, e.g. bioreactor setup [41-43], the functional difference of each therapeutic product leads to various culture requirements, including the medium formulation [44], mass transfer (nutrients and oxygen) [42], mechanical stress [41], cell density, and sometimes the microenvironment [45]. The bioreactor and bioprocess should be designed and optimized accordingly for each product. For example, while monoclonal antibody production by CHO was usually harvested when cell viability dropped to 50% to maximize the titer [46], T cell culture for adoptive therapy should maintain viability >80% for high cell quality.

Each cell culture platform has its advantage and limitation for different application. The commonly used static culture platforms, such as T flask and petri dish, are convenient

in initial research but hard to scale up. Platforms with mixing mechanism are convenient to provide a homogeneous physiologically and chemically desired microenvironment. Stirred tank bioreactor is most widely used in biopharmaceutical processes [42]. It provides a closed system with delicate temperature, pH, and oxygen control. Seeding, feeding, and sampling can be done automatically without interrupting the cell culture. The challenges of process development for a stirred tank bioreactor cell culture include the medium screening, parameter optimization, feeding formulation and strategy, and scale up from 1mL frozen vial to benchtop scale (2L or 5L) production and industrial scale (1000L and more) production [47, 48].

Downstream processing presents another critical challenge to the quality of cancer therapeutic product [49]. Each therapeutic protein drug, antibody, or ADC needs a customized strategy to achieve purity and yield. After the culture process optimization, the increased product titer and the corresponding change of impurity composition demands a modified purification. While general principles on chromatography are used to guide protein purification [50], high-throughput assay and automatic screening platform have been recently used to facilitate the purification through biophysical and biochemical characterization [51, 52]. The challenges in therapeutic cell culture purification appear in a different way. For example, the magnetic beads in T cell activation need to be completely removed [53]. It becomes a bottleneck as the production scale increases.

### **Rational design in process engineering**

Process development can be complicated with the interaction of each parameter. Rational design identifies targets based on systemic understanding of the intracellular and

extracellular cell regulation [54-56]. The targets then guide the genetic engineering [57], culture medium design and optimization [58-60], culture process design [61], and downstream product purification [62]. As demand for pharmaceutical manufacturing development grows, process analytical technology becomes increasingly important. Methods that have been widely used in traditional bioprocesses, such as factorial design, response surface methodology, and design-of-experiments (DoE) [63], and various emerging modeling methods [64] and Omics-based methods [65, 66], provide powerful approaches to reduce the number of experiments needed.

Over the course of this dissertation research, a novel target was identified for neuroendocrine tumor treatment, and the specific targeting mAb was developed. A high titer mAb production and purification platform was established on CHO cells from fed-batch cell culture. The cancer treatment efficacy of mAb was enhanced through the ADC technology with an improved process. Additionally, high quality human T cell biomanufacturing was investigated to accelerate the emerging cellular cancer therapy. Rational design for process development was guided by an Omics-based mathematical model, which integrated the proteomics, metabolomics, and production kinetics. Our systematic understanding of bioprocess contributes to novel cancer therapy development.

CHAPTER 2

NOVEL THERAPY DEVELOPMENT FOR NEUROENDORINE TUMOR

by

JIANFA OU, XIAO GUANG (MARGARET) LIU

In preparation

Format adapted for dissertation

## **Abstract**

Novel therapeutic strategies are in high demand for pancreatic neuroendocrine tumors (PanNET) treatment because tumors often present with multiple metastases at the time of discovery, and lead to limited therapeutic options. Monoclonal antibodies (mAb) based immunotherapy is one of the most promising target therapies. We used hybridoma technology to develop a novel mAb targeting SSTR, which is highly expressed on PanNET cells. Binding affinity of our novel anti-SSTR mAb was 6 times higher than the commercial antibody. Efficient and specific binding were observed on SSTR receptor through *in vitro* and *in vivo* studies. Antibody-drug conjugate with strong toxicity and specific targeting was successfully developed by conjugating the in-house anti-SSTR mAb to chemical drug Monomethyl auristatin E. An efficient therapy was developed for PanNET treatment in this study.

**Keywords:** Pancreatic neuroendocrine tumor, Novel therapy, Monoclonal antibody, Antibody-drug conjugate

## 1 Introduction

Patients with pancreatic neuroendocrine tumors (PanNETs) have limited therapeutic options [1]. Surgery is the only curative option for isolated tumors, but the tumors often present with multiple metastases, making complete resections almost impossible [2]. Other forms of therapy including chemoembolization, radiofrequency ablation, cryoablation, and chemotherapy show limited efficacy [3]. Novel therapeutic strategies are in high demand for PanNET treatment. As a new generation of cancer treatment method, targeted therapy has shown its strength by interfering with the tumor growth and progression [4]. The target identification relies heavily on our understanding of the cancer's molecular behavior. An efficient approach is comparative proteomics analysis between cancer and normal samples. Targeting candidates are those present in cancer cells only, or those expressed more in cancer cells. Anti-HER2 (human epidermal growth factor receptor 2 protein) antibody, trastuzumab, can greatly suppress the HER2+ tumor growth [5].

There are multiple types of target therapies, such as hormone therapy [6], signal transduction inhibitor [7], apoptosis inducer [8], monoclonal antibodies (mAb) based immunotherapy [9], and mAb-based toxic molecule delivery [10]. Antibody is a well-established class of drug for cancer therapeutics because of its high tolerance by humans. The recent advancements of mAb have achieved reduced immunological rejection [11], improved effector functions [12], and optimized pharmacokinetics [13]. Moreover, engineering of antigen-binding affinity and specificity was practical on antibodies [14]. The streamlining of development and optimization makes antibody drugs the most rapidly expanding pharmaceuticals for cancer treatment. More than 30 monoclonal antibodies have

been approved for use with many more under clinical trial [15]. However, there still are challenges for novel therapeutic antibody development, including the side effects caused by non-specific binding, the lack of efficacy because of low affinity and cytotoxicity, and high production cost [16]. There are several factors contributing to the price of antibody drugs, such as the development expense, manufacturing, and the large required dosage.

Generally, antibody cancer treatment extends survival time, but rarely cures the cancer [15]. So far most of the antibody for cancer treatment targets the tumor cells and blocks cell proliferation [17]. The cytotoxic effect is weak compared to standard chemotherapy agents. Therefore, improved efficacy is an important goal of antibody therapy [16, 18]. While the target and targeting affinity affects the immune response intensity [19], pharmacokinetics (PK) determines the response duration, thus increasing the antitumor activity [20]. However, PK optimization requires a time-consuming Fc engineering and repeated in vivo studies [21]. Antibody-drug conjugate (ADC) technique is another strategy to improve the antibody drug efficacy. A typical ADC structure consists of a mAb, a spacer/linker, and a cytotoxic reagent/payload. The mAb is responsible for specifically targeting the tumor and activating internalization. The cytotoxic reagent is then released after linker cleavage or mAb degradation [22]. It selectively delivers lethal agents to tumor cells and minimizes side effects to patients. The increased potency will reduce the treatment dosage, drug cost, and the cost for administration.

In this chapter, we identified a somatostatin receptor (SSTR) for NET treatment. In house monoclonal antibody was generated by hybridoma, a widely used technology that fuses B cells with the immortalized myeloma cells [23]. Antibodies with strong specificity and high affinity were screened. To improve therapeutic efficacy, we propose to conjugate

the drug candidates with antibodies that specifically bind to somatostatin receptors (SSTRs) expressed on the surface of PanNETs cells.

## **2 Materials and method**

### *2.1 Cell line and cell culture*

The human NET cancer cell line BON was grown in DMEM/F12 medium supplemented with 10% fetal bovine serum (FBS) and 4 mM L-glutamine in T25 flask. All basal media, supplements and reagents used in this study were purchased from Thermo Fisher Scientific (Waltham, MA) unless otherwise specified.

### *2.2 Hybridoma generation*

SSTR peptide design, mouse immunization, and fusion of myeloma cells (Sp2/0) with immune spleen cells were finished by ProMab (Richmond, CA). Mouse immunization was confirmed by Western Blot screening. Hybridoma clones were evaluated by sandwich enzyme-linked immunosorbent assay (ELISA) following the previous described procedure [24]. Specifically, a 96-well plate was coated with SSTR peptides. The anti-SSTR mAb was captured and detected using an anti-mouse IgG (HRP-linked) antibody. 3,3',5,5'-Tetramethylbenzidine (Thermo Fisher Scientific, Waltham, MA) was added for blue color development. The plate was read at 450 nm after adding H<sub>2</sub>SO<sub>4</sub> as stop solution.

### *2.3 Antibody purification*

Spent medium of hybridoma culture was collected for anti-SSTR mAb purification, using Bio-Rad NGC system (Bio-Rad, Hercules, CA) equipped with a UNOsphere SUPRA column. The process included column equilibration, sample loading, column washing, and

antibody elution. The equilibration buffer was comprised of 0.02 M sodium phosphate and 0.02 M sodium citrate at pH 7.5. Elution buffer contained 0.02 M sodium citrate and 0.1 M sodium chloride at pH 3.0. The pH of eluted mAb was neutralized to 7.0 with 1 M Tris solution.

#### *2.4 Confocal Imaging*

The animal model, mouse xenograft, and human patient tissue were provided by Dr. Herbert Chen's lab. Tissues were washed with saline and treated by 10% formalin or 4% PFA overnight at room temperature. The fixed tissues were washed with PBS and 50% ethanol sequentially, and stored in 70% ethanol before paraffin embedding. The embedded samples were sliced at 3-5  $\mu\text{m}$ , fixed on covered glass, and dewaxed before imaging. The BON cells were grown on a glass coverslip (Warner Instruments, Hamden, CT), which was mounted on the stage of an Olympus IX81 confocal laser scanning microscope (Center Valley, PA) and equilibrated at 37°C in PBS containing 10% inactivated goat serum and 1% BSA. At 16-24h before imaging, the cells were transduced with CellLight Late Endosomes-RFP (BacMam 2.0). The AF647 labelled mAb was incubated with tissue slices at 4°C overnight or BON cells at 37°C. Lasers of 543 and 633nm were used for excitation.

#### *2.5 Antibody drug conjugate preparation*

*Synthesis of linker-Monomethyl auristatin E (MMAE) payload* 18.20  $\mu\text{mol}$  potent molecule MMAE, 16.38  $\mu\text{mol}$  Mc-Val-Cit-PABC-PNP, and 3.64  $\mu\text{mol}$  hydroxybenzotriazole were dissolved and mixed in 500  $\mu\text{L}$  dimethylformamide. Then 18.20  $\mu\text{mol}$  pyridine was added to the mixture after 2 min, and 20  $\mu\text{mol}$  trifluoroacetic acid

(TFA) was added after 24 h. the solvents were removed by vacuum pump and the conjugates were purified by a Waters HPLC system equipped with 600 Controller/Pump and 996 PDA detector (Waters, Milford, MA) using a reversed-phase C<sub>18</sub> column with 5 μm C18(2) 100 Å and 250 x 10 mm.

*ADC production* 5 mg/mL mAb solved in 50 mM borate buffer at pH 8.0 was reduced with 1 mM dithiothreitol (DTT) at 37 °C for 1 h, followed by repeated buffer exchange in Pierce dialysis column using PBS buffer containing 1 mM pentetic acid. The linker-MMAE payload was mixed with the reduced mAb with payload:mAb molar ratio of 6.6, and incubated at 4 °C for 1 h. The reaction was terminated by adding 20-fold molar excess of cysteine over payload and the final products were purified by G-25 gel filtration.

## 2.6 Toxicity Evaluation

*In vitro toxicity* Cells were seeded at 96 well plates with VCD 0.05x10<sup>6</sup> cells/mL and volume 75 μL. After 24h incubation, equal volume of medium containing the ADC was added, and the cells were further incubated for 3 days. The actual liquid volume was then measured and working solution of CellTiter-Glo® Luminescent Cell Viability Assay Kit (Promega, Madison, WI) was added at equal amount before reading the luminescence with a Synergy H1 Hybrid Multi-Mode Microplate Reader (BioTek, Winooski, VT).

*In vivo efficacy* Animal tumor model was generated by injecting 5x10<sup>6</sup> cells BON cells to immunodeficient mice, and tumors were allowed to grow for 7 days. ADC was injected for treatment every 6 days with total dosage of 8mg/kg.

### 3 Result and discussion

#### 3.1 Overview of Novel antibody development for targeted therapy

An overview of Novel antibody development was shown in Figure 1, including target identification, antibody generation by mouse immunization, single clone screening, single clone scale-up, adaptation, and antibody production and evaluation. Our previous proteomics, western, and qPCR studies revealed several promising targets for cancer treatment, one of which is SSTR. Parts of the SSTR peptides were selected and synthesized by ProMab (CA). After immunization, the mice spleen cells were isolated and fused with Sp2/0 cells to generate hybridoma cells. The clones were ranked based on specific binding to the SSTR peptides, followed by top clone scale-up. Hybridoma cells were cultured in spinner flasks to produce anti-SSTR mAb for further evaluation.

#### 3.2 Target confirmation

*In vitro confirmation* Shown in Figure 2A, commercial antibody (labelled with AF647, red) binding was clearly visualized under CLSM. A strong binding was observed on the mouse xenograft generated from BON cell line, and observed on the human NET tissues. The time lapse study (Figure 2B) revealed the efficient interaction between mAb and surface receptor. The surface binding happened after 10 min incubation. The internalized mAb eventually co-localized with the late endosome over the 40 min observation.

*In vivo confirmation* The specific targeting was confirmed by *in vivo* study (Figure 3). The AF647 labelled anti-SSTR mAb was injected into mice at a dosage of 8mg/kg body weight. After 24 h, the mice were sacrificed, and tissue slices were taken from different

locations for imaging, including tumor xenograft, brain, and liver. Strong fluorescent signal was observed on the tumor slice, while other body parts had no signal.

*Preliminary application* Conjugating the cytotoxic drugs with antibodies specific for somatostatin receptors can reduce the systemic toxic effect to normal organ and tissues. Novel ADC for PanNET treatment was successfully developed by conjugating the antibody to chemical drugs. Figure 4 indicated that the anti-SSTR ADC specifically bound to the tumor and inhibited the growth. ADC was injected on Day 0, Day 6, and Day 12 with a total dosage of 8mg/kg body weight. The tumor sizes of control group and treated group were both 90mm<sup>3</sup> at the beginning. On Day 6 tumors of control groups were around 210mm<sup>3</sup> while the treated tumors had no significant growth. The tumor growth rate increased after Day 12 because of the high total cancer cell number. On Day 20, the tumor size of the control group (1580mm<sup>3</sup>) was more than twice larger than the treated group (760mm<sup>3</sup>). No severe side effect was noticed on the ADC treated mice. The efficacy of an ADC is affected by antibody binding efficacy, ADC preparation process, and product purity and integrity. By developing our in house mAb, we expected to produce a mAb with high specificity, affinity and binding efficiency. The ADC preparation process optimization will be discussed in Chapter 3. More characterization of ADC will also be presented.

### *3.3 Development and evaluation of in house novel antibody*

Hybridoma clones that effectively expressed novel antibody were screened by ELISA following the published procedures. The reading was positively related to the combination of antibody titer and antigen binding efficiency. Shown in Figure 5, two

peptides from the SSTR protein were used to evaluate 40 clones. The clones had different binding efficiency to peptide A and peptide B (Figure 5). For example, clone 1 had the strongest binding to peptide B but the binding to peptide A was very low. Clone 24 was selected considering the balance between antigen A and antigen B. The mAb of clone 24 had 93% positive binding after incubation at 37°C for 30 min (Figure 6A). Comparatively, the commercial antibody had 16% positive binding. The binding affinity of our novel antibody was increased by almost 6 folds.

Additionally, ADC was prepared with the novel anti-SSTR mAb and its toxicity was evaluated. Shown in Figure 6B, the relative viability of BON cells dropped to 60% and 20% after treating with ADC of commercial mAb and ADC of in house mAb, respectively. More cytotoxic reagent acted on the cells due to the high affinity of in house mAb. As low as 0.5nM ADC caused observable toxicity to BON cells after 3 days' treatment. The increased ADC toxicity indicated the promising application of our novel mAb on cancer treatment, which will be evaluated in the next step.

#### **4 Ongoing work and next steps**

By now we have generated and evaluated the anti-SSTR antibody from mice. The mouse antibody has weak interaction with human target [25], short life-time [26], and inefficient effector function [10]. Humanization has largely overcome the disadvantages of the mouse-based antibody development [27, 28]. Our antibody sequencing is undergoing variable domain and leader sequencing. The heavy chain and light chain will be aligned. Afterwards, the complementarity-determining regions (CDRs), or antigen-binding loops, will be transferred to a human IgG to generate a chimeric antibody [29, 30]. The humanized

antibody will eventually be produced by a pre-established platform, such as Chinese Hamster Ovary (CHO) cells. We will describe a CHO-based mAb manufacturing system in Chapter 3.

Nowadays antibody drug development is an iterative process. After an antibody is produced for a target, optimization may be needed to meet the designed clinical outcome with guidelines from existing drugs. It generates a strategy called bio-superior, also known as biobetter or next generation. As a validation process, the success or failure of an antibody drug guides the selection of new targets.

## **5 Conclusion**

SSTR was identified for specific antibody targeting because of its high expression on PanNET. The commercial anti-SSTR antibody showed efficient specific binding *in vitro* and *in vivo*. Our in house anti-SSTR mAb was developed using hybridoma technology. Its binding affinity was 6 times higher than the commercial antibody. The best clone was selected for antibody production. Novel ADC was successfully developed by conjugating the in house anti-SSTR mAb to chemical drug MMAE. The specific binding and strong toxicity of ADC were achieved, proven by the low viability (20%) of PanNET cells after treatment.

## Reference

1. Batchelor, E., P. Madaj, and A.G. Gianoukakis, *Pancreatic neuroendocrine tumors*. *Endocrine research*, 2011. **36**(1): p. 35-43.
2. Halfdanarson, T.R., et al., *Pancreatic neuroendocrine tumors (PNETs): incidence, prognosis and recent trend toward improved survival*. *Annals of oncology*, 2008. **19**(10): p. 1727-1733.
3. Bilimoria, K.Y., et al., *Prognostic score predicting survival after resection of pancreatic neuroendocrine tumors: analysis of 3851 patients*. *Annals of surgery*, 2008. **247**(3): p. 490-500.
4. Sawyers, C., *Targeted cancer therapy*. *Nature*, 2004. **432**: p. 294.
5. Matsui, Y., et al., *Suppression of tumor growth in human gastric cancer with HER2 overexpression by an anti-HER2 antibody in a murine model*. *International journal of oncology*, 2005. **27**(3): p. 681-685.
6. Fournier, A., et al., *Use of different postmenopausal hormone therapies and risk of histology-and hormone receptor-defined invasive breast cancer*. *Journal of clinical oncology: official journal of the American Society of Clinical Oncology* *Journal of clinical oncology: official journal of the American Society of Clinical Oncology*, 2008. **26**(8): p. 1260.
7. Steeg, P.S., *Metastasis suppressors alter the signal transduction of cancer cells*. *Nature Reviews Cancer*, 2003. **3**(1): p. 55.
8. Taraphdar, A.K., M. Roy, and R. Bhattacharya, *Natural products as inducers of apoptosis: Implication for cancer therapy and prevention*. *Current science*, 2001: p. 1387-1396.

9. Mellman, I., G. Coukos, and G. Dranoff, *Cancer immunotherapy comes of age*. Nature, 2011. **480**(7378): p. 480.
10. Carter, P., *Improving the efficacy of antibody-based cancer therapies*. Nature Reviews Cancer, 2001. **1**(2): p. 118.
11. Little, M., et al., *Of mice and men: hybridoma and recombinant antibodies*. Immunology Today, 2000. **21**(8): p. 364-370.
12. Hoogenboom, H.R. and P. Chames, *Natural and designer binding sites made by phage display technology*. Immunology Today, 2000. **21**(8): p. 371-378.
13. Glennie, M.J. and P.W.M. Johnson, *Clinical trials of antibody therapy*. Immunology Today, 2000. **21**(8): p. 403-410.
14. Halin, C. and D. Neri, *Antibody-based targeting of angiogenesis*. Critical Reviews™ in Therapeutic Drug Carrier Systems, 2001. **18**(3).
15. Liu, J.K.H., *The history of monoclonal antibody development – Progress, remaining challenges and future innovations*. Annals of Medicine and Surgery, 2014. **3**(4): p. 113-116.
16. Carter, P.J., *Potent antibody therapeutics by design*. Nature Reviews Immunology, 2006. **6**: p. 343.
17. Carter, P., *Improving the efficacy of antibody-based cancer therapies*. Nat Rev Cancer, 2001. **1**(2): p. 118-29.
18. Adams, G.P. and L.M. Weiner, *Monoclonal antibody therapy of cancer*. Nature biotechnology, 2005. **23**(9): p. 1147.
19. Leabman, M.K., et al. *Effects of altered FcγR binding on antibody pharmacokinetics in cynomolgus monkeys*. in *MAbs*. 2013. Taylor & Francis.

20. Wang, W., E. Wang, and J. Balthasar, *Monoclonal antibody pharmacokinetics and pharmacodynamics*. *Clinical Pharmacology & Therapeutics*, 2008. **84**(5): p. 548-558.
21. Zalevsky, J., et al., *Enhanced antibody half-life improves in vivo activity*. *Nature biotechnology*, 2010. **28**(2): p. 157-159.
22. Stump, B. and J. Steinmann, *Conjugation process development and scale-up*, in *Antibody-Drug Conjugates*. 2013, Springer. p. 235-248.
23. Köhler, G. and C. Milstein, *Continuous cultures of fused cells secreting antibody of predefined specificity*. *Nature*, 1975. **256**(5517): p. 495.
24. Lequin, R.M., *Enzyme immunoassay (EIA)/enzyme-linked immunosorbent assay (ELISA)*. *Clinical chemistry*, 2005. **51**(12): p. 2415-2418.
25. Ober, R.J., et al., *Differences in promiscuity for antibody–FcRn interactions across species: implications for therapeutic antibodies*. *International immunology*, 2001. **13**(12): p. 1551-1559.
26. Presta, L.G., *Engineering antibodies for therapy*. *Current pharmaceutical biotechnology*, 2002. **3**(3): p. 237-256.
27. Kipriyanov, S.M. and F. Le Gall, *Generation and production of engineered antibodies*. *Molecular biotechnology*, 2004. **26**(1): p. 39-60.
28. Gonzales, N.R., et al., *Minimizing the immunogenicity of antibodies for clinical application*. *Tumor Biology*, 2005. **26**(1): p. 31-43.
29. Riechmann, L., et al., *Reshaping human antibodies for therapy*. *Nature*, 1988. **332**(6162): p. 323.
30. Lonberg, N., *Human antibodies from transgenic animals*. *Nature biotechnology*, 2005. **23**(9): p. 1117.

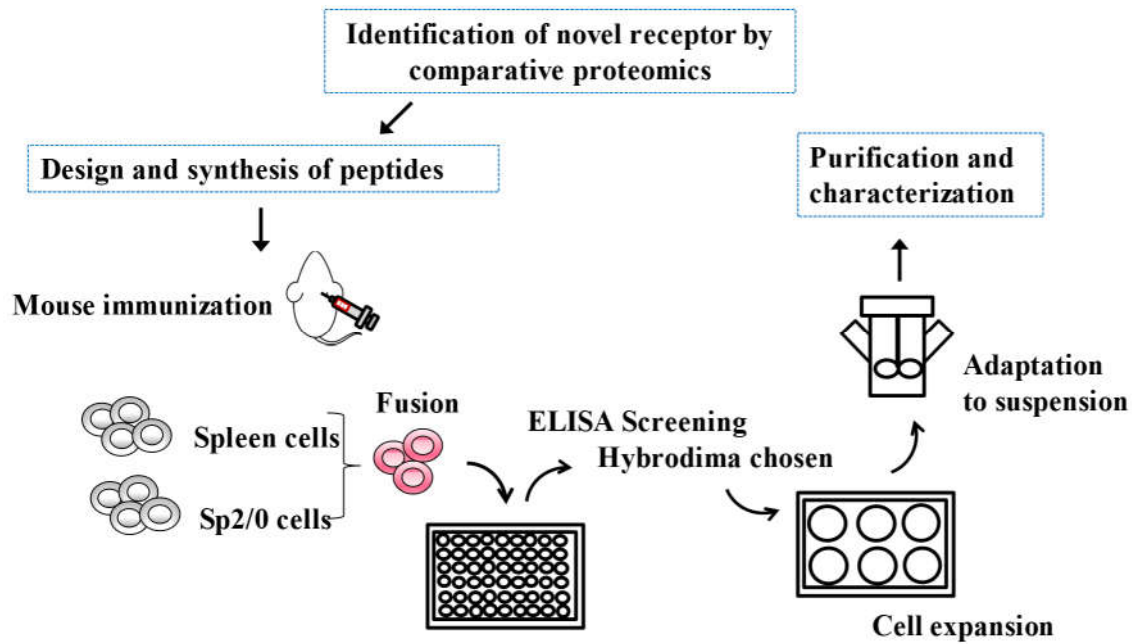
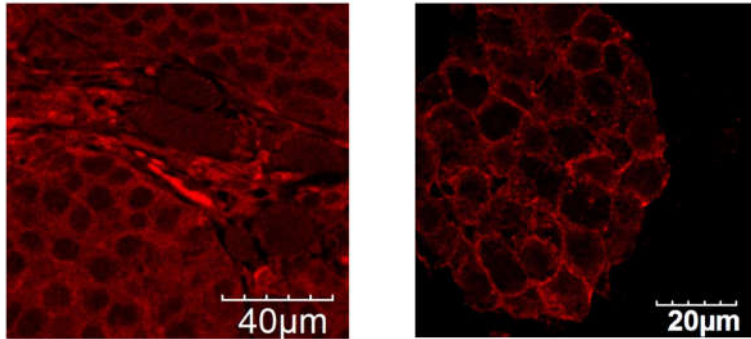


**Figure 1.** Novel antibody development overview

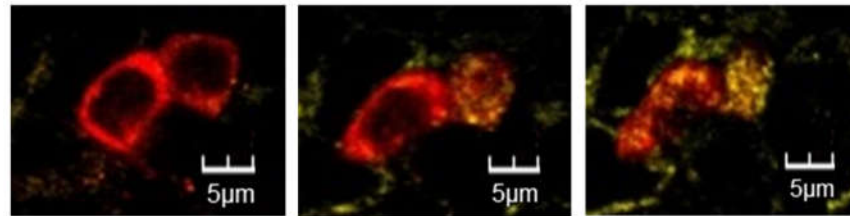
### Fixed tissue staining



Mouse xenograft

Human patient tissue

### Live cell (BON) staining



10 min

30 min

40 min

**Figure 2.** Specific binding of antibody candidate

Staining conditions: Alexa Fluor (AF) 647-labeled commercial anti-SSTR mAb was incubated with tissues (4 °C overnight) or incubated with cells (37 °C over 40 min) at 2 µg/mL in PBS buffer containing 10% inactivated goat serum and 1% BSA.

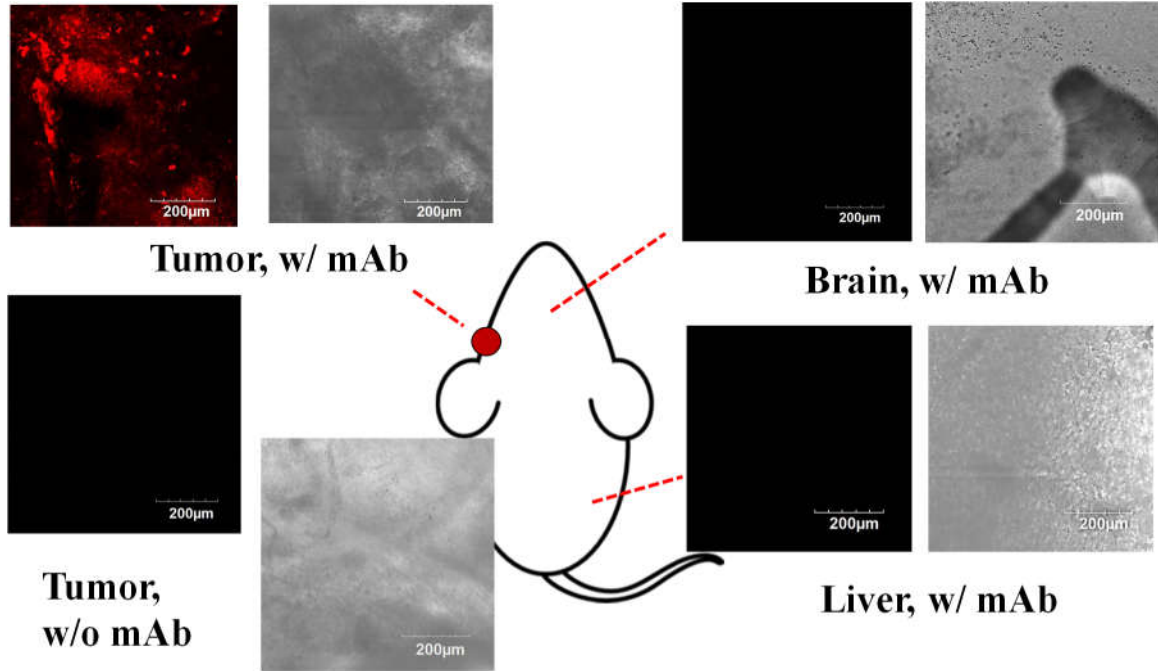


**Figure 3.** *In vivo* evaluation of antibody specific targeting

The AF647 labelled anti-SSTR mAb was injected into mice at a dosage of 8mg/kg body weight. After 24 h, the mice were sacrificed, and tissue slices were taken from different locations for imaging.

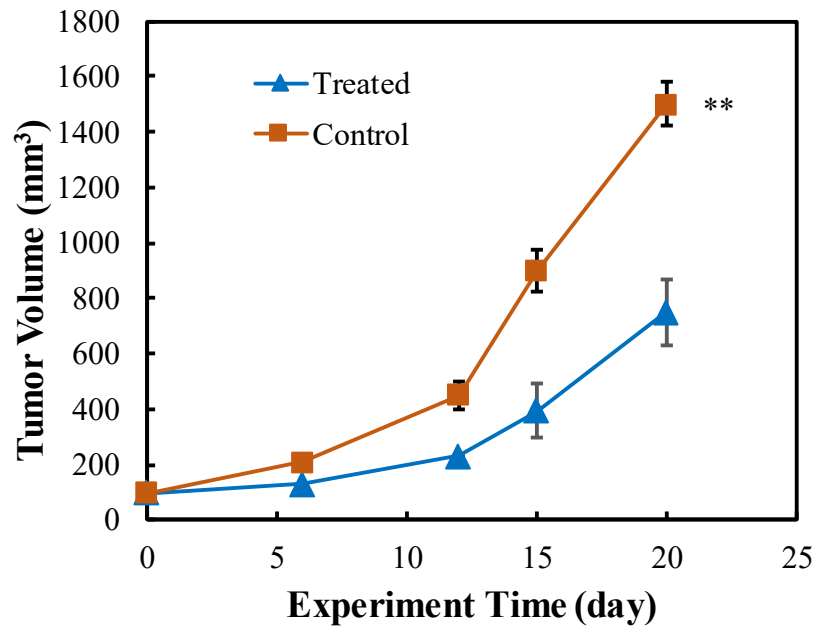


**Figure 4.** ADC in vivo efficacy assay

Animal tumor model was generated by injecting  $5 \times 10^6$  cells BON cells to immunodeficient mice, and tumors were allowed to grow for 7 days. ADC was injected for treatment every 6 days with total dosage of 8mg/kg.

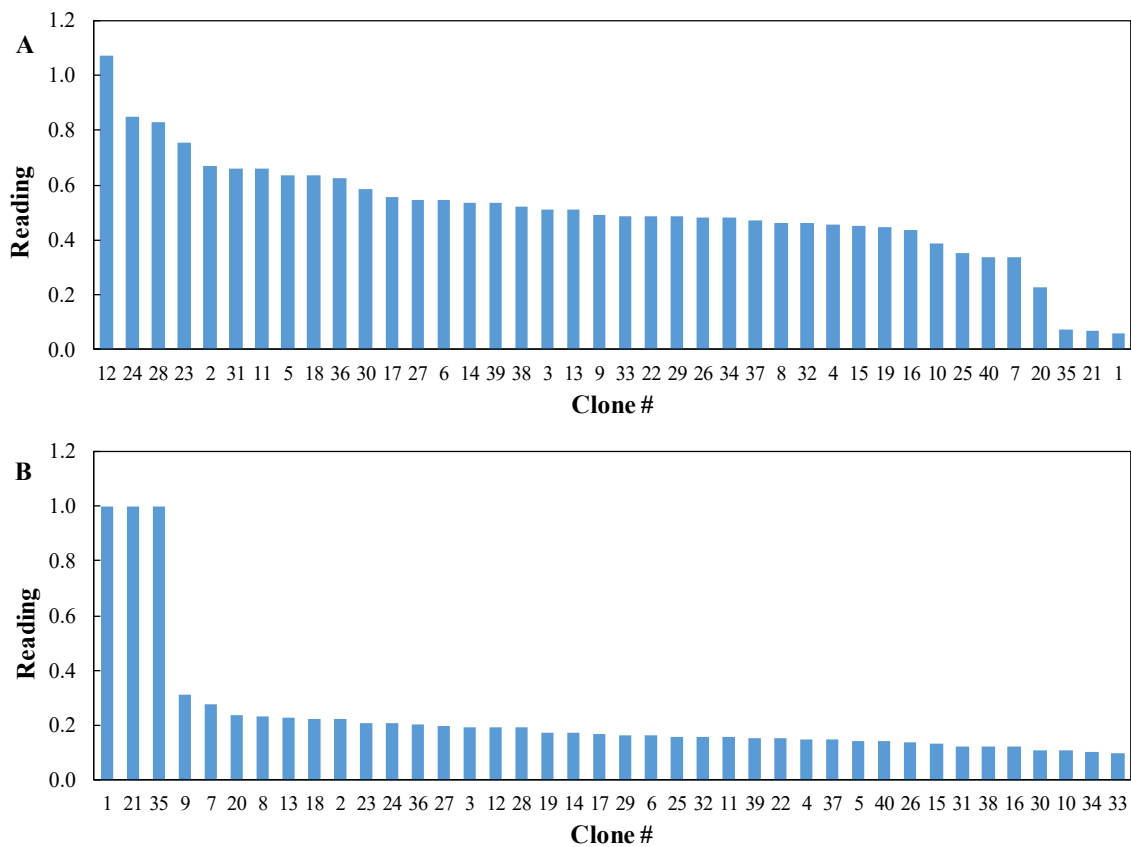


**Figure 5.** ELISA ranking of novel anti-SSTR antibody from hybridoma using peptide A and peptide B

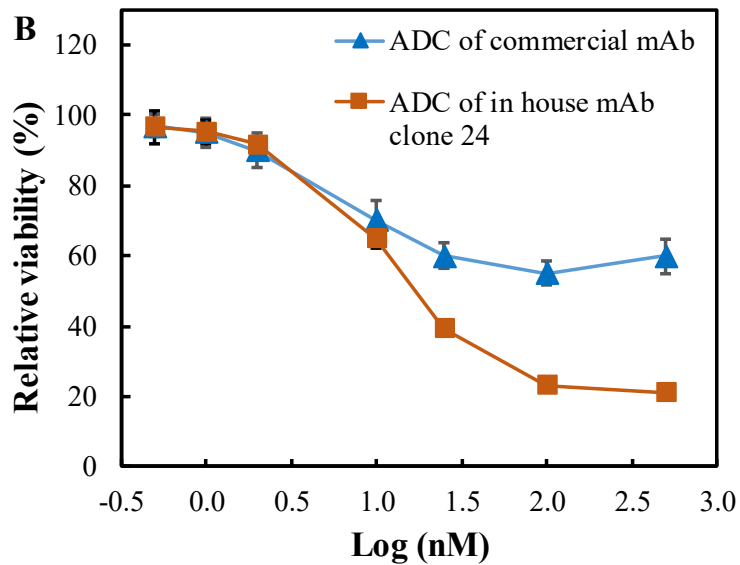
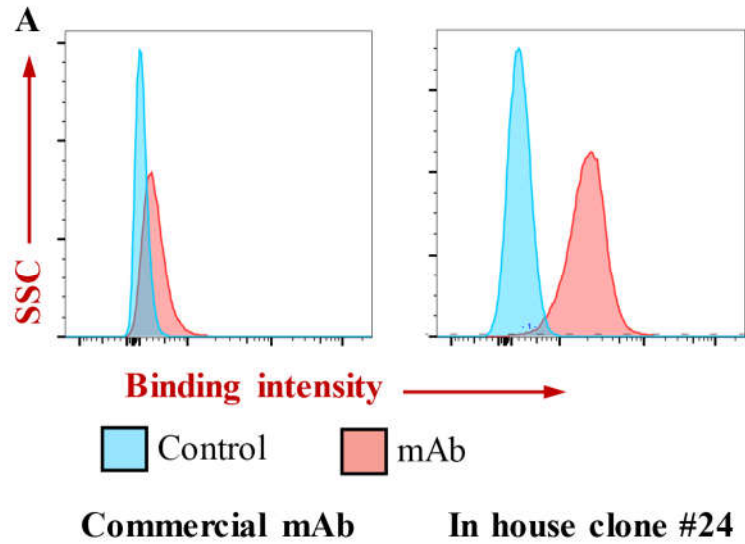


**Figure 6.** Increased binding and ADC toxicity comparing to commercial antibody

**(A)** Flow cytometry analysis of receptor binding of purified in house anti-SSTR mAb (clone #24) and the commercial anti-SSTR mAb to SSTR<sup>+</sup> BON cell line. Staining conditions: Alexa Fluor (AF) 647-labeled mAb was incubated with cells at 5  $\mu$ g/million cells at 37 °C for 30 min.

**(B)** Evaluation of ADCs constructed with in house anti-SSTR mAb and the commercial anti-SSTR mAb. ▲ MMAE-commercial mAb, ■ MMAE-in house mAb.

CHAPTER 3

BIOPROCESS DEVELOPMENT OF ANTIBODY-DRUG CONJUGATE  
PRODUCTION FOR CANCER TREATMENT

by

JIANFA OU, YINGNAN SI, KAHYONG GOH, NORIO YASUI, YICHEN GUO,  
JIAJIA SONG, LIZHONG WANG<sup>3</sup>, RENATA JASKULA-SZTUL, JINDA FAN,  
LUFANG ZHOU, RUNHUA LIU, AND XIAOGUANG (MARGARET) LIU

Submitted to PLOS One

Format adapted for dissertation

## **Abstract**

Antibody drug conjugate (ADC) is a class of targeted cancer therapies that combine the advantages of monoclonal antibody (mAb)'s specific targeting and chemotherapy's potent cytotoxicity. The therapeutic effect of ADC is significantly affected by its bioproduction process. This study aims to develop an effective ADC production process using anti-HER2 mAb-drug as a model therapeutic. First, a high titer ( $>2$  g/L) of mAb was produced by Chinese hamster ovary cells from fed-batch cell culture. Both live-cell confocal microscopy imaging and flow cytometry analysis demonstrated that the produced mAb and ADC had strong and specific binding to HER2<sup>+</sup> cell line BT474. Second, various conjugation conditions of mAb and drug, including linker selection, ratio of drug and mAb, and conjugation approaches, were investigated to improve the production yield and product quality. Finally, the ADC structure and biological quality were evaluated by SDS-PAGE and anti-breast cancer toxicity study, respectively. The ADC with integral molecular structure and high cytotoxicity (IC<sub>50</sub> of 1.95 nM) was produced using the optimized production process. The robust bioproduction process could guide the development of ADC-based biopharmaceuticals.

**Keywords:** antibody-drug conjugate; bioprocess development; toxicity; breast cancer

## 1 Introduction

As an effective targeted therapy, antibody-drug conjugate (ADC) has been developed to treat solid tumors while minimizing the side effects on normal cells [1-3]. It drew great attention after the first ADC, gemtuzumab ozogamicin (Mylotarg®) for acute myelocytic leukemia treatment, was approved by the FDA in 2000 [4]. The high clinical need led to two recently approved ADCs, i.e. the CD30-targeting Brentuximab vedotin (Adcetris®) to treat relapsed Hodgkin lymphoma and systemic anaplastic large cell lymphoma and HER2-targeting Trastuzumab emtansine (Kadcyla®) to treat relapsed or chemotherapy refractory HER2<sup>+</sup> breast cancer [5, 6]. Nowadays there are nearly 60 ADCs in clinical trials and this number continues to grow [7].

ADC is typically composed of monoclonal antibody (mAb), spacer or linker, and cytotoxic reagent or payload. The mAb enables ADC to circulate in the bloodstream until it binds to the tumor specific surface antigen. After binding, ADC is internalized via the receptor-mediated endocytosis, forms late endosome, undergoes lysosomal degradation, releases the toxic drug into the cytoplasm, and eventually leads to cancer cell death [8-10]. The challenges in ADC construction include: 1) high-quality mAb that specifically targets and delivers drugs to cancer cells, 2) suitable linker which is stable in circulation but quickly releases the payload after endocytosis, and 3) efficient and robust conjugation process to achieve high biological activity, high stability and reduced heterogeneity [11]. Two conjugation approaches, lysine- and cysteine-based, were developed to produce ADC. In lysine-based conjugation, the potent small molecule can directly react with antibody through the modified lysine while it needs accurate process control to reduce batch-to-batch variation and product heterogeneity [12, 13]. In cysteine-based conjugation, the

cytotoxic drug can conjugate with the thiols generated from disulfide bond reduction, but it is important to use site-specific conjugation or novel linker to achieve high stability and structural integrity of ADC [14, 15]. In addition to conjugation process, the high-quality mAb production and potent free drug selection are also very important for ADC production.

The objective of this study was to develop an effective and robust bioproduction process of ADC. Several key parameters, i.e. mAb production, linker selection, conjugation conditions, and end product purification, were investigated. The HER2-targeting ADC was used as a model biopharmaceutical. Both the molecular integrity and the anti-breast cancer toxicity of constructed ADCs were evaluated. The data collected in this study could benefit the ADC-based anti-cancer therapy development.

## **2 Materials and methods**

### *2.1 Cell lines and cell culture*

The seed culture of our in-house CHO DG44/anti-HER2 mAb was maintained in Dynamis™ medium, supplemented with 8 mM L-glutamine, 500 nM methotrexate and anti-clumping agent (0.3% v/v) in 125-mL shaker flask at 37 °C, 5% CO<sub>2</sub> and 130 rpm in a humidified incubator (Caron, Marietta, OH). Methotrexate was removed one passage before the mAb production in bioreactor. The HER2<sup>+</sup> human breast cancer cell line BT474 (ATCC, Manassas, VA) was cultivated in DMEM/F12 medium supplemented with 10% fetal bovine serum (FBS) and 4 mM L-glutamine in T25 flask. The control cell line MDA-MB-231 (ATCC) was grown in DMEM containing 10% FBS and 4 mM L-glutamine in

T25 flask. All basal media, supplements and reagents used in this study were purchased from Thermo Fisher Scientific (Waltham, MA) unless otherwise specified.

## *2.2 Optimization of anti-HER2 mAb production*

*Bioproduction optimization* The established procedure of fed-batch cell culture in 2-L stirred-tank bioreactor for mAb production was described in our previous publication [16]. The mAb production cultures were seeded with viable cell density (VCD) of  $0.3\text{-}0.5 \times 10^6$  cells/mL in Dynamis™ medium supplemented with 6 g/L glucose and 8 mM glutamine. The nutrient EfficientFeeding C+ was fed to the cell culture broth on Day 3, 5, 7 and 9 during mAb production. The bioreactor production process parameters were controlled at 37 °C, pH 7.0, DO 70% and agitation 70 rpm. The bioreactor was sampled daily to monitor cell growth, glucose, glutamine and anti-HER2 mAb titer. The VCD and viability were measured by cell counter (Thermo Fisher Scientific). Glucose concentration was measured by HemoCue® Glucose 201 DM System, glutamine concentration was analyzed using YSI (YSI, Yellow Springs, OH), and mAb was titrated using a Bio-Rad NGC system. The glucose concentration was maintained at 2-6 g/L and glutamine concentration was maintained at 2-8 mM through feeding concentrated solution of glucose and glutamine, respectively. The mAb production was stopped when viability reached <50%, and antibody was harvested by centrifugation and filtration for purification. Similar fed-batch culture was performed in shaker flask at 37 °C, 5% CO<sub>2</sub> and 130 rpm in a humidified incubator without pH and DO control.

*Purification and evaluation* Small-scale anti-HER2 mAb was purified using NAb™ Protein A Plus Spin Kit. Large-scale mAb purification using Bio-Rad NGC system

(Bio-Rad, Hercules, CA) equipped with a UNOsphere SUPrA column was conducted according to the manufacturer's protocols, including column equilibration, sample loading, column washing, and antibody elution. The equilibration buffer was comprised of 0.02 M sodium phosphate and 0.02 M sodium citrate at pH 7.5. Elution buffer contained 0.02 M sodium citrate and 0.1 M sodium chloride at pH 3.0. The pH of eluted mAb was neutralized to 7.0 with 1 M Tris solution. The mAb purity was examined by SDS-PAGE under natural condition using NuPAGE™ 4-12% Bis-Tris Protein Gels (1.0 mm, 10-well) and a PowerPac™ Basic Power Supply (Bio-Rad). The surface binding of our anti-HER2 mAb was analyzed using BD LSRII flow cytometer (BD Biosciences, San Jose, CA) after incubating cells with 1 µg of Alexa Fluor 488-labeled mAb/million cells on ice for 30 min.

### *2.3 Bioprocess development of ADC construction*

The diagram of ADC construction is shown in Figure 1, including both lysine-based conjugation and cysteine-based conjugation.

*Synthesis of rebridging linker* The rebridging linker was synthesized following the published protocol [17] with minor modification. Briefly, 3.91 mmol 6-aminohexanoic acid was mixed with 3.91 mmol 3,4-dibromofuran-2,5-dione in 20 mL of acetic acid. After stirring for 10 min at room temperature, the solution was heated at 100 °C for 18 h. The solvent was removed by vacuum and the rebridging linker was purified with silica gel with eluent solution of dichloromethane/ethyl acetate 0-40%.

*Synthesis of linker-MMAE payload* The peptide-based traditional Maleimidocaproyl(Mc)-Val-Cit-PABC-PNP linker or the rebridging linker were reacted with monomethyl auristatin E (MMAE). In the construction of traditional linker-MMAE

payload, 18.20  $\mu\text{mol}$  potent molecule MMAE, 16.38  $\mu\text{mol}$  Mc-Val-Cit-PABC-PNP, and 3.64  $\mu\text{mol}$  hydroxybenzotriazole were dissolved and mixed in 500  $\mu\text{L}$  dimethylformamide. Then 18.20  $\mu\text{mol}$  pyridine was added to the mixture after 2 min, and 20  $\mu\text{mol}$  trifluoroacetic acid (TFA) was added after 24 h. In the construction of rebridging linker-MMAE payload, 13.55  $\mu\text{mol}$  N,N'-diisopropylcarbodiimide, 13.55  $\mu\text{mol}$  N,N-diisopropylethylamine, and 33.85  $\mu\text{mol}$  synthesized rebridging linker were mixed in 0.25 mL dichloromethane, followed by frequent mixing for 1 h at room temperature. Then 13.55  $\mu\text{mol}$  MMAE was added and frequently mixed for additional 16 h. After linker-MMAE conjugates were synthesized, the solvents were removed by vacuum pump and the conjugates were purified by a Waters HPLC system equipped with 600 Controller/Pump and 996 PDA detector (Waters, Milford, MA). A reversed-phase C<sub>18</sub> column with 5  $\mu\text{m}$  C18(2) 100 Å and 250 x 10 mm (Phenomenex Luna®; Torrance, CA) was used with gradient elution buffer of Phase A (water+0.1% TFA) and Phase B (acetonitrile). The purified products were confirmed by Agilent 6500 Series Accurate-Mass Q-TOF LC/MS (Agilent Technologies, Santa Clara, CA).

*ADC production* The anti-HER2 mAb produced in this study was used to generate all conjugates. The lysine-based ADC was produced following a previously developed method with modification [18]. Briefly, the crosslinker Sulfo-SMCC was mixed with 5 mg/mL mAb in PBS and incubated for 30 min at room temperature. The excessive crosslinker was removed by repeated buffer exchange using Pierce™ Protein Concentrator. Then with cytotoxic mertansine (DM1) reacted with the SMCC-modified mAb at different molar ratios (4:1, 8:1 and 16:1) for 30 min. The final product was purified by PD MidiTrap™ G-25 (GE Healthcare, Little Chalfont, United Kingdom) gel filtration.

The cysteine-based ADC was constructed using two conjugation approaches, i.e. sequential conjugation and *in situ* conjugation [19, 20]. In sequential conjugation, 5 mg/mL mAb solved in 50 mM borate buffer at pH 8.0 was reduced with 1 mM dithiothreitol (DTT) at 37 °C for 1 h, followed by repeated buffer exchange in Pierce dialysis column using PBS buffer containing 1 mM pentetic acid. Then the traditional linker-MMAE and rebridging linker-MMAE payloads were mixed with the reduced mAb with payload:mAb molar ratio of 6.6 and 4.4, respectively, and incubated at 4 °C for 1 h. The reaction was terminated by adding 20-fold molar excess of cysteine over payload and the final products were purified by G-25 gel filtration. In *in situ* conjugation, 7 equivalent of tris (2-carboxyethyl) phosphine (TCEP) was used to reduce 5 mg/mL mAb in 50 mM borate buffer, pH 8.0. The payload was added simultaneously with TCEP at 7 equivalent. After incubation at 37 °C for 2 h, the product was purified by G-25 gel filtration.

#### 2.4 Characterization of ADCs

*Drug-antibody ratio and structure* The integrity of ADC structure was analyzed using SDS-PAGE. The average drug-antibody ratio (DAR) was calculated using the following equation [21, 22]:

$$DAR = \frac{\epsilon_{mAb}^{248 \text{ or } 252} \cdot R - R \cdot \epsilon_{mAb}^{280}}{R \cdot \epsilon_{Drug}^{280} - \epsilon_{Drug}^{248 \text{ or } 252}} \quad (1)$$

Where  $R = A_{248}/A_{280}$  = Absorbance ratio.  $\epsilon_{mAb}^{248/252} = 9.41 \times 10^4 \text{ M}^{-1}\text{cm}^{-1}$ ,  $\epsilon_{mAb}^{280} = 2.34 \times 10^5 \text{ M}^{-1}\text{cm}^{-1}$ ,  $\epsilon_{MMAE}^{248} = 1.5 \times 10^3 \text{ M}^{-1}\text{cm}^{-1}$ ,  $\epsilon_{MMAE}^{280} = 1.59 \times 10^4 \text{ M}^{-1}\text{cm}^{-1}$ ,  $\epsilon_{DMI}^{252} = 2.64 \times 10^5 \text{ M}^{-1}\text{cm}^{-1}$ ,  $\epsilon_{DMI}^{280} = 5.23 \times 10^3 \text{ M}^{-1}\text{cm}^{-1}$ . The UV absorbance was measured using a NanoDrop™ 2000 Spectrophotometer.

*Surface binding and internalization* The live-cell confocal laser scanning microscopy technique was utilized to evaluate the surface binding capability and internalization of mAb and ADC in HER2<sup>+</sup> BT474 cell line. The BT474 cells were seeded on glass coverslips (Warner Instruments, Hamden, CT) and transduced with BacMam 2.0 CellLight Late Endosomes-RFP and BacMam GFP Transduction Control to stain late endosomes and cytoplasm of BT474 cells, respectively, overnight. The transduced cells were rinsed twice with PBS buffer, stained with 2 µg/mL Alexa Fluor™ 647 labeled anti-HER2 mAb in a PBS buffer containing 10% inactivated goat serum and 1% bovine serum albumin (BSA), and incubated at 37 °C under the microscope. The dynamic imaging profiles were captured using a confocal microscope (Olympus IX81, Center Valley, PA) every 20 min until ADC trafficked to late endosomes for lysosomal degradation to release drugs intracellularly.

*Anti-breast cancer toxicity evaluation* The HER2<sup>+</sup> BT474 cells and control cells were seeded in 96-well plates with seeding density of  $0.05 \times 10^6$  cells/mL in 75 µL DMEM/F12 or DMEM complete medium, and incubated at 37 °C for 24 h. Equal volume of medium containing ADCs, free drugs (positive control), or PBS (control) was added to the well-plate cultures to initiate the anti-cancer toxicity study. After incubation at 37 °C for 3 days, the culture volume in well plate was measured. The working solution of CellTiter-Glo® Luminescent Cell Viability Assay Kit (Promega, Madison, WI) was added at equal amount before reading the luminescence with a Synergy H1 Hybrid Multi-Mode Microplate Reader (BioTek, Winooski, VT). The luminescent signal was proportional to the number of cells, and used to calculate the relative viability in each treatment.

### 3 Results

#### 3.1 mAb production and purification

Feeding cell culture nutrients and accurately controlling bioproduction process parameters are important to improve mAb production. In this study, the anti-HER2 mAb was produced by CHO DG44/IgG from fed-batch cell culture in both shaker flask and stirred-tank bioreactor. Figure 2a showed the diagram of stirred-tank bioreactor connected to the automatic control panel of temperature, pH, DO and agitation, gas stations, and feeding pumps. Figure 2b showed the flowchart of mAb purification using NGC chromatography system.

*Production* The kinetics profiles of CHO cell growth and mAb production were presented in Figure 3 and the production parameters were summarized Table 1. Both shaker flask culture and bioreactor culture effectively produced mAb within 11 days. It was found that the specific growth rate was  $\mu = 0.028 \pm 0.002 \text{ h}^{-1}$  in shaker flask and  $0.033 \pm 0.001 \text{ h}^{-1}$  in bioreactor. The VCD in bioreactor was  $18.1 \times 10^6$  cells/mL, which was slightly higher than the VCD of  $14.3 \times 10^6$  cells/mL in shaker flask. The final anti-HER2 mAb titer was  $2335.2 \pm 56.3 \text{ mg/L}$  and  $1278.2 \pm 62.5 \text{ mg/L}$ , and the specific production rate was  $30.00 \pm 2.14 \text{ pg/cell/day}$  and  $19.60 \pm 0.55 \text{ pg/cell/day}$  in bioreactor and shaker flask, respectively. It is clear that the mAb production was improved by 58% and cell growth was increased by 26% in bioreactor as compared to shaker flask.

*mAb characterization* The purified anti-HER2 mAbs were characterized using SDS-PAGE gel together with the FDA approved Trastuzumab (Figure 4a). The results showed that our in-house anti-HER2 mAb had an expected protein size of 150 kDa and

similar purity as Trastuzumab. A strong surface binding of mAb to the HER2 receptor is critical to achieve a high anti-cancer toxicity or efficacy of HER2-targeting ADC and to minimize the side effects caused by the non-specific targeting. Flow cytometry analysis was performed to quantitate and compare the cell surface binding of our anti-HER2 mAb and Trastuzumab to BT474 and control cells. Figure 4b revealed that Trastuzumab showed strong surface binding to BT474 cells but no binding to negative control cells, and our in-house anti-HER2 mAb had similar surface binding as Trastuzumab. These data indicated that the generated ADC had strong and specific surface binding to HER2 receptor in breast cancer.

### *3.2 Bioprocess Development of ADC Construction*

In this study, we evaluated the factors that affected ADC yield and quality, including potent drugs; conjugation approaches; molar ratio among drug, linker, and mAb; linker selection; and product purification.

*Potent drugs* Two potent chemical drugs, i.e. MMAE and DM1, that induce apoptosis by blocking the polymerization of tubulin, were used to investigate the cysteine- and lysine- based conjugation production process [5, 23]. Figure 5a described the dose-dependent anti-breast cancer toxicity using free drugs. It is shown that the viability of HER2<sup>+</sup> BT474 cells was reduced by MMAE to 12% at concentration of 12 nM and 6% at 60 nM, and the viability was decreased by DM1 to 62% at 12 nM and 11% at 60 nM. As a negative control, mAb was not toxic to breast cancer cells in this study.

*Conjugation approach* In lysine-based conjugation, the Sulfo-SMCC linker reacted with the 10 chemically accessible lysine residues in mAb, and generated mAb-DM1 ADCs

with DARs of 0-10. As shown in the SDS-PAGE gel (Figure 5b), the structure of mAb in ADC was not obviously changed by conjugation at lysine. In cysteine-based conjugation, the cysteine was reduced to generate free thiol groups and generated ADCs with DARs of 2, 4, 6 or 8. Although the attractive non-covalent bonds could maintain the structure of mAb [24], the break of inter-chain disulfides significantly reduced the stability of ADCs, which was confirmed by the heterologous structure of mAb in ADCs (Figure 5b).

*Molar ratio of drug:linker:mAb* Three different ratios of drug:linker:mAb (4:4:1, 8:4:1 and 16:8:1) were evaluated in the lysine-based conjugation and generated three DM1-carrying ADCs, including DM1-ADC1, DM1-ADC2 and DM1-ADC4. The DARs of these three ADCs were  $3.15 \pm 0.20$ ,  $3.68 \pm 0.10$  and  $4.51 \pm 0.13$ , respectively. It is clear that DAR was increased by 16% when the drug amount doubled, and increased by 36% when the drug amount quadrupled and linker amount doubled. These DAR data were consistent with previous studies [15, 21]. Figure 5b revealed that all these ADCs had integral structure although a small portion of aggregation was observed, which could be caused by the hydrophobicity of the linker and payload [15]. The ADC4 showed a higher anti-breast cancer toxicity with  $IC_{50}$  value of 3.88 nM than that of ADC1 with  $IC_{50}$  value of 63.16 nM and ADC2 with  $IC_{50}$  value of 23.67 nM (Figure 5c). Therefore, the higher ratio of drug and linker in the lysine-based conjugation improved the DAR and anti-cancer toxicity of ADC.

*Purification method* In addition to G25 column, protein A column was also tested in ADC purification. After lysine-based conjugation using the same drug:linker:mAb of 8:4:1, DM1-ADC2 and DM1-ADC3 were purified using G25 and protein A, respectively. The recovery rate of DM1-ADC2 was  $96.1 \pm 4.8\%$ , much higher than the recovery rate ( $65.8 \pm 5.9\%$ ) of DM1-ADC3. However, DM1-ADC3 showed higher cytotoxicity than

DM1-ADC2, with IC<sub>50</sub> of 5.07 nM vs. IC<sub>50</sub> of 23.67 nM (Figure 5c). These results indicated that G25 column significantly improved ADC recovery rate but slightly reduced the anti-cancer toxicity as compared to protein A column.

*Rebridging linker* A rebridging linker that can cross link the reduced cysteine was employed to maintain the mAb structure in cysteine-based ADC (Figure 1c). It is found that the rebridged ADC had less single chain, i.e. 2H, H and L (Figure 5b), and also showed higher cytotoxicity than the non-bridged ADC (Figure 5d).

*Sequential vs in situ conjugation* Both sequential and *in situ* conjugations were applied in the construction of mAb-MMAE using rebridging linker and traditional linker. The SDS-PAGE showed that the *in situ* conjugation significantly increased the production of ADC via improving the content of stable structure (2H+2L, 2H+L, 1H+L, H+L).

### 3.3 Binding and Internalization of ADC

Live-cell confocal microscopy imaging technique was used to monitor the surface binding and internalization of ADC in breast cancer cell. The dynamic profiles of confocal imaging was presented in Figure 6. No binding or internalization was observed on the negative control MDA-MB-468 cells, which is consistent with previous study [25]. After mixing the AF647 labeled anti-HER2 mAb-MMAE ADC (red color) with the HER2<sup>+</sup> BT474 cells (blue color), the ADC bound to cell surface within 20 min. Then the ADC is quickly internalized, which is triggered by the receptor-mediated endocytosis [26], properly localized at late endosome (green color) for lysozyme degradation within 40 min [27], and continuously accumulated intracellularly within 60 min [28].

## 4 Discussion

The production process of ADC can significantly affect its quality and yield [29]. This study used HER2-targeting ADC as a model therapeutics to evaluate and optimize the ADC bioproduction process, including mAb production, linker selection, conjugation approach, and purification method.

The mAb enables ADC to specifically target the surface receptor in cancer cells. The high quality of mAb, such as glycosylation, sialylation and stability, can improve the biological function of ADC, and the high productivity can significantly reduce the development and production cost of ADC. In this study, a high-titer and high-quality HER2-targeting mAb was produced from a fed-batch cell culture in stirred-tank bioreactor. Fed-batch process has been widely used in mAb production, which can regulate its post-translational modification and productivity [30, 31]. The flow cytometry analysis and confocal microscopy imaging demonstrated that our mAb had strong and specific surface binding capability.

Previous studies showed that the heterogeneity of DAR could diminish the in vivo solubility, impair binding capability, and influence pharmacokinetic/pharmacodynamic efficacy of ADC [21, 32-34]. This study showed that our lysine-based ADC conjugation process generated ADCs with a good range of DAR (i.e. 3.1-4.5). The cysteine-based conjugation caused the structural loss of disulfide bonds, which caused a high heterogeneity of ADC. Several strategies were developed to impair the ADC structure caused by cysteine reduction, such as engineering cysteine residue [35, 36], introducing unnatural amino acids [37], and utilizing additional enzymes in ADC conjugation process [38, 39]. However, these techniques were time consuming and had limited application

scenarios. The linker bridging technique was developed to repair ADC structure, optimize DAR and simplify conjugation operation [17, 20, 40]. This study used the rebridging linker in cysteine-based conjugation, which improved the ADC integrity and anti-cancer toxicity. Literature also reported that the ADC constructed with non-cleavable linker showed higher anti-cancer toxicity and stability in vitro [41], and improved anti-cancer efficacy and pharmacokinetic performance in vivo [25, 42]. Therefore, novel linker development is an effective approach to optimize the bioproduction process of ADC.

The comparison between our study and reported data was summarized in Table 2. It is clear that the ADCs that were prepared with the optimized process showed high anti-cancer toxicity and the IC<sub>50</sub> values were similar to previous publications, but the viability of cancer cells post treatment was lower than most reported data, indicating a better cytotoxicity. In addition, the anti-cancer toxicity was affected by ADC preparation process, targeted cell line, treatment timeline, detection assay, etc.

## **5 Conclusions**

ADC is a promising targeted therapy for cancer treatment. This study developed a robust ADC production process by investigating mAb production and conjugation conditions. The collected results or observations can be used to guide ADC development and production, which will accelerate the ADC-based anti-cancer therapy development and eventually benefit cancer patients.

## References

1. Bouchard, H., C. Viskov, and C. Garcia-Echeverria, *Antibody-drug conjugates-a new wave of cancer drugs*. *Bioorg Med Chem Lett*, 2014. **24**(23): p. 5357-63.
2. Drake, P.M. and D. Rabuka, *An emerging playbook for antibody-drug conjugates: lessons from the laboratory and clinic suggest a strategy for improving efficacy and safety*. *Curr Opin Chem Biol*, 2015. **28**: p. 174-80.
3. Bunn, P.A., Jr., et al., *Small Cell Lung Cancer: Can Recent Advances in Biology and Molecular Biology Be Translated into Improved Outcomes?* *J Thorac Oncol*, 2016. **11**(4): p. 453-74.
4. Larson, R.A., et al., *Final report of the efficacy and safety of gemtuzumab ozogamicin (Mylotarg) in patients with CD33-positive acute myeloid leukemia in first recurrence*. *Cancer*, 2005. **104**(7): p. 1442-52.
5. Younes, A., U. Yasothan, and P. Kirkpatrick, *Brentuximab vedotin*. *Nat Rev Drug Discov*, 2012. **11**(1): p. 19-20.
6. Verma, S., et al., *Trastuzumab emtansine for HER2-positive advanced breast cancer*. *N Engl J Med*, 2012. **367**(19): p. 1783-91.
7. Diamantis, N. and U. Banerji, *Antibody-drug conjugates--an emerging class of cancer treatment*. *Br J Cancer*, 2016. **114**(4): p. 362-7.
8. Stump, B. and J. Steinmann, *Conjugation process development and scale-up*, in *Antibody-Drug Conjugates*. 2013, Springer. p. 235-248.

9. Pabst, M., et al., *Modulation of drug-linker design to enhance in vivo potency of homogeneous antibody-drug conjugates*. J Control Release, 2017. **253**: p. 160-164.
10. Trail, P.A., G.M. Dubowchik, and T.B. Lowinger, *Antibody drug conjugates for treatment of breast cancer: Novel targets and diverse approaches in ADC design*. Pharmacol Ther, 2018. **181**: p. 126-142.
11. Hughes, B., *Antibody–drug conjugates for cancer: poised to deliver?* 2010, Nature Publishing Group.
12. Marcoux, J., et al., *Native mass spectrometry and ion mobility characterization of trastuzumab emtansine, a lysine-linked antibody drug conjugate*. Protein Sci, 2015. **24**(8): p. 1210-23.
13. Nanna, A.R., et al., *Harnessing a catalytic lysine residue for the one-step preparation of homogeneous antibody-drug conjugates*. Nat Commun, 2017. **8**(1): p. 1112.
14. Panowski, S., et al., *Site-specific antibody drug conjugates for cancer therapy*. MAbs, 2014. **6**(1): p. 34-45.
15. Tsuchikama, K. and Z. An, *Antibody-drug conjugates: recent advances in conjugation and linker chemistries*. Protein Cell, 2016.
16. Xu, N., et al., *Comparative proteomic analysis of three Chinese hamster ovary (CHO) host cells*. Biochemical Engineering Journal, 2017. **124**: p. 122-129.

17. Behrens, C.R., et al., *Antibody-Drug Conjugates (ADCs) Derived from Interchain Cysteine Cross-Linking Demonstrate Improved Homogeneity and Other Pharmacological Properties over Conventional Heterogeneous ADCs*. Mol Pharm, 2015. **12**(11): p. 3986-98.
18. Liu, C., et al., *Eradication of large colon tumor xenografts by targeted delivery of maytansinoids*. Proc Natl Acad Sci U S A, 1996. **93**(16): p. 8618-23.
19. Doronina, S.O., et al., *Development of potent monoclonal antibody auristatin conjugates for cancer therapy*. Nat Biotechnol, 2003. **21**(7): p. 778-84.
20. Schumacher, F.F., et al., *Next generation maleimides enable the controlled assembly of antibody-drug conjugates via native disulfide bond bridging*. Org Biomol Chem, 2014. **12**(37): p. 7261-9.
21. Zhang, H., et al., *Therapeutic potential of an anti-HER2 single chain antibody-DMI conjugates for the treatment of HER2-positive cancer*. Signal Transduct Target Ther, 2017. **2**: p. 17015.
22. Fishkin, N., *Maytansinoid-BODIPY Conjugates: Application to Microscale Determination of Drug Extinction Coefficients and for Quantification of Maytansinoid Analytes*. Mol Pharm, 2015. **12**(6): p. 1745-51.
23. LoRusso, P.M., et al., *Trastuzumab emtansine: a unique antibody-drug conjugate in development for human epidermal growth factor receptor 2-positive cancer*. Clin Cancer Res, 2011. **17**(20): p. 6437-47.

24. Adem, Y.T., et al., *Auristatin antibody drug conjugate physical instability and the role of drug payload*. *Bioconjug Chem*, 2014. **25**(4): p. 656-64.
25. Lewis Phillips, G.D., et al., *Targeting HER2-positive breast cancer with trastuzumab-DM1, an antibody-cytotoxic drug conjugate*. *Cancer Res*, 2008. **68**(22): p. 9280-90.
26. Xu, S., *Internalization, Trafficking, Intracellular Processing and Actions of Antibody-Drug Conjugates*. *Pharm Res*, 2015. **32**(11): p. 3577-83.
27. Zemskov, E.A., et al., *Cell-surface transglutaminase undergoes internalization and lysosomal degradation: an essential role for LRP1*. *J Cell Sci*, 2007. **120**(Pt 18): p. 3188-99.
28. Nejadmoghaddam, M.R., et al., *Placenta-specific1 (PLAC1) is a potential target for antibody-drug conjugate-based prostate cancer immunotherapy*. *Sci Rep*, 2017. **7**(1): p. 13373.
29. Perez, H.L., et al., *Antibody-drug conjugates: current status and future directions*. *Drug Discov Today*, 2014. **19**(7): p. 869-81.
30. Sommerfeld, S. and J. Strube, *Challenges in biotechnology production—generic processes and process optimization for monoclonal antibodies*. *Chemical Engineering and Processing: Process Intensification*, 2005. **44**(10): p. 1123-1137.
31. Yang, J.D., et al., *Fed-batch bioreactor process scale-up from 3-L to 2,500-L scale for monoclonal antibody production from cell culture*. *Biotechnol Bioeng*, 2007. **98**(1): p. 141-54.

32. Shen, B.Q., et al., *Conjugation site modulates the in vivo stability and therapeutic activity of antibody-drug conjugates*. Nat Biotechnol, 2012. **30**(2): p. 184-9.
33. Debaene, F., et al., *Innovative native MS methodologies for antibody drug conjugate characterization: High resolution native MS and IM-MS for average DAR and DAR distribution assessment*. Anal Chem, 2014. **86**(21): p. 10674-83.
34. Lyon, R.P., et al., *Reducing hydrophobicity of homogeneous antibody-drug conjugates improves pharmacokinetics and therapeutic index*. Nat Biotechnol, 2015. **33**(7): p. 733-5.
35. Junutula, J.R., et al., *Site-specific conjugation of a cytotoxic drug to an antibody improves the therapeutic index*. Nat Biotechnol, 2008. **26**(8): p. 925-32.
36. Junutula, J.R., et al., *Rapid identification of reactive cysteine residues for site-specific labeling of antibody-Fabs*. J Immunol Methods, 2008. **332**(1-2): p. 41-52.
37. Hofer, T., et al., *Molecularly defined antibody conjugation through a selenocysteine interface*. Biochemistry, 2009. **48**(50): p. 12047-57.
38. Jeger, S., et al., *Site-specific and stoichiometric modification of antibodies by bacterial transglutaminase*. Angew Chem Int Ed Engl, 2010. **49**(51): p. 9995-7.
39. Boeggeman, E., et al., *Site Specific Conjugation of Fluoroprobes to the Remodeled Fc N-Glycans of Monoclonal Antibodies Using Mutant Glycosyltransferases: Application for Cell Surface Antigen Detection*. Bioconjugate Chem, 2009. **20**(6): p. 1228-1236.

40. Nunes, J.P., et al., *Functional native disulfide bridging enables delivery of a potent, stable and targeted antibody-drug conjugate (ADC)*. Chem Commun (Camb), 2015. **51**(53): p. 10624-7.
41. Kellogg, B.A., et al., *Disulfide-linked antibody-maytansinoid conjugates: optimization of in vivo activity by varying the steric hindrance at carbon atoms adjacent to the disulfide linkage*. Bioconjug Chem, 2011. **22**(4): p. 717-27.
42. Oflazoglu, E., et al., *Combination of the anti-CD30-auristatin-E antibody-drug conjugate (SGN-35) with chemotherapy improves antitumour activity in Hodgkin lymphoma*. Br J Haematol, 2008. **142**(1): p. 69-73.
43. Bryant, P., et al., *In Vitro and In Vivo Evaluation of Cysteine Rebridged Trastuzumab-MMAE Antibody Drug Conjugates with Defined Drug-to-Antibody Ratios*. Mol Pharm, 2015. **12**(6): p. 1872-9.
44. Sun, M.M., et al., *Reduction-alkylation strategies for the modification of specific monoclonal antibody disulfides*. Bioconjug Chem, 2005. **16**(5): p. 1282-90.
45. Badescu, G., et al., *Bridging disulfides for stable and defined antibody drug conjugates*. Bioconjug Chem, 2014. **25**(6): p. 1124-36.
46. Junutula, J.R., et al., *Engineered thio-trastuzumab-DMI conjugate with an improved therapeutic index to target human epidermal growth factor receptor 2-positive breast cancer*. Clin Cancer Res, 2010. **16**(19): p. 4769-78.

**Table 1** Summary of fed-batch cell culture in bioreactor

<b>Cell culture</b>	<b>Shaker flask</b>	<b>Bioreactor</b>
$\mu$ ( $\text{h}^{-1}$ )	0.028 $\pm$ 0.002	0.033 $\pm$ 0.001
VCD <sub>Max</sub> ( $\times 10^6$ cells/mL)	14.26 $\pm$ 0.63	18.12 $\pm$ 0.48
mAb <sub>Max</sub> (mg/L)	1278.2 $\pm$ 62.5	2335.2 $\pm$ 56.3
qmAb (pg/cell/day)	19.60 $\pm$ 0.55	30.00 $\pm$ 2.14
qGlucose (pg/cell/day)	-137.65 $\pm$ 2.19	-162.90 $\pm$ 5.80

**Table 2** Summary of ADC cytotoxicity assay

<b>Toxicity</b>	<b>DM1-ADC</b>		<b>MMAE-ADC</b>	
	This Study a*	Literature <sup>*</sup>	This study a*	Literature
<b>IC<sub>50</sub> (nM)</b>	3.88	2.71-4.26 <sup>a</sup> and 0.24 <sup>b</sup> [25], 4.7 <sup>a</sup> [43]	1.95	2.7-13.8 <sup>c**</sup> [44], 0.60 <sup>a**</sup> [45]
<b>Viability (%)</b>	<10	50-60 <sup>a</sup> and 30-35 <sup>b</sup> [25], 40 <sup>b</sup> [46]	<10	5-15 <sup>c**</sup> [19], 25 <sup>a**</sup> [45]

**Note:** Cell lines: <sup>a</sup>BT474, <sup>b</sup>SK-BR-3, and <sup>c</sup>Karpas 299; assay timeline: \*3 days and \*\*4

days.

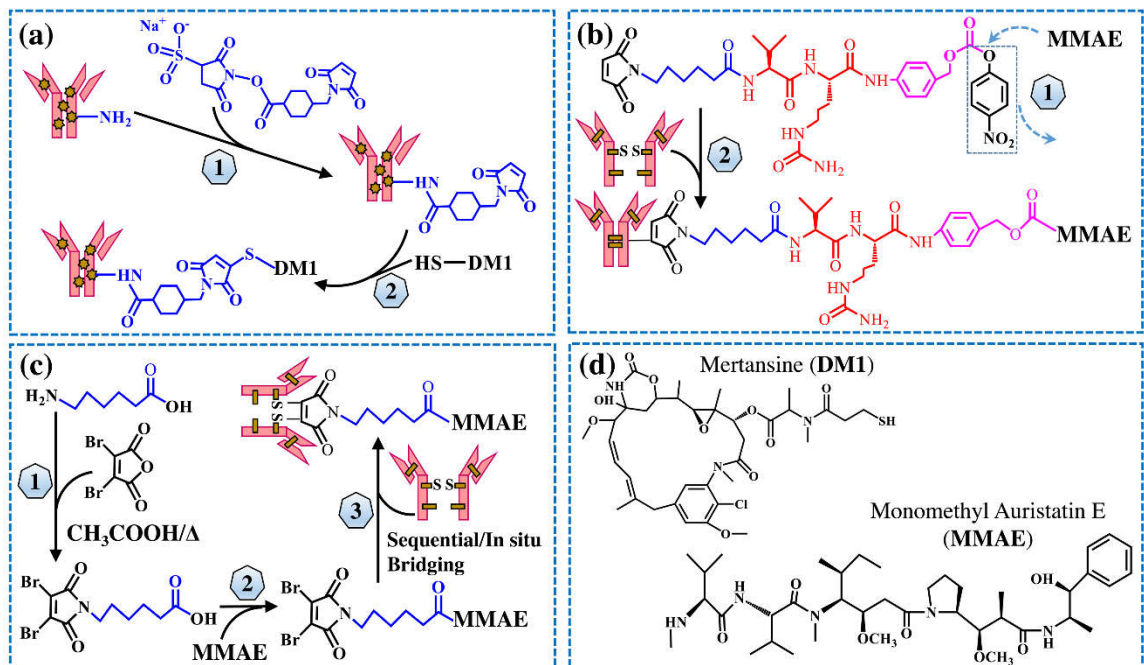


**Figure 1.** The diagram of ADC construction. **(a)** Lysine-based conjugation of mAb-DM1: 1) mAb modification by cross linker Sulfo-SMCC, and 2) conjugation of DM1 with the purified mAb-SMCC. **(b)** Cysteine-based conjugation of mAb-MMAE using traditional linker: 1) synthesis of Mc-Val-Cit-PABC-PNP linker-MMAE payload, and 2) conjugation of payload with the DTT/TCEP reduced mAb. **(c)** Cysteine-based conjugation of mAb-MMAE using rebridging linker: 1) synthesis of rebridging linker, 2) synthesis of rebridging linker-MMAE payload, and 3) conjugation of payload with the DTT/TCEP reduced mAb. **(d)** Structures of free drugs MMAE and DM1.

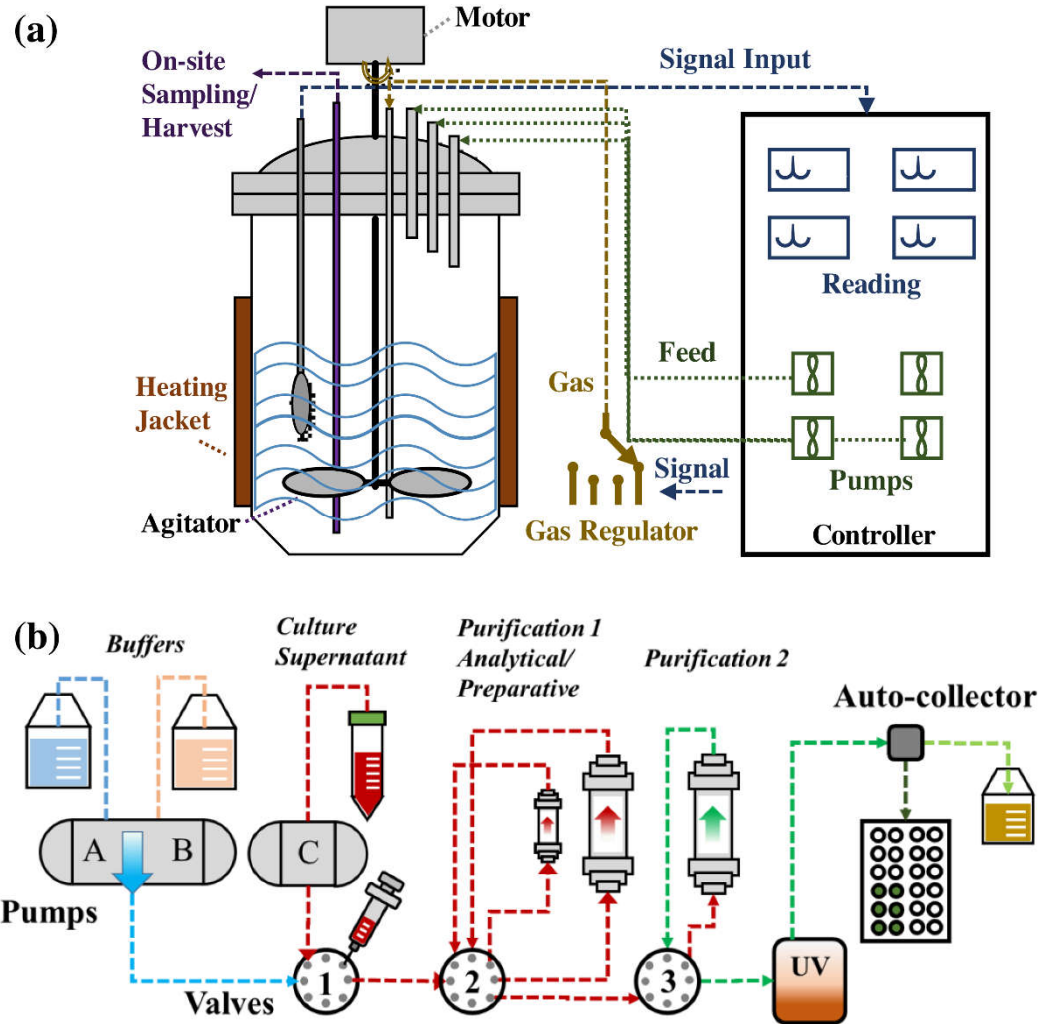


**Figure 2.** Anti-HER2 mAb production and purification. (a) Fed-batch production in stirred-tank bioreactor. (b) The purification process of mAb.

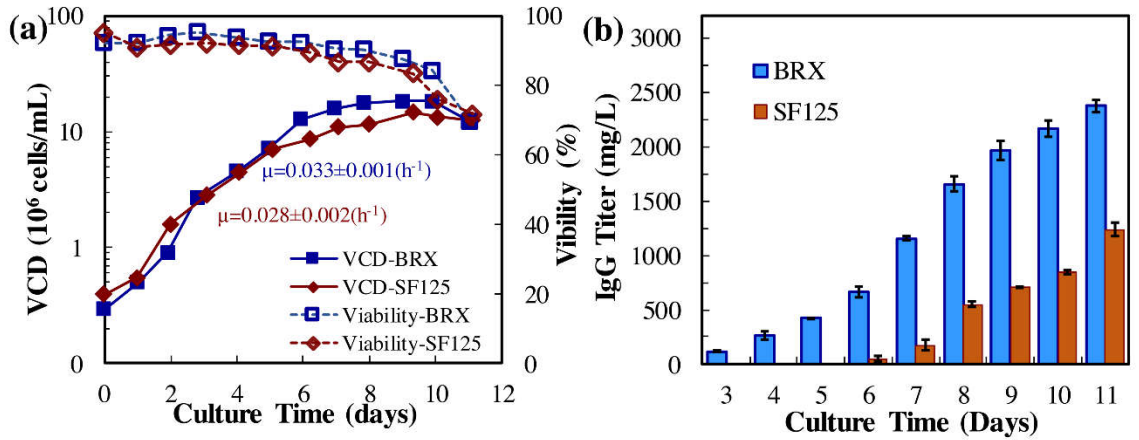


**Figure 3.** Anti-HER2 mAb production in fed-batch cell culture. (a) CHO/IgG (anti-HER2 mAb) cell growth in shaker flask (SF125) and 2-L stirred-tank bioreactor (BRX).  $\blacklozenge/\blacklozenge$ : SF125 with working volume of 30 mL, Temp 37 °C, agitation 130 rpm, and CO<sub>2</sub> 5%.  $\blacksquare/\blacksquare$ : BRX with working volume of 1 liter, Temp 37 °C, agitation 70 rpm, and DO 70%. (b) Anti-HER2 mAb production.

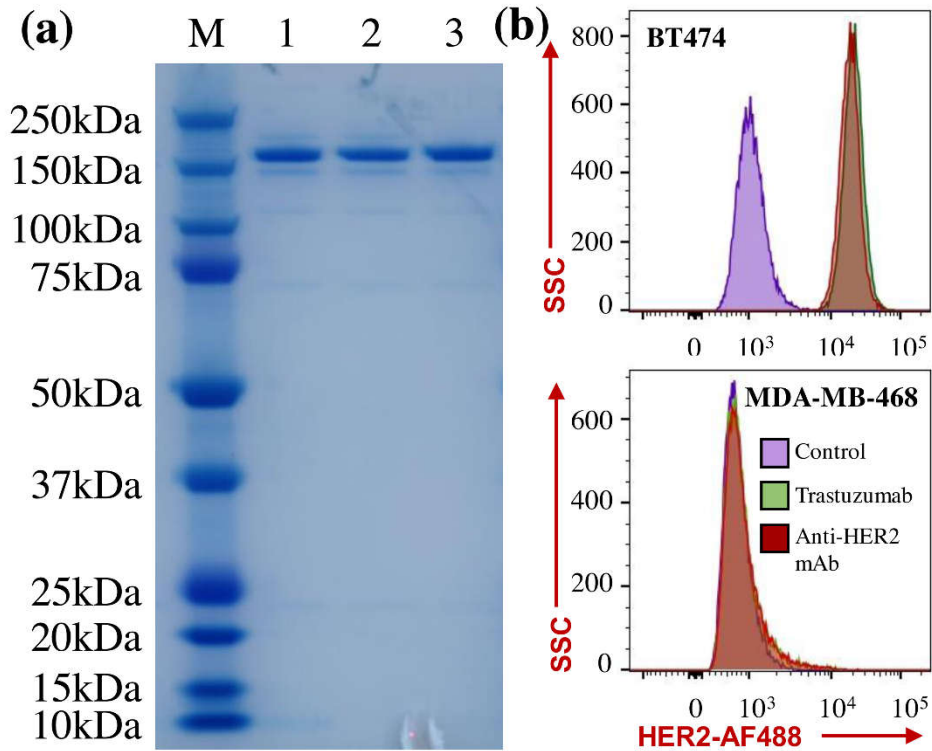


**Figure 4.** Evaluation of mAb purity and surface binding to HER2 receptor. **(a)** SDS-PAGE gel. M: marker, 1: anti-HER2 mAb purified by small-scale protein A purification kit, 2: anti-HER2 mAb purified by large-scale NGC system, 3: FDA approved Trastuzumab. Protein samples were loaded with 1  $\mu\text{g}$ /well. **(b)** Flow cytometry analysis of receptor binding of purified anti-HER2 mAb and Trastuzumab to HER2<sup>+</sup> BT474 cell line and negative control MDA-MB-468 cell line. Staining conditions: Alexa Fluor (AF) 488-labeled mAb was incubated with cells at 1  $\mu\text{g}$ /million cells on ice for 30 min.

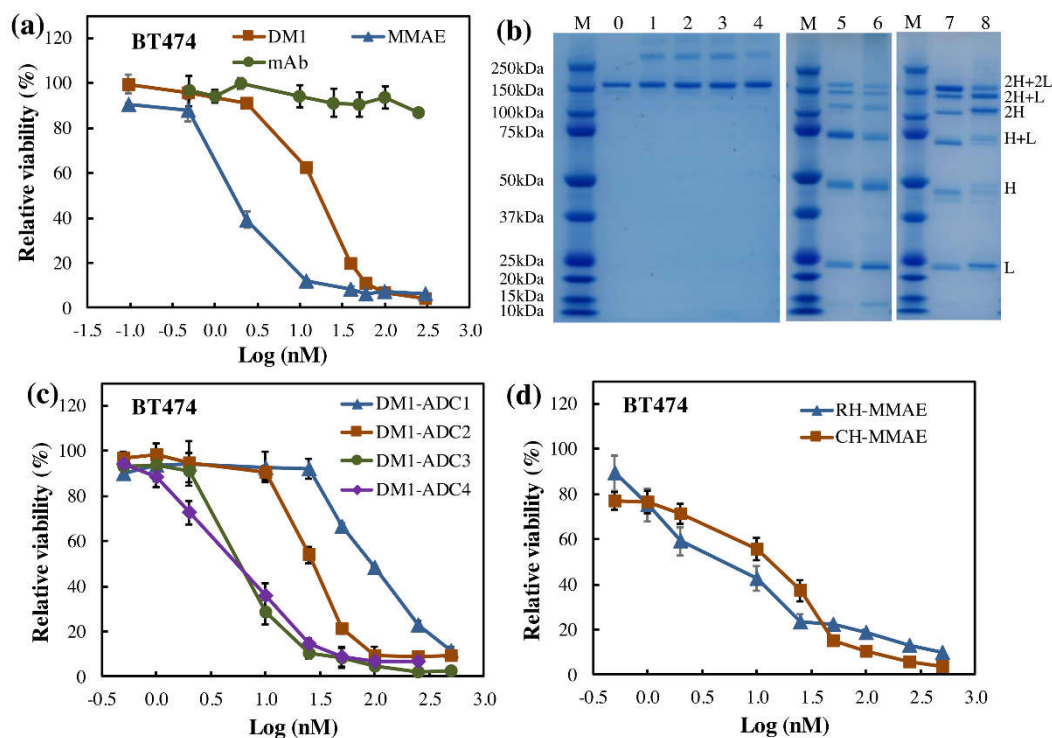


**Figure 5.** Evaluation of ADCs constructed in different production processes. **(a)** Anti-cancer toxicity of free drugs. ▲ MMAE, ■ DM1, ● mAb. **(b)** SDS-PAGE of ADCs. M: marker, 0: purified mAb, 1-4: lysine-based DM1-carrying ADCs (named as DM1-ADC1-4) with drug:linker:mAb ratio of 4:4:1, 8:4:1, 8:4:1, and 16:8:1, respectively. DM1-ADC1 and ADC2 were purified using G25 column, and DM1-ADC3 and ADC4 were purified using protein A column. 5-8: Cysteine-based ADCs. 5: ADC from sequential conjugation with rebridging linker. 6: ADC from sequential conjugation with traditional linker. 7: ADC from *in situ* conjugation with rebridging linker (named as MMAE-ADC1). 8: ADC from *in situ* conjugation with traditional linker (named as MMAE-ADC2). ADC samples were loaded to SDS-PAGE gel with 2  $\mu$ g/well. **(c)** Anti-cancer toxicity of lysine-based anti-HER2 mAb-DM1 ADCs. ▲ DM1-ADC1, ■ DM1-ADC2, ● DM1-ADC3, ◆ DM1-ADC4. **(d)** Anti-cancer toxicity of anti-HER2 mAb-MMAE ADCs. ▲ MMAE-ADC1, ■ MMAE-ADC2.

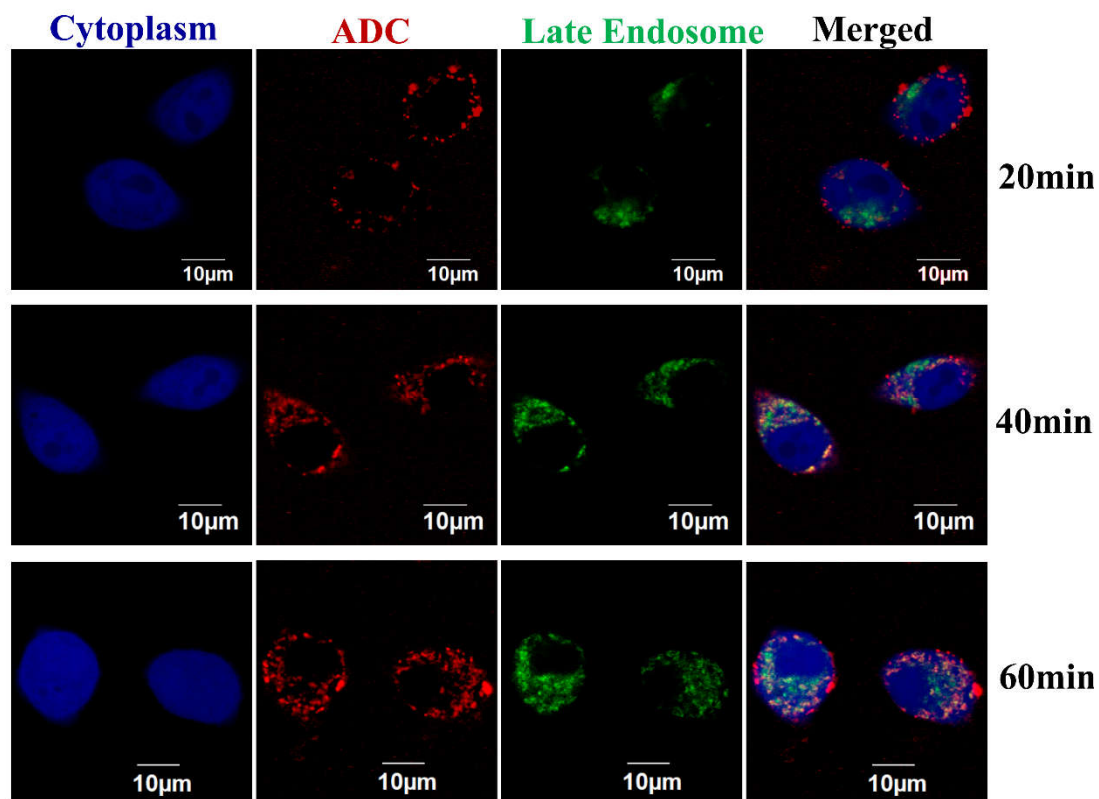


**Figure 6.** Surface binding and internalization process of ADC by confocal laser scanning microscopy. The BT474 cells were transduced with BacMam 2.0 CellLight Late Endosomes-RFP and BacMam GFP Transduction Control to stain late endosomes (green) and cytoplasm (blue), respectively. The DM1-ADC4 (red) was labeled with Alexa Fluor 647 and stained cells at 2  $\mu\text{g}/\text{mL}$  in PBS buffer containing 10% inactivated goat serum and 1% BSA. The cytoplasm, late endosome, and ADC were excited by lasers with wavelength of 488 nm, 543 nm, and 633 nm.

CHAPTER 4

HIGH QUALITY HUMAN T CELL BIOMANUFACTURING IN STIRRED-TANK  
BIOREACTOR

by

JIANFA OU, XIAOGUANG (MARGARET) LIU

In preparation

Format adapted for dissertation

## **Abstract**

As T cell therapy grows, a robust biomanufacturing protocol is urgently needed for high quality human T cell production. In this study, a protocol was established to grow T cells in a stirred tank bioreactor with control of pH, temperature, and dissolved oxygen. PBMC was isolated from fresh human blood. The CD4<sup>+</sup> and CD8<sup>+</sup> T cells were purified and stimulated by anti-CD3/anti-CD28 beads in a suspension system. After 4 days' activation, beads were removed and cells were seeded in 40mL to 2L bioreactor systems for large scale culture. After 4 days' culture, the high-quality cells can be 1) harvested for treatment/research, 2) re-stimulated for further scale-up, and 3) frozen and used at the right time. Cell type, activation signal, inhibitory signal, memory type, and cytokine production were monitored by flow cytometry to ensure high cell quality. This system had high consistency and robustness among patients. Our method will facilitate novel T cell therapy development.

**Keywords:** Human T cell; manufacturing; stirred tank bioreactor; large scale culture

## 1 Introduction

Adoptive T cell therapies have found significant applications in viral-associated disease, reduced leukocytes caused by chemotherapy and irradiation therapy, and direct cancer treatment. T cells can obtain the ability to target cancers by either tumor-infiltrating, or by being genetically engineered to express chimeric antigen receptors (CAR) that are specifically expressed by tumors. As an emerging technique, CAR T-cell therapy has successfully treated patients with adult B-cell non-Hodgkin's lymphoma and childhood acute lymphoblastic leukemia [1-3]. More targets are under evaluation for novel CAR T-cell therapy development [4].

Prior to adoptive transfer for T cell cancer therapy, an efficient *in vitro* expansion is needed to achieve sufficient cell numbers. There are currently limits to the quality and quantity of CAR-T cells that we are able to produce. Only small batches of CAR-T cells can be cultivated at one time using static flasks and spinner-based bioreactor systems. Even smaller is the amount of viable CAR-T cells once the production process is completed. Due to the limited amount of blood that can be obtained from a patient, one major challenge of the therapy is the expansion of T cells using a cGMP-compliant culture system. The classic static culture method, including the usage of flasks or gas-permeable bags, relies on oxygen diffusion [5]. It requires a large working volume and a large number of flasks to generate billions of T cells, as cell productivity is limited by the flask area. Thus, this method requires intense work load for culture manipulation. Additionally, the culture parameters including pH, temperature, and dissolved oxygen are hard to control. The low efficiency and large variation causes hurdles for developing the T cell therapy. Moreover, personalized autologous cell manufacturing encounters different challenges compared to

the cell line manufacturing. For example, the accommodation of multiple parallel productions is critical for the therapy to be commercialized. Regardless of our significant knowledge in conventional cell manufacturing and bioreactor design, the fundamental difference of T cell cultures with other products makes it difficult to be applied directly. Considering the natural suspension status of T cells, the alternative strategies to static culture have been extensively discussed. Scalable bioreactor with enough parameter control is a solution for this challenge. Besides, the operational flexibility of bioreactor gives it the potential to deal with various clinical applications [6, 7].

Multiple expansion devices have been manufactured based on permeable membrane, such as the GE WAVE bioreactor [8, 9] and G-Rex bioreactor [10], to allow perfusion culture. The expansion of 100-fold in batch culture was reported using the G-Rex system [11]. A study of pentaviral-specific T cells was reported using culture vessel with gas-permeable membrane at the bottom [12]. The GE WAVE platform was used to manufacture T cell to support clinical trials [13]. It uses a rocking platform to induce waves to medium and provide oxygen to support cell growth. With the combination of a perfusion system, a cell density of  $10 \times 10^6$  cells/mL was reported [1, 14, 15]. But the continuous medium raises the cost and the facility requirement. Additionally, Miltenyi CliniMACS Prodigy system has shown its potential for T cell expansion after its successful isolation and culture of NK cells. It combines cell washing, magnetic cell separation, and cell cultivation [16, 17]. However, the current platforms rely on intensive labor, which raises risks in quality control. The scale up process is a big challenge as the change of batch size significantly affects the homogeneity of oxygen and nutrients, as well as the shear-stress profile. Careful optimization of monitor, control, and operation, is desired when applying

the stirred tank culture on a cell type in order to keep the cell properties unchanged [18]. A more robust system is urgently needed. Stirred tank bioreactor has been widely used in biopharmaceutical manufacturing [19]. Nevertheless, there are limited reports about its application in T cell manufacturing. Its value is severely underestimated.

In the present study, we developed a protocol to grow T cells in a stirred tank bioreactor with controlled pH, temperature, and dissolved oxygen. Our process also optimized the materials and timing for T cell stimulation. Stimulation reagent was removed before the proliferation. Application of simplified T cell expansion method will accelerate the dissemination of T cell cancer treatment, and provide patients more convenience to use the efficient treatment. With an efficient expansion system based on homogeneous mixing, automation will be more readily practical, and makes the manufacturing easy to be compiled with cGMP. Our protocol contributes to an important step to a well-controlled and cost-efficient manufacturing process.

## **2 Materials and Methods**

### *2.1 Materials*

All basal media, supplements and reagents used in this study were purchased from Thermo Fisher Scientific (Waltham, MA) unless otherwise specified.

### *2.2 T cell isolation*

Peripheral blood mononuclear cells (PBMCs) were provided by StemExpress (Folsom, CA) collecting from healthy donors under written informed consent. CD4<sup>+</sup> and CD8<sup>+</sup> T cells were isolated using Dynabeads® CD4 and CD8 positive isolation kit

following the instructions, respectively. Generally, the PBMC were washed with buffer 1 (Ca<sup>2+</sup> and Mg<sup>2+</sup> free PBS, 0.1% BSA, 2mM EDTA, pH 7.4). PBMC were incubated with isolation beads on ice for 20 min with gentle mixing. CD4<sup>+</sup> and CD8<sup>+</sup> T cells were captured by magnetic beads. While held on a magnet, the supernatant was removed and the bead and cell complex were washed with buffer 1 twice. The bead and cell complex was treated by detach reagent for 45 min at room temperature. The magnetic beads were removed with the magnet. The released T cells were washed with culture medium twice.

### *2.3 T cell stimulation and cell culture*

CD4<sup>+</sup> and CD8<sup>+</sup> T cells were seeded at 0.5x10<sup>6</sup>/mL in T flask or shake flask. Two types of activation reagents were used. 1) Dynabeads® Human T-Activator CD3/CD28 beads (Thermo Fisher Scientific) were added to the culture at cell:bead ratio 1:1. Magnetic beads were removed by a magnet after 4 days' activation. 2) ImmunoCult™ Human CD3/CD28 T Cell Activator (Stemcell Technologies, Vancouver, Canada) was added at 25 µL/mL culture on Day 0. Three types of media were used for evaluation: AIM-V Medium CTS (Thermo Fisher Scientific), OpTmizer CTS (Thermo Fisher Scientific), and ImmunoCult-XF T Cell expansion medium (Stemcell Technologies). Activation and cell culture were supplemented with 30IU/mL IL-2 unless otherwise specified. The bioreactor production process parameters were controlled at 37 °C, pH 7.4, DO 70% and agitation 70 rpm. Shake flasks were maintained at 37 °C, 5% CO<sub>2</sub> and shaking frequency 125 rpm. Spinner flasks were maintained at 37 °C, 5% CO<sub>2</sub> and agitation 50 rpm. The pH of T flasks, shake flasks and spinner flasks were adjusted to 7.4 once a day with 0.5M Na<sub>2</sub>CO<sub>3</sub>. The

bioreactor, shake flask, and spinner flask were sampled daily to monitor cell growth. The VCD and viability were measured by cell counter (Thermo Fisher Scientific).

#### *2.4 Flow Cytometry Analysis*

The following conjugated antibodies were purchased from BioLegend (San Diego, CA): anti-CD8a (FITC), anti-CD45RO (PerCP-Cy5.5), anti-PD-1 (PE), anti-CCR7 (PE-Cy7), anti-CD27 (APC), anti-CD4 (APC-Cy7), anti-CD45RA (BV510), anti-CD223 (PerCP-Cy5.5), anti-CD3 (PE), anti-KLRG1 (PE-Cy7), anti-CD278 (APC), anti-CD4 (APC-Cy7), anti-CD134 (BV510), anti-IFN- $\gamma$  (FITC), anti-IL-2 (PE), anti-IL-4 (APC). For surface staining, cells were harvested and washed with staining buffer (PBS, 1% BSA) at 400g for 7 min, and treated with Fc Receptor Blocking Solution (Biolegend 1 $\mu$ L/1x10<sup>6</sup> cells) at 4°C for 15 min. Cells were then stained with antibodies and LIVE/DEAD Blue Dead Cell Stain (Thermo Fisher Scientific) at 4°C for 30 min. Cells were washed with staining buffer twice before analysis. Supplies for intra-cellular staining were purchased from BioLegend. Activation Cocktail was added to cell culture and incubated for 2h. Monensin was then added and incubated for 4 h. Cells were harvested, washed with PBS once, and resuspended in fixation solution (500  $\mu$ L/1x10<sup>6</sup> cells). After incubating in dark for 20 min at 4 °C, cells were washed with Intracellular Staining Perm Wash Buffer five times. Anti-IFN- $\gamma$ , anti-IL-2, and anti-IL-4 antibodies were used for staining at 37°C for 30 min. Finally, cells were washed with Intracellular Staining Perm Wash Buffer twice and resuspended in staining buffer for analysis.

### **3 Results**

#### *3.1 Efficient T cell biomanufacturing in stirred-tank bioreactor*

Figure 1 gave an overview of the process design with the key control factors. The manufacturing process contained the PBMC isolation from patient, which was followed by the magnetic bead-based CD4<sup>+</sup> or CD8<sup>+</sup> T cells isolation. The purified T cells were stimulated with magnetic beads coated with anti-CD3 mAb/anti-CD28 mAb. After 4 days, the beads were removed and the stimulated cells were transferred to a seeding bottle connected to the stirred-tank bioreactor. In the closed system, the temperature, pH, dissolved oxygen (DO), and agitation, closed system were controlled automatically. Samples were taken from the on-site sampling port to monitor cell number and cell quality. Cells were harvested at the maximum VCD and formulated for infusion. The bioreactor was open for the optional second stimulated cell culture.

#### *3.2 Medium and feeding optimization*

There are multiple marketed media for T cell culture in static mode. It is important to evaluate their performance in the well mixed system. The seeding culture was scaled up in the AIM-V medium for 3 days in T75 after removing the stimulation magnetic beads. Then the CD4<sup>+</sup> T cells were seeded in different medium to evaluate the growth (Figure 2A). The media was supplemented with 30IU/mL IL-2 on day 0. The OpTmizer and ImmunoCult media had similar VCD<sub>max</sub> at 2.83x10<sup>6</sup> cells/mL and 3.48 x10<sup>6</sup> cells/mL, which were 50% higher than that of the AIM-V medium (Table 1). Though the OpTmizer medium showed slower growth rate compared to the ImmunoCult medium, it maintained

high viability of 80% on day 6, while the others had dropped to 59.0% and 45.8%. Therefore, the OpTmizer medium was used in the rest of the study.

Feeding is an important factor in various cell cultures. IL-2 at 30IU/mL or higher was essential to maintain the cell grow and viability (Figure 2B), consistent with previous reports [20]. Even though the T cell can produce IL-2 with the stimulatory signal, the autocrine reduced as the cell grew, resulting in the need for recombinant human IL-2 supplement to maintain proliferation[21]. Neither non-essential amino acid or essential amino acid helped the cell growth. We noticed significant cell growth (5 fold) during the seeding culture scale-up process, though there was only 3-fold growth from day 0 to day 4. The stimulation strategy and scaled up process seemed to be more impactful for efficient cell growth.

### *3.3 Seeding time and stimulation on T cell growth*

A general time schedule is shown in Figure 3a. The T cells were isolated and stimulated on day -4, and cells were harvested on day 0 for directed bioreactor seeding or scale-up before seeding. Figure 3b showed the growth with seeding culture with 0 day, 2 days, and 5 days' scale up. The seeding culture from day 0 showed the highest VCDmax at  $8.33 \times 10^6$  cells/mL with viability of 93.0%. The culture with 2 days' additional scale-up had VCDmax at  $1.89 \times 10^6$  cells/mL, while the culture after 4 days' scale up lost all growth potential. It indicated that Day 4 was a right time for restimulation. A very fast cell growth with doubling time  $13.0 \pm 0.2$  h was observed (Table 1); it was consistent with the in vivo studies that T cells can divide multiple times a day [22, 23]. Figure 3c showed that second stimulation led to lower VCDmax at  $3.98 \times 10^6$  cells/mL, compared to the first stimulation

with VCD<sub>max</sub> at 8.33x10<sup>6</sup> cells/mL. It was probably caused by the loss of CD28 on T cell membranes, resulting in a weaker stimulation signal each turn [21]. Regardless of the possible multiple restimulations, our strategy combining the first two stimulations can proliferate T cells for >500,000 folds.

We compared two forms of stimulation reagents, e.g. anti-CD3 and anti-CD28 antibodies coated on magnetic beads and the same antibodies in a soluble tetramer form. As shown in Figure 3d, T cells received the signal from both methods during the first two days, and had the fastest growth rate between Day -2 to Day 0. On Day 4, the soluble tetramer anti-CD3/anti-CD28 led to lower proliferation (9 folds) compared to the bead bound antibodies (90 folds). The proper spatial effect was critical to delivering a strong CD3/CD28 signal simultaneously [24, 25]. Additionally, the soluble antibodies lost the effect on Day 2, indicating that anti-CD3 and anti-CD28 antibodies lost the function due to prolonged exposure to the culture [26]. Therefore, removing these antibodies before biomanufacturing can improve the product purity without losing the activation effect.

### *3.4 Robust process scale-up*

The T cell proliferation was evaluated in containers with different working volume, e.g. 10mL (T flask), 30mL (shake flask), and 80mL (spinner). Shown in Figure 4a, they had similar VCD<sub>max</sub> at 3.65-4.05x10<sup>6</sup> cells/mL, whereas their viabilities were 52%, 80%, and 83%, respectively. The gentle mixing in the spinner prolonged T cell survival. Same as acute immune response, cell death happened after quick expansion without a stationary phase. A large scale culture was established in a 2L stirred tank bioreactor using the first stimulated CD4<sup>+</sup> T cell. With the automatic pH and DO control, the stirred tank bioreactor

had VCDmax at  $6.40 \times 10^6$  cells/mL, which was 60% higher than the spinner culture ( $3.98 \times 10^6$  cells/mL). In addition to high viability, the cell purity was confirmed by the high percentage of  $CD3^+CD4^+$  or  $CD3^+CD8^+$  T cells after proliferation (Table 2). We have applied this strategy on T cells from five donors. The total cell number was increased by 132 to 1011 folds after the 1st stimulation (Figure 5).

To evaluate the  $CD4^+$  and  $CD8^+$  T cell collaboration, we seeded them with ratio 2:1 on Day 0 in the spinner suspension system. Shown in Figure 6, the ratio was 1.5:1 on Day 2 and remained the same on Day 4, with total VCDmax  $4.38 \times 10^6$  cells/mL. The  $CD4^+$  and  $CD8^+$  T cell single cultures were seeded at  $0.4\text{-}0.5 \times 10^6$  cells/mL, respectively. They reached  $2.8\text{-}2.9 \times 10^6$  cells/mL on Day 2 with the same growth rate. The  $CD8^+$  T cell then stopped growing. It indicated that  $CD4^+$  T cells can boost the growth and maintained the activation signal of  $CD8^+$  T cell. The collaboration of  $CD4^+$  and  $CD8^+$  T cell could be used to improve the manufacturing process.

### *3.5 Proliferation status and cell quality evaluation by surface protein*

*T cell activation signal* The effector T cells, effector memory T cells, and central memory T cells were proliferated with the signal controlled by the CD3/T cell receptor (TCR) and CD28 receptor (Figure 7a). T cells respond to anti-CD3 resembles to the antigen activation, while anti-CD28 provided an essential expansion signal by promoting the lymphocyte survival [27, 28]. The method can maintain the variety of polyclonal antigen-primed T cells as a cell pool, which was confirmed by inducible cytokine secretion later. It was optional to stimulate them with the peptide [26], antigen-presenting cells (APCs) [29], or genetic engineering [30], to generate antigen specific T cells for adoptive T cell therapy

or CAR-T cancer therapy. We observed that the T cell size was positively related to its proliferation potential, while the maximum size was observed on Day 0 and decreased gradually over the course of 4 days, consistent with previous study[21]. Programmed cell death protein 1 (PD-1) was linked to cell cycle control [31] and upregulated upon TCR activation by antigen stimulation or by the CD3 bypass [32-34]. Its expression level is related to the strength of TCR signaling (Figure 7c) [35]. The high level PD-1 (>90%) on Day 0 indicated that the T cells were sufficiently activated after 4 days' stimulation. On Day 4, PD-1 decreased to <15% when the T cell proliferation stopped, similar to the initial status where PD-1 expression is low or moderate in healthy humans [36]. The restimulated cells on Day 8 had lower PD-1 than Day 0, which indicated the need for stronger or longer restimulation signal. Costimulatory signaling receptor ICOS was significantly elevated to >99% after the CD3/CD28 stimulation and maintained at high levels during the expansion. At the same time, the OX40 and CD27 signaling receptors, which both belonged to TNF receptors nerve growth factor receptor (TNFRSF), had little or no change during the expansion. This was consistent with previous reports [27, 37, 38]. The high level of inducible T cell costimulator (ICOS) molecule was proven beneficial to immunotherapy [39].

*T cell inhibition signal* The expression of lymphocyte activation gene 3 protein (LAG-3), an inhibitory receptor related to T cell exhaustion [40] and releasing suppressive signal [27], decreased from >95% (Day -4) to 23.3±11.9% and 61.6±15.8% (Day 0) after stimulation on CD4<sup>+</sup> and CD8<sup>+</sup> T cells, respectively, and rested at <10% (Day 4). Additionally, the expression of killer cell lectin-like receptor subfamily G member 1 (KLRG1), a phenotypic marker related to exhausted T cells [40] and impaired T cell

antitumor effect [41], was very low before and after the expansion, consistent with previous publications [42, 43]. It indicated a low inhibitory signal [44].

*Memory T cell/naïve T cell* The memory T cell/naïve T cell ratio was expected to vary significantly among donors of different ages and health condition[45], and we noticed the large variation of CD45RO<sup>+</sup> T cells before stimulation (Table 2). All T cells adopted a memory phenotype after activation with a CD45RA<sup>+</sup>LowCD45RO<sup>+</sup>High population because the naïve cell had no or weak growth [46], due to the lack of additional antigen stimulation and certain cytokines such as IL-4, IL-7, and IL-15 [47]. There was a slight decrease from Day 0 to Day 4 of CCR7<sup>+</sup> population, which was a marker of central memory cells [48], while the CD45RO<sup>+</sup> was >90% all the time, probably because the effector memory T cells grew faster under the bioreactor condition after removing the stimulation signal [49, 50]. Besides, the central memory T cell can differentiate to effector memory T cells [51, 52].

In summary, the T cells were functional after expansion based on the surface protein analysis.

### 3.6 Cell function evaluation by cytokine production

We measured the intracellular cytokine production by the expanded T cells after a short time stimulation with PMA and monensin. Generally, the expanded T cells were functional as they were able to produce IFN- $\gamma$ , IL-2, and IL-4 cytokines after stimulating with PMA and monensin.

CD4<sup>+</sup> T cells In addition to cell surface molecules, cytokine secretion is a widely accepted paradigm to distinguish T cell subsets [53]. CD4<sup>+</sup> T-helper cells were divided into two major groups, namely T-helper type 1 (Th1) and T-helper type 2 (Th2) cells. IFN-

$\gamma$  was the signature cytokine generated by Th1 to activate the macrophage function, whereas IL-4 was a signature cytokine of Th2 associated with strong antibody response [54, 55]. Both Th1 and Th2 can produce IL-2 [53]. Shown in Table 3, there were 61.8%, 95.6%, and 38.2% CD4<sup>+</sup> T cells producing IFN- $\gamma$ , IL-2, and IL-4 after the 4 days' stimulation, whereas the number was 54.2%, 76.4%, and 6.5% before stimulation. Therefore, there were more Th1 after the biomanufacturing, the same as the unstimulated population. There was a high IL-2<sup>+</sup> population, because the expression level of IFN- $\gamma$  and IL-4 T cells were generally lower than IL-2. Th1 cells were critical to eliminate intracellular organisms, such as viral pathogens [56], and cancer cells [57], while Th2 played an important role against parasitic infections [58].

CD8<sup>+</sup> T cells The CD8<sup>+</sup> T cell mostly produced IFN- $\gamma$  and IL-2 cytokines (Tc1 subset) (Table 3), consistent with the previous reports about its similarity to Th1 CD4<sup>+</sup> T cell [55, 59]. IFN- $\gamma$  is directly related to the CD8<sup>+</sup> T cells cytotoxic function against tumors and viruses [60]. It can promote CD8<sup>+</sup> T-cell motility and enhances target killing [60]. Its high expression ratio (50.1%) in this study indicated that CD8<sup>+</sup> remained cytotoxic after expansion. The temporary increase on Day 0 may be caused by the TCR activation. Memory CD8<sup>+</sup> T cell is a major source of IFN- $\gamma$  [61]. The CD8<sup>+</sup> T cell function was further supported by high expression of IL-2, which was related to the antigen response ability [62], and induced proinflammatory cytokine secretion, such as IL-6, IL-1b, IFN- $\gamma$ , and TNF- $\alpha$  [20]. We also found a small percentage of CD8<sup>+</sup> T cell (Tc2 subset) producing Th2 cytokine IL-4, same as previous reports [63, 64]. The Tc2 was important for CD8<sup>+</sup> cell function, as it helped for IgM and IgG synthesis by B cells, regardless of its lower cytotoxicity [55].

## 4 Discussion

In this study, we successfully developed a scalable manufacturing process for CD4<sup>+</sup> and CD8<sup>+</sup> human T cells. The medium and stimulation strategy were optimized. More than 5 billion T cells can be grown over a 4 days' culture in our stirred tank bioreactor. The proliferated T cells had good quality, confirmed by 12 surface proteins and 3 cytokines.

*Robust Biomanufacturing process development* Removing the stimulation beads before large scale culture will benefit the cost and simplify the culture process in the stirred-tank bioreactor. We notice that the cell number expanded by 5-10 folds from Day -4 to Day 0. Most of the expansion happened between Day -2 to Day 0, when most of the cells were no longer attached to the beads. Besides, the anti-CD3 or anti-CD28 mAb lost 90% of their binding ability in 5 days [26]. There is no need for prolonged stimulation. Repeated stimulation was used to keep the cell growing in some studies [26]. However, it should be avoided for high quality T cell culture, because the severity of T cell exhaustion, which reduced the T cell function against infections and tumors [40], is correlated to the stimulation level, i.e. antigen exposure time or amount [65]. The total process, from cell stimulation to harvest, took 8 days with consistent expansion folds. It was simpler and more efficient compared to the static culture taking 2-3 weeks for 100 fold expansion [21] and WAVE system [66, 67]. The nutrient feeding from regular cell culture had no significant effect on the T cell. Probably because the signaling for T cell growth has not yet been maximized. The cytokine IL-2 was found critical to maintain cell growth and viability during the biomanufacturing process, as it regulated the T cell survival, proliferation, and differentiation [39]. The addition of cytokines can be optimized in the next step.

*CD4<sup>+</sup> and CD8<sup>+</sup> T cell collaboration* Functional CD4<sup>+</sup> T cell was proved to be important for the CD8<sup>+</sup> T cell cytotoxicity [68, 69]. The presence of CD4<sup>+</sup> T cell was important for the initial priming and secondary response of CD8<sup>+</sup> T cells to the antigen [70, 71]. As we describe above, the change of surface markers PD-1 and LAG-3 indicated decreased activation signal during the culture. On Day 2, the PD-1<sup>+</sup> percentages of CD4<sup>+</sup> and CD8<sup>+</sup> T cells were 11.3±2.6% and 11.1±3.6%, while the corresponding LAG3<sup>+</sup> percentages were 11.2±4.2% and 50.6±11.3%. The CD8<sup>+</sup> T cell proliferation signal was slightly higher in the coculture than the single culture.

*Cell quality* The function of expanded T cells was confirmed by a combination of surface and activation markers with intracellular cytokines [72]. A single protein was not enough to identify the T cell exhaustion or activation [35]. For example, PD-1 is related to the T cell exhaustion state, where the T cells lose their robustness and become inefficient in fighting disease because the use of different transcriptional programs [40]. It was successfully used to indicate the stimulation signal strength in this study with other protein markers. It is important to harvest or restimulate the T cells before apoptosis happens. Previous studies determined the need for restimulation by cell size [21]. Cell surface protein expression, such as PD-1, gave a more precise indicator to determine the proliferation status. The CD3/CD28 stimulation showed its benefit on cell function with a highly diverse TCR repertoire after the proliferation [21]. Expansion of antigen-specific T Cells can be improved by changing the anti-CD3 to anti-CD28 ratio or changing the total stimulation time, while anti-CD3 or anti-CD28 alone cannot stimulate cell expansion [26]. Differentiation of T-cell effector subsets can be skewed by the addition of cytokines in the culture. For example, IFN- $\gamma$  plus IL-12 led to Th1 cell differentiation, IL-4 helped Th2 cell

development, while IL-4 plus TGF- $\beta$  resulted in Th9 cells [58]. The differentiation of Th17 [73], Th22 [74], Tfh [75], and more were also reported. The central memory T cells showed higher anti-tumor toxicity than the effector memory T cells in vivo [76, 77]. An anti-CD3 + anti-CD28 + IL-7 + IL-15 stimulation method was reported to improve T cell specific cytotoxicity [78]. Refining the T cell to a specific phenotype, a.k.a. T cell polarization, is a cutting edge of clinical research [79], and more importantly, it is compatible with our system.

The release criteria of CAR-T product mostly includes the total cell number, cell viability ( $\geq 70\%$ ), residual bead number ( $\leq 100$  beads/ $3 \times 10^6$  cells), sterility such as bacteria, fungi, and mycoplasma, and endotoxin [80]. The criteria also include the immunophenotyping (CD3<sup>+</sup> cells  $\geq 80\%$  and CAR related phenotypes) and the unwanted autonomous growth ( $< 2 \times 10^4$  cells/mL for cells without cytokines) [81]. The in vivo soluble cytokine assessment, including IL-2, IL-7, IL-15, IL-12, TNF- $\alpha$ , and IFN- $\gamma$  [82], was often used to evaluate the CAR-T therapy [83]. Unfortunately, severe cytokine storm was reported post T infusion [82, 84], indicating the need for better quality control. It is important to develop criteria for specific T cell subsets, as the previous quality criteria focus on the cell mixture derived from PBMC.

Future direction A stimulation without targeting specific antigen was used in this study for proof of concept. In the next step, we will use this novel platform to engineer and produce CAR-T cells that target specific cancers. We used defined subpopulations of T cells, e.g. CD4<sup>+</sup> and CD8<sup>+</sup> T cells, to explore more details of cell quality. We will compare the discovery to a leukapheresis mixture, which is currently used in CAR-T cell therapy, and guide the optimization of mixture culture cell quality. We also plan to develop a closed

cell harvest system to take the manufacturing one step closer to clinical practice [[13](#)]. Some cutting edge researches, such as replacing autologous T cells with new cell sources, will also benefit T cell manufacturing [[85](#)].

## Reference

1. Wang, X. and I. Riviere, *Clinical manufacturing of CAR T cells: foundation of a promising therapy*. Mol Ther Oncolytics, 2016. **3**: p. 16015.
2. Kochenderfer, J.N., et al., *B-cell depletion and remissions of malignancy along with cytokine-associated toxicity in a clinical trial of anti-CD19 chimeric-antigen-receptor-transduced T cells*. Blood, 2012. **119**(12): p. 2709-20.
3. Rodgers, D.T., et al., *Switch-mediated activation and retargeting of CAR-T cells for B-cell malignancies*. Proc Natl Acad Sci U S A, 2016. **113**(4): p. E459-68.
4. Zhu, X., et al., *Patient-derived glioblastoma stem cells are killed by CD133-specific CAR T cells but induce the T cell aging marker CD57*. Oncotarget, 2015. **6**(1): p. 171-84.
5. Jin, J., et al., *Simplified method of the growth of human tumor infiltrating lymphocytes (TIL) in gas-permeable flasks to numbers needed for patient treatment*. Journal of immunotherapy (Hagerstown, Md.: 1997), 2012. **35**(3): p. 283.
6. Ferreira, G. and A. Jungbauer, *Bioreactor design for clinical-grade expansion of stem cells*. Biotechnol J, 2013. **8**(6): p. 634-5.
7. Martin, I., D. Wendt, and M. Heberer, *The role of bioreactors in tissue engineering*. Trends in biotechnology, 2004. **22**(2): p. 80-86.
8. Somerville, R.P., et al., *Clinical scale rapid expansion of lymphocytes for adoptive cell transfer therapy in the WAVE® bioreactor*. Journal of Translational Medicine, 2012. **10**(1): p. 69.

9. Shukla, A.A. and U. Gottschalk, *Single-use disposable technologies for biopharmaceutical manufacturing*. Trends in biotechnology, 2013. **31**(3): p. 147-154.
10. Bajgain, P., et al., *Optimizing the production of suspension cells using the G-Rex "M" series*. Mol Ther Methods Clin Dev, 2014. **1**: p. 14015.
11. Vera, J.F., et al., *Accelerated production of antigen-specific T-cells for pre-clinical and clinical applications using Gas-permeable Rapid Expansion cultureware (G-Rex)*. Journal of immunotherapy (Hagerstown, Md.: 1997), 2010. **33**(3): p. 305.
12. Papadopoulou, A., et al., *Activity of broad-spectrum T cells as treatment for AdV, EBV, CMV, BKV, and HHV6 infections after HSCT*. Science translational medicine, 2014. **6**(242): p. 242ra83-242ra83.
13. Donia, M., et al., *Simplified protocol for clinical-grade tumor-infiltrating lymphocyte manufacturing with use of the Wave bioreactor*. Cytotherapy, 2014. **16**(8): p. 1117-20.
14. Hollyman, D., et al., *Manufacturing validation of biologically functional T cells targeted to CD19 antigen for autologous adoptive cell therapy*. Journal of immunotherapy (Hagerstown, Md.: 1997), 2009. **32**(2): p. 169.
15. Levine, B., *Performance-enhancing drugs: design and production of redirected chimeric antigen receptor (CAR) T cells*. Cancer gene therapy, 2015. **22**(2): p. 79.
16. Kumaresan, P., et al., *Automated Cell Enrichment of Cytomegalovirus-specific T cells for Clinical Applications using the Cytokine-capture System*. Journal of visualized experiments: JoVE, 2015(104).

17. Stroncek, D.F., et al., *Preliminary evaluation of a highly automated instrument for the selection of CD34+ cells from mobilized peripheral blood stem cell concentrates*. *Transfusion*, 2016. **56**(2): p. 511-517.
18. Roh, K.H., R.M. Nerem, and K. Roy, *Biomanufacturing of Therapeutic Cells: State of the Art, Current Challenges, and Future Perspectives*. *Annu Rev Chem Biomol Eng*, 2016. **7**: p. 455-78.
19. Li, F., et al., *Cell culture processes for monoclonal antibody production*. *MAbs*, 2010. **2**(5): p. 466-79.
20. Siegel, J.P. and R.K. Puri, *Interleukin-2 toxicity*. *Journal of Clinical Oncology*, 1991. **9**(4): p. 694-704.
21. Levine, B.L., et al., *Effects of CD28 costimulation on long-term proliferation of CD4+ T cells in the absence of exogenous feeder cells*. *The Journal of Immunology*, 1997. **159**(12): p. 5921-5930.
22. KajaMurali-Krishna and J. DAltman, *Counting Antigen-Specific CD8 T Cells: A Reevaluation of Bystander Activation during Viral Infection*. *Immunity*, 1998.
23. Butz, E.A. and M.J. Bevan, *Massive Expansion of Antigen-Specific CD8+ T Cells during an Acute Virus Infection*. *Immunity*, 1998. **8**(2): p. 167-175.
24. Garlie, N.K., et al., *T cells coactivated with immobilized anti-CD3 and anti-CD28 as potential immunotherapy for cancer*. *Journal of immunotherapy (Hagerstown, Md.: 1997)*, 1999. **22**(4): p. 336-345.
25. Thompson, J.A., et al., *A Phase I Trial of CD3/CD28-activated T Cells (Xcellerated T Cells) and Interleukin-2 in Patients with Metastatic Renal Cell Carcinoma*. *Clinical Cancer Research*, 2003. **9**(10): p. 3562-3570.

26. Kalamasz, D., *Optimization of Human T-Cell Expansion Ex Vivo Using Magnetic Beads Conjugated with Anti-CD3 and Anti-CD28 Antibodies*. 2004.
27. Chen, L. and D.B. Flies, *Molecular mechanisms of T cell co-stimulation and co-inhibition*. *Nat Rev Immunol*, 2013. **13**(4): p. 227-42.
28. Boise, L.H., et al., *CD28 costimulation can promote T cell survival by enhancing the expression of Bcl-xL*. *Immunity*, 1995. **3**(1): p. 87-98.
29. Sallusto, F., J. Geginat, and A. Lanzavecchia, *Central memory and effector memory T cell subsets: function, generation, and maintenance*. *Annu Rev Immunol*, 2004. **22**: p. 745-63.
30. Hoyos, V., et al., *Engineering CD19-specific T lymphocytes with interleukin-15 and a suicide gene to enhance their anti-lymphoma/leukemia effects and safety*. *Leukemia*, 2010. **24**(6): p. 1160-70.
31. Patsoukis, N., D. Sari, and V.A. Boussiotis, *PD-1 inhibits T cell proliferation by upregulating p27 and p15 and suppressing Cdc25A*. *Cell Cycle*, 2012. **11**(23): p. 4305-9.
32. Honda, T., et al., *Tuning of antigen sensitivity by T cell receptor-dependent negative feedback controls T cell effector function in inflamed tissues*. *Immunity*, 2014. **40**(2): p. 235-247.
33. Okazaki, T., et al., *A rheostat for immune responses: the unique properties of PD-1 and their advantages for clinical application*. *Nat Immunol*, 2013. **14**(12): p. 1212-8.

34. Chikuma, S., et al., *PD-1-Mediated Suppression of IL-2 Production Induces CD8<sup>+</sup> T Cell Anergy In Vivo*. *The Journal of Immunology*, 2009. **182**(11): p. 6682-6689.
35. Simon, S. and N. Labarriere, *PD-1 expression on tumor-specific T cells: Friend or foe for immunotherapy?* *Oncoimmunology*, 2017. **7**(1): p. e1364828.
36. Duraiswamy, J., et al., *Phenotype, function, and gene expression profiles of programmed death-1(hi) CD8 T cells in healthy human adults*. *J Immunol*, 2011. **186**(7): p. 4200-12.
37. Croft, M., *The role of TNF superfamily members in T-cell function and diseases*. *Nat Rev Immunol*, 2009. **9**(4): p. 271-85.
38. Shen, C.-J., et al., *Chimeric antigen receptor containing ICOS signaling domain mediates specific and efficient antitumor effect of T cells against EGFRvIII expressing glioma*. *Journal of Hematology & Oncology*, 2013. **6**(1): p. 33.
39. Sim, G.C., et al., *IL2 Variant Circumvents ICOS<sup>+</sup> Regulatory T-cell Expansion and Promotes NK Cell Activation*. *Cancer Immunol Res*, 2016. **4**(11): p. 983-994.
40. Wherry, E.J. and M. Kurachi, *Molecular and cellular insights into T cell exhaustion*. *Nat Rev Immunol*, 2015. **15**(8): p. 486-99.
41. Li, L., et al., *KLRG1 restricts memory T cell antitumor immunity*. *Oncotarget*, 2016. **7**(38): p. 61670-61678.
42. Curran, M.A., et al., *Combination CTLA-4 Blockade and 4-1BB Activation Enhances Tumor Rejection by Increasing T-Cell Infiltration, Proliferation, and Cytokine Production*. *PLOS ONE*, 2011. **6**(4): p. e19499.

43. Song, C., et al., *Eomesodermin is required for antitumor immunity mediated by 4-1BB-agonist immunotherapy*. *OncoImmunology*, 2014. **3**(2): p. e27680.
44. Henson, S.M. and A.N. Akbar, *KLRG1--more than a marker for T cell senescence*. *Age (Dordr)*, 2009. **31**(4): p. 285-91.
45. Hodes, R.J., *Aging and the immune system*. *Immunol Rev*, 1997. **160**: p. 5-8.
46. Iezzi, G., K. Karjalainen, and A. Lanzavecchia, *The duration of antigenic stimulation determines the fate of naive and effector T cells*. *Immunity*, 1998. **8**(1): p. 89-95.
47. Sprent, J., *Burnet oration. T-cell survival and the role of cytokines*. *Immunol Cell Biol*, 2001. **79**(3): p. 199-206.
48. Sallusto, F., et al., *Functional subsets of memory T cells identified by CCR7 expression*, in *Lymphoid Organogenesis*. 2000, Springer. p. 167-171.
49. Kaech, S.M. and W. Cui, *Transcriptional control of effector and memory CD8+ T cell differentiation*. *Nat Rev Immunol*, 2012. **12**(11): p. 749-61.
50. Masopust, D. and J.M. Schenkel, *The integration of T cell migration, differentiation and function*. *Nat Rev Immunol*, 2013. **13**(5): p. 309-20.
51. Yim, C.Y., et al., *Use of N-acetyl cysteine to increase intracellular glutathione during the induction of antitumor responses by IL-2*. *The Journal of Immunology*, 1994. **152**(12): p. 5796-5805.
52. Roederer, M., et al., *Cytokine-stimulated human immunodeficiency virus replication is inhibited by N-acetyl-L-cysteine*. *Proceedings of the National Academy of Sciences*, 1990. **87**(12): p. 4884-4888.

53. Zhu, J., H. Yamane, and W.E. Paul, *Differentiation of effector CD4 T cell populations*. *Annu Rev Immunol*, 2010. **28**: p. 445-89.
54. Mosmann, T.R. and R.L. Coffman, *TH1 and TH2 cells: different patterns of lymphokine secretion lead to different functional properties*. *Annu Rev Immunol*, 1989. **7**: p. 145-73.
55. Mosmann, T.R., L. Li, and S. Sad, *Functions of CD8 T-cell subsets secreting different cytokine patterns*. *Semin Immunol*, 1997. **9**(2): p. 87-92.
56. Trinchieri, G., *Interleukin-12: a cytokine produced by antigen-presenting cells with immunoregulatory functions in the generation of T-helper cells type 1 and cytotoxic lymphocytes*. *Blood*, 1994. **84**(12): p. 4008-4027.
57. Knutson, K.L. and M. Disis, *Tumor antigen-specific T helper cells in cancer immunity and immunotherapy*. *Cancer Immunology, Immunotherapy*, 2005. **54**(8): p. 721-728.
58. Coghill, J.M., et al., *Effector CD4(+) T cells, the cytokines they generate, and GVHD: something old and something new*. *Blood*, 2011. **117**(12): p. 3268-3276.
59. Fong, T.A. and T.R. Mosmann, *Alloreactive murine CD8+ T cell clones secrete the Th1 pattern of cytokines*. *The Journal of Immunology*, 1990. **144**(5): p. 1744-1752.
60. Bhat, P., et al., *Interferon-gamma derived from cytotoxic lymphocytes directly enhances their motility and cytotoxicity*. *Cell Death Dis*, 2017. **8**(6): p. e2836.
61. Kambayashi, T., et al., *Memory CD8+ T Cells Provide an Early Source of IFN- The Journal of Immunology*, 2003. **170**(5): p. 2399-2408.

62. Pearce, E.J., et al., *Downregulation of Th1 cytokine production accompanies induction of Th2 responses by a parasitic helminth, Schistosoma mansoni*. The Journal of Experimental Medicine, 1991. **173**(1): p. 159-166.
63. Salgame, P., et al., *Differing lymphokine profiles of functional subsets of human CD4 and CD8 T cell clones*. Science, 1991. **254**(5029): p. 279-282.
64. Sad, S., R. Marcotte, and T.R. Mosmann, *Cytokine-induced differentiation of precursor mouse CD8<sup>+</sup> T cells into cytotoxic CD8<sup>+</sup> T cells secreting Th1 or Th2 cytokines*. Immunity, 1995. **2**(3): p. 271-279.
65. Wherry, E.J., et al., *Viral Persistence Alters CD8 T-Cell Immunodominance and Tissue Distribution and Results in Distinct Stages of Functional Impairment*. Journal of Virology, 2003. **77**(8): p. 4911-4927.
66. Singh, H., et al., *Manufacture of T cells using the Sleeping Beauty system to enforce expression of a CD19-specific chimeric antigen receptor*. Cancer Gene Ther, 2015. **22**(2): p. 95-100.
67. Kaiser, A.D., et al., *Towards a commercial process for the manufacture of genetically modified T cells for therapy*. Cancer Gene Ther, 2015. **22**(2): p. 72-8.
68. Monsurro, V., et al., *Functional Heterogeneity of Vaccine-Induced CD8<sup>+</sup> T Cells*. The Journal of Immunology, 2002. **168**(11): p. 5933-5942.
69. Woodland, D.L. and R.W. Dutton, *Heterogeneity of CD4<sup>+</sup> and CD8<sup>+</sup> T cells*. Current Opinion in Immunology, 2003. **15**(3): p. 336-342.
70. Janssen, E.M., et al., *CD4<sup>+</sup> T cells are required for secondary expansion and memory in CD8<sup>+</sup> T lymphocytes*. Nature, 2003. **421**: p. 852.

71. Shedlock, D.J., et al., *Role of CD4 T Cell Help and Costimulation in CD8 T Cell Responses During *Listeria monocytogenes* Infection*. The Journal of Immunology, 2003. **170**(4): p. 2053-2063.
72. Kalos, M., *Biomarkers in T cell therapy clinical trials*. Journal of Translational Medicine, 2011. **9**(1): p. 138.
73. Manel, N., D. Unutmaz, and D.R. Littman, *The differentiation of human T(H)-17 cells requires transforming growth factor-beta and induction of the nuclear receptor RORgammat*. Nat Immunol, 2008. **9**(6): p. 641-9.
74. Ness-Schwickerath, K.J., C. Jin, and C.T. Morita, *Cytokine Requirements for the Differentiation and Expansion of IL-17A- and IL-22-Producing Human V $\gamma$ 2V $\delta$ 2 T Cells*. The Journal of Immunology, 2010.
75. Baumjohann, D., et al., *The microRNA cluster miR-17 approximately 92 promotes TFH cell differentiation and represses subset-inappropriate gene expression*. Nat Immunol, 2013. **14**(8): p. 840-8.
76. Klebanoff, C.A., et al., *Central memory self/tumor-reactive CD8<sup>+</sup> T cells confer superior antitumor immunity compared with effector memory T cells*. Proc Natl Acad Sci U S A, 2005. **102**(27): p. 9571-6.
77. Barber, D.L., E.J. Wherry, and R. Ahmed, *Cutting Edge: Rapid In Vivo Killing by Memory CD8 T Cells*. The Journal of Immunology, 2003. **171**(1): p. 27-31.
78. Gargett, T. and M.P. Brown, *Different cytokine and stimulation conditions influence the expansion and immune phenotype of third-generation chimeric antigen receptor T cells specific for tumor antigen GD2*. Cytotherapy, 2015. **17**(4): p. 487-495.

79. Levine, B.L., et al., *Global Manufacturing of CAR T Cell Therapy*. *Molecular Therapy - Methods & Clinical Development*, 2017. **4**: p. 92-101.
80. June, C.H., et al., *Use of chimeric antigen receptor-modified T cells to treat cancer*. 2016, Google Patents.
81. Cooper, L.J., et al., *Human application of engineered chimeric antigen receptor (CAR) T-cells*. 2017, Google Patents.
82. Brentjens, R., et al., *Treatment of Chronic Lymphocytic Leukemia With Genetically Targeted Autologous T Cells: Case Report of an Unforeseen Adverse Event in a Phase I Clinical Trial*. *Molecular Therapy*, 2010. **18**(4): p. 666-668.
83. Porter, D.L., et al., *Chimeric Antigen Receptor–Modified T Cells in Chronic Lymphoid Leukemia*. *New England Journal of Medicine*, 2011. **365**(8): p. 725-733.
84. Morgan, R.A., et al., *Case Report of a Serious Adverse Event Following the Administration of T Cells Transduced With a Chimeric Antigen Receptor Recognizing ERBB2*. *Molecular Therapy*, 2010. **18**(4): p. 843-851.
85. Themeli, M., I. Rivière, and M. Sadelain, *New cell sources for T cell engineering and adoptive immunotherapy*. *Cell stem cell*, 2015. **16**(4): p. 357-366.
86. Morvan, P.Y., et al., *Distinct pattern of IL-2 and IFN-gamma gene expression in CD4 and CD8 T cells: cytofluorometric analysis at a single cell level using non-radioactive probes*. *Cell Mol Biol (Noisy-le-grand)*, 1995. **41**(7): p. 945-57.
87. Nakamura, K., et al., *IL-4-producing CD8+ T cells may be an immunological hallmark of chronic GVHD*. *Bone Marrow Transplantation*, 2005. **36**: p. 639.
88. Lam, B.S., et al., *Rapid expansion of functional human T cells using a novel serum-free and xeno-free culture medium*, in *CCIC 2015*. 2015: Vancouver, BC.

89. Smith, C., et al., *Ex vivo expansion of human T cells for adoptive immunotherapy using the novel Xeno-free CTS Immune Cell Serum Replacement*. Clin Transl Immunology, 2015. 4(1): p. e31.
90. BILLER, H., *Interferon-g secretion of peripheral blood CD81 T lymphocytes in patients with bronchial asthma: In vitro stimulus determines cytokine production*. 2001.

**Table 1** Summary of the representative data of the developed novel human T cell biomanufacturing in stirred-tank bioreactor.

<b>Biomanufacturing Parameters</b>		<b>Scale</b> (mL)	<b>VCD<sub>max</sub></b> (10 <sup>6</sup> cells/mL)	<b>TVCN</b> (10 <sup>6</sup> cells)	<b>Viability<sup>a</sup></b> (%)	<b>μ</b> (h <sup>-1</sup> )	<b>Td</b> (h)
<b>Medium</b>	AIM-V	30	1.90±0.11	56.9±3.2	76.8±2.5 <sup>b</sup>	0.030±0.001	23.2±0.8
	Optimizer	30	2.83±0.12	84.8±3.6	87.5±1.4 <sup>b</sup>	0.030±0.004	23.1±2.9
	ImmunoCult	30	3.49±0.52	104.6±15.5	91.8±1.1 <sup>b</sup>	0.041±0.000	17.1±0.2
<b>Feed</b>	2U/mL IL2	30	1.08±0.11	32.3±3.2	88.5±0.7 <sup>c</sup>	0.038±0.006	18.3±2.7
	30U/mL IL2	30	1.31±0.05	39.2±1.5	86.5±2.1 <sup>c</sup>	0.038±0.006	18.3±2.7
<b>Seed and stimulation</b>	1 <sup>st</sup> stimulated Day 0 seed	80	8.33±0.11	666.0±8.5	93.0±1.4	0.053±0.001	13.0±0.2
	1 <sup>st</sup> stimulated Day 2 seed	80	1.89±0.04	151.2±3.4	95.0±1.4	0.029±0.002	23.8±1.5
	1 <sup>st</sup> stimulated Day 5 seed	80	0.55±0.02	44.1±2.0	96.0±1.4	0.007±0.001	99.5±17.2
	2 <sup>nd</sup> stimulated Day 0 seed	80	3.98±0.06	318.4±4.5	93.0±0.0	0.042±0.002	16.7±0.7
<b>Scale-up</b>	T75	10	4.05±0.13	40.5±1.3	90.5±0.7	0.034±0.002	20.4±0.9
	SF125	30	3.65±0.18	109.4±5.3	91.5±2.1	0.041±0.001	16.9±0.4
	Spinner	80	3.98±0.06	318.4±4.5	93.0±0.0	0.042±0.002	16.7±0.7
	Bioreactor	800	6.40±0.46	5120.0±367.7	94.0±1.4	0.046±0.002	15.2±0.7

<sup>a</sup> Expanded cell viability was affected by seeding culture viability, medium switching, and preparation duration; <sup>b</sup> Seeding culture was prepared in AIM-V medium with viability 86.5%, switching to a different medium reduced the viability; <sup>c</sup> Prolonged seeding culture preparation reduced the final viability.

**Table 2** Evaluation of cell surface markers of human CD4<sup>+</sup> and CD8<sup>+</sup> T cells produced in the new biomanufacturing process.

Function	Marker	Day -4		Day 0		Day 2		Day 4		Day 8 (restimulated)	
		CD4 <sup>+</sup>	CD8 <sup>+</sup>	CD4 <sup>+</sup>	CD8 <sup>+</sup>						
Cell type	CD4 <sup>+</sup>	99.1±0.5	0.7±0.0	99.0±1.1	0.8±0.0	99.6±0.2	0.6±0.3	99.6±0.4	0.4±0.2	98.6±1.1	0.3±0.0
	CD8 <sup>+</sup>	0.8±0.1	99.5±0.0	0.4±0.3	99.8±0.0	0.3±0.1	99.3±0.0	0.4±0.4	93.8±0.0	0.4±0.1	99.0±0.1
	CD3 <sup>+</sup> (stimulation)	97.8±2.6	98.2±2.2	97.5±2.8	92.6±8.4	99.4±0.7	96.3±4.1	98.3±2.3	91.7±7.7	95.1±3.7	96.8±0.5
Activation signal	PD-1 <sup>+</sup> /CD279 <sup>+</sup> (related to TCR signalling)	5.7±4.3	6.5±5.6	84.5±4.3	84.7±4.3	30.3±24. 6	7.0±3.8	8.1±3.9	3.3±2.5	63.1±6.0	67.9±15. 6
	ICOS <sup>+</sup> /CD278 <sup>+</sup> (costimulation receptor)	30.3±19. 9	13.3±10. 8	99.6±0.1	99.5±0.6	99.7±0.2	99.2±1.0	99.5±0.6	91.2±12. 7	99.8±0.2	99.8±0.2
	OX40 <sup>+</sup> /CD134 <sup>+</sup> (costimulation receptor)	1.8±1.3	0.1±0.1	2.7±1.6	1.7±1.3	0.2±0.2	0.1±0.1	0.3±0.5	0.1±0.1	0.4±0.3	0.0±0.0
	CD27 <sup>+</sup> (costimulation receptor)	83.3±2.7	64.1±5.1	83.1±9.9	95.4±1.1	87.9±4.7	86.6±4.0	92.3±3.4	89.7±1.3	67.2±2.4	88.5±1.7
Inhibitory signal	LAG-3 <sup>+</sup> /CD223 <sup>+</sup>	95.0±6.2	97.6±2.8	23.3±11. 9	61.6±15. 8	11.0±5.8	24.0±12. 7	4.4±1.2	4.9±4.0	16.4±8.6	47.4±8.6
	KLRG1 <sup>+</sup>	0.9±0.4	1.4±0.7	5.5±2.5	7.9±2.3	7.5±0.7	6.6±1.0	6.7±2.3	6.4±3.4	6.4±1.5	4.7±0.4
Memory type	CCR7 <sup>+</sup> (central memory T cell)	19.4±7.6	6.0±1.0	90.7±6.6	86.5±8.0	78.3±5.8	70.1±5.2	81.7±5.5	68.5±6.4	39.1±9.9	29.2±7.2
	CD45RO <sup>+</sup> (memory T cell)	86.7±4.0	57.4±13. 6	97.0±4.4	99.7±0.4	98.4±1.9	93.5±7.8	98.6±0.9	94.1±2.6	99.6±0.3	99.0±0.1
	CD45RA <sup>+</sup> (naïve T cell)	13.9±3.0	55.3±6.6	2.4±1.1	3.5±2.6	3.7±2.3	3.6±2.4	0.7±0.3	1.1±0.7	1.9±1.5	3.4±0.9

Samples were collected from the culture shown in Figure 3-5.

**Table 3** Cytokine production summary

Data source	Cytokines secretion	Un-stimulated		Bead detachment <sup>b</sup>		Harvest	
		CD4 <sup>+</sup>	CD8 <sup>+</sup>	CD4 <sup>+</sup>	CD8 <sup>+</sup>	CD4 <sup>+</sup>	CD8 <sup>+</sup>
This study <sup>a</sup>	IFN- $\gamma$	46.2-54.2	50.9-62.0	15.6-20.8	20.3-34.8	21.1-31.1	39.8-50.9
	IL-2	64.9-76.7	19.8-39.5	79.8-95.6	77.2-93.8	75.7-95.9	74.5-96.1
	IL-4	4.6-6.5	1.7-3.5	4.2-8.7	10.2-19.9	6.0-9.1	5.2-8.2
Literature	IFN- $\gamma$	17-23[86]	27-37[86]			23-47 <sup>d</sup> [88]	42-72 <sup>d</sup> [88]
		6.7-38.9[87]	20-58.4[87]			15-41 <sup>c</sup> [89]	4-42 [90]
							10-41 <sup>c</sup> [89]
	IL-2	60[86]	25-35[86]			53-78 <sup>c</sup> [89]	49-97 <sup>c</sup> [89]
	IL-4	0.2-4.9[87]	0.1-1.6[87]			19-47 <sup>d</sup> [88]	0-21 <sup>d</sup> [88]

<sup>a</sup> Data of this study was collected at duplication.

<sup>b</sup> Previous researches didn't have the bead detachment before cell expansion.

<sup>c</sup> 14 days' culture. <sup>d</sup> 21 days' culture.

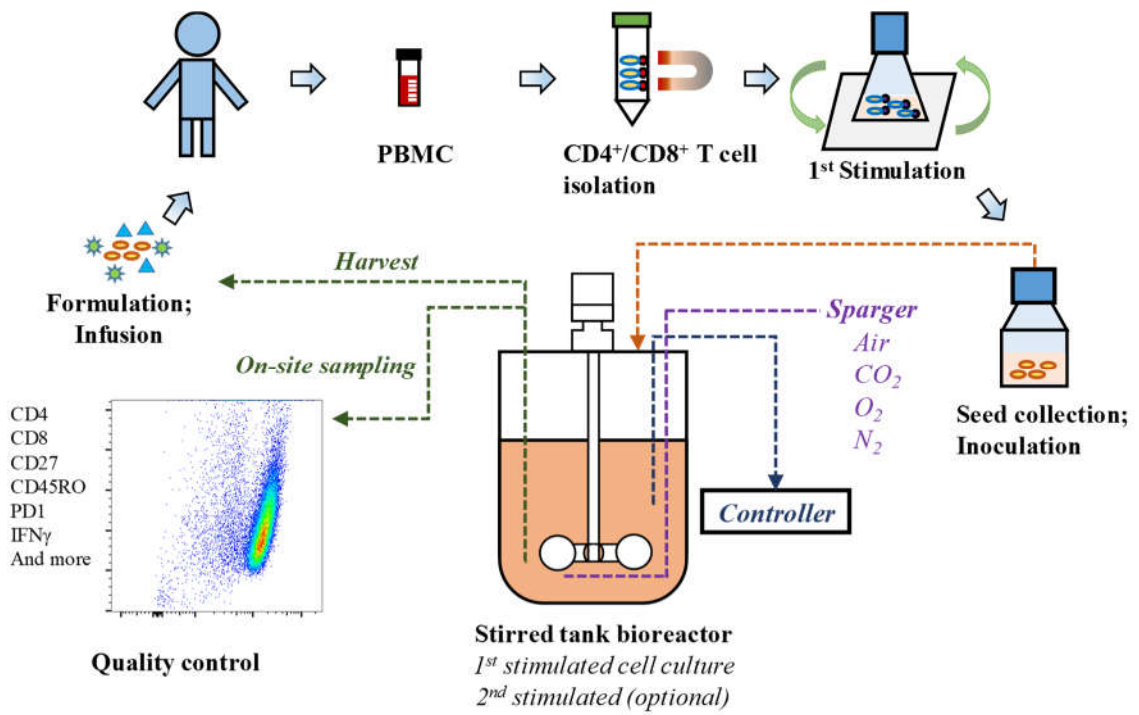


**Figure 1.** High quality T cell manufacturing process design

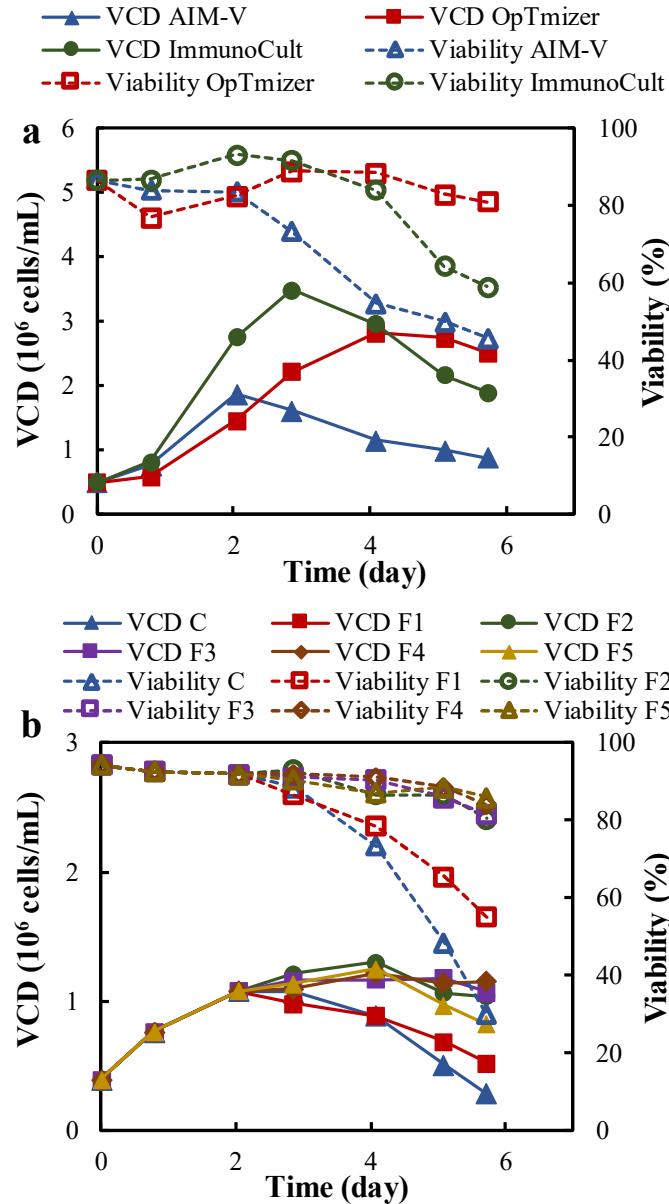


**Figure 2. Medium and feeding optimization**

a, Three medium formulations were evaluated to identify the best basal medium for cell growth. Seeding culture was stimulated with magnetic beads coated with anti-CD3 mAb/anti-CD28 mAb for four days and then scaled up for 3 days in the AIM-V medium supplemented with 30 IU/mL IL-2.

b, Effect of feeding on cell growth in OpTmizer medium with the schedule as above.

C: no feeding control, no IL-2;

F1: 2 IU/mL IL-2 was added on Day 0, 2, and 4;

F2: 30 IU/mL IL-2 was added on Day 0, 2, and 4;

F3: 60 IU/mL IL-2 was added on Day 0, 2, and 4;

F4: 30 IU/mL IL-2 was added on Day 0, 2, and 4; 1% non-essential amino acid was added on Day 2 and 4;

F5: 30 IU/mL IL-2 was added on Day 0, 2, and 4; 1% essential amino acid was added on Day 2 and 4.

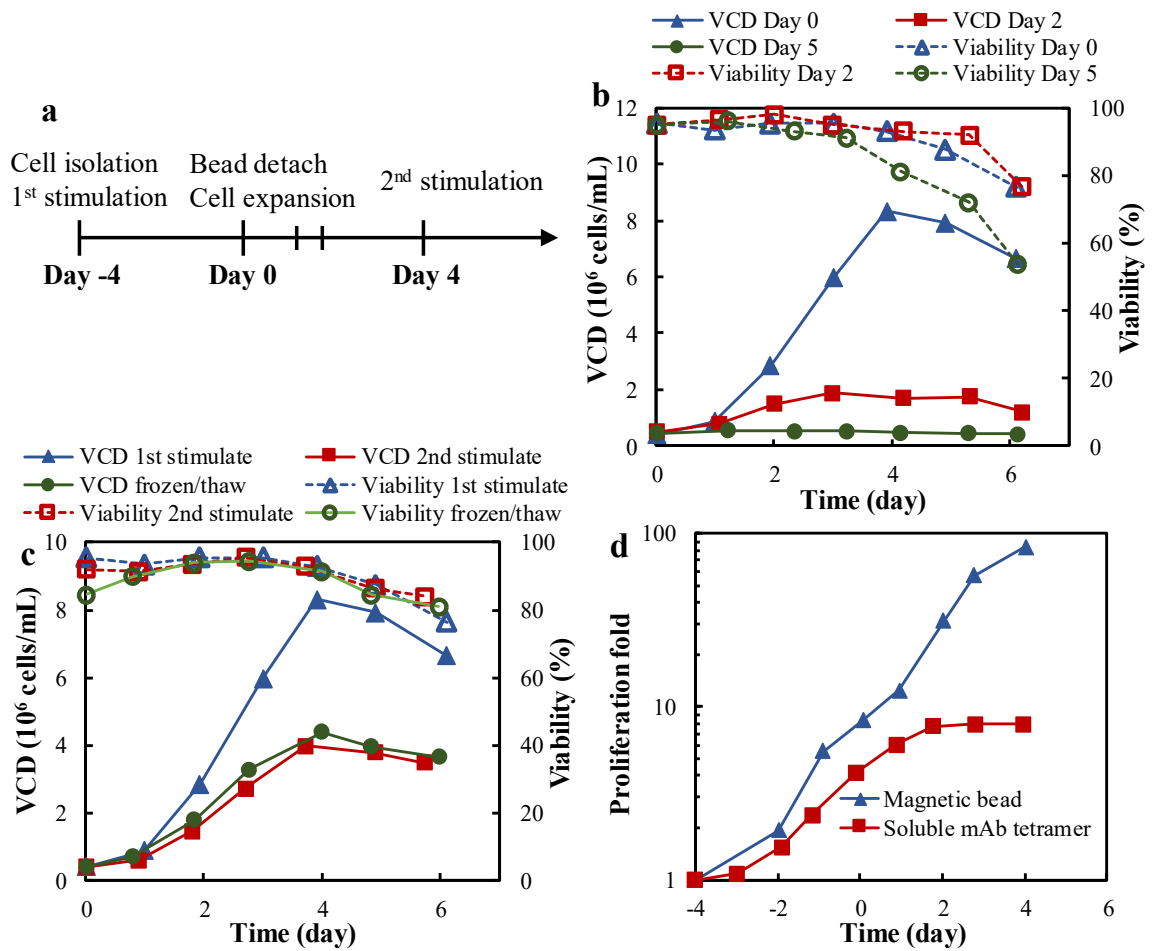


**Figure 3. Cell growth potential affected by seeding time and stimulation strategy**

a, Process development timeline. Fresh medium was added on Day -1 to maintain VCD below  $1 \times 10^6$  cells/mL.

b, Cell proliferation potential with the seeding culture from day 0, day 2 and day 5.

c, Comparison of 1<sup>st</sup> and 2<sup>nd</sup> stimulation.

d, Comparison of restimulation with the anti-CD3 mAb/anti-CD28 mAb bead and restimulation with the soluble mAb tetramer.

OpTmizer medium was used in the evaluation supplemented with 30 IU/mL IL-2 on Day 0, 2, and 4.

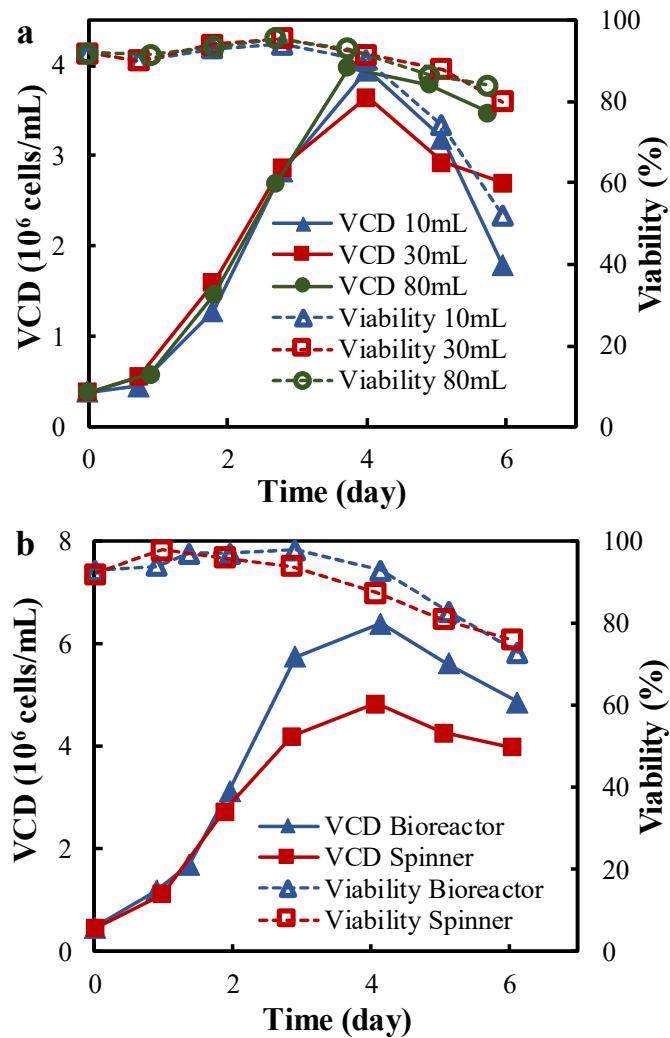


**Figure 4. Human T cell biomanufacturing scale up.**

a, Comparison of culture volume and container using the restimulated CD4<sup>+</sup> T cell.

b, Large scale culture in 2L stirred tank bioreactor using the 1<sup>st</sup> stimulated CD4<sup>+</sup> T cell.

OpTmizer medium was used in the evaluation supplemented with 30 IU/mL IL-2 on Day 0, 2, and 4.

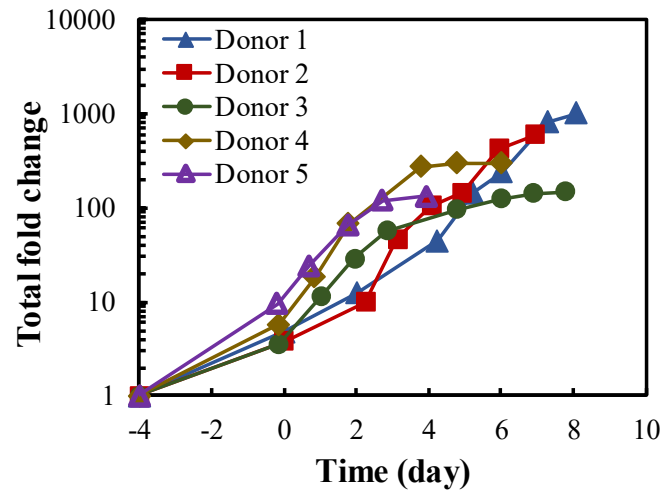


**Figure 5. Robustness of the developed scalable human T cell biomanufacturing.** Total cell expansion fold was consistent among various donors.

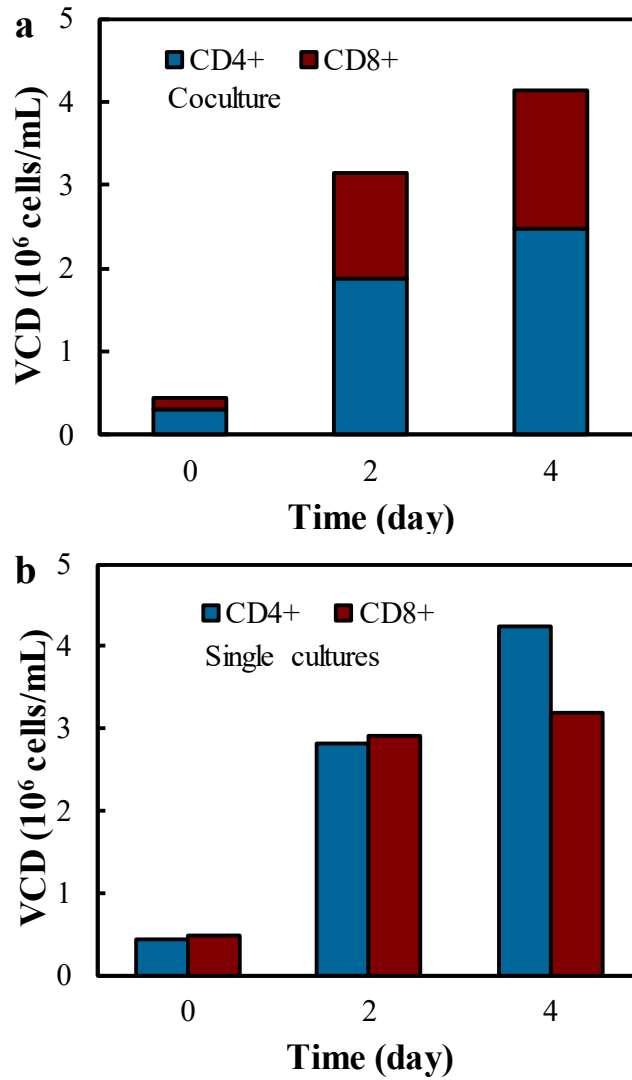


**Figure 6. CD4<sup>+</sup> and CD8<sup>+</sup> cells coculture**

a, CD4<sup>+</sup> and CD8<sup>+</sup> T cell coculture. CD4<sup>+</sup>:CD8<sup>+</sup> cell ratios were 2.0:1.0, 1.5:1.0, and 1.5:1.0 on Day 0, 2, and 4. CD8<sup>+</sup> cell grew faster in the coculture with CD4<sup>+</sup> cell.

b, CD4<sup>+</sup> and CD8<sup>+</sup> T cell individual culture.

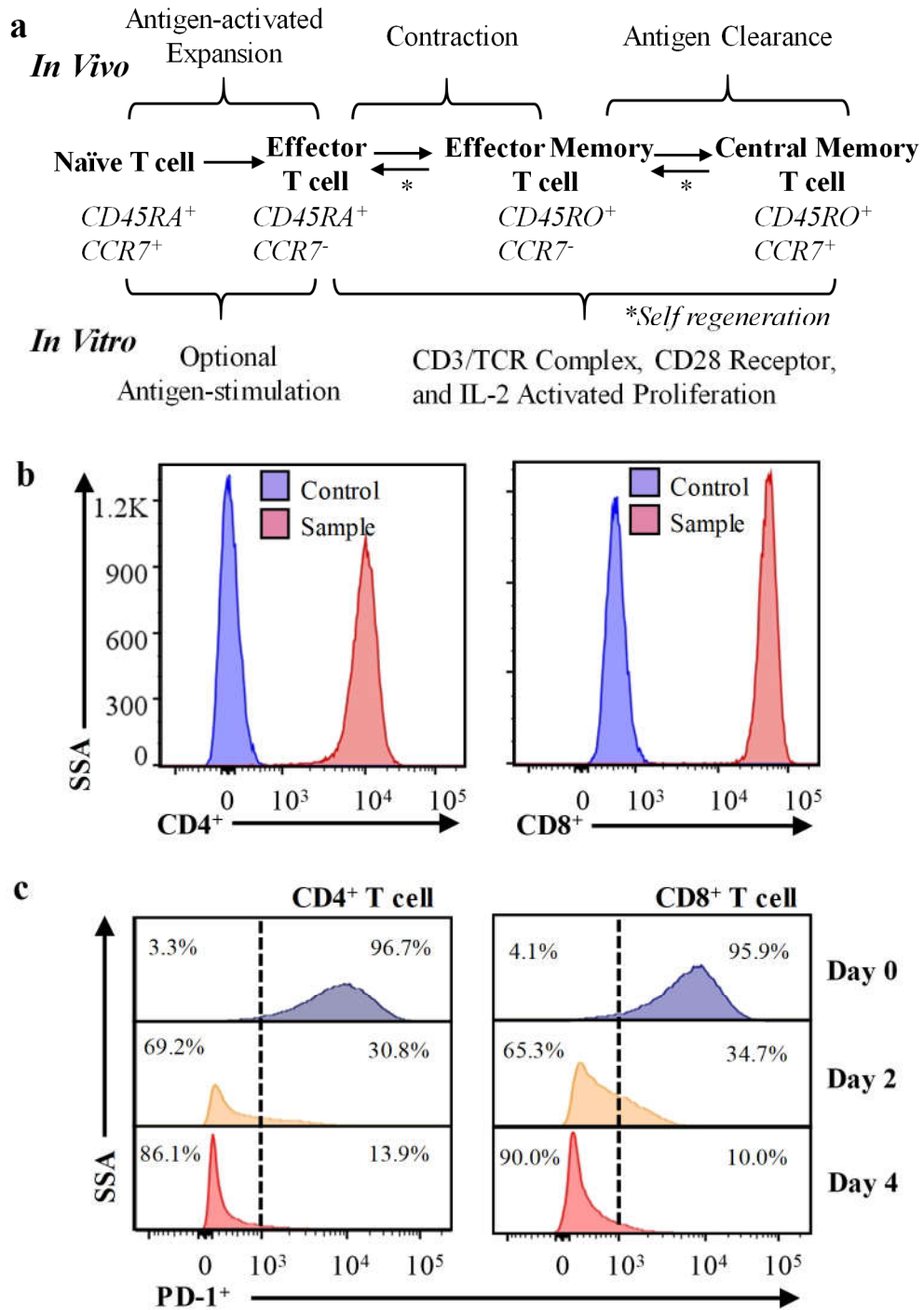


**Figure. 7. T cell quality and status evaluation**

a, Diagram of T cell proliferation and differentiation pathway

b, CD4<sup>+</sup> and CD8<sup>+</sup> T cells purity. Both cell types showed high 99% purity after the expansion.

c, Proliferation signal. PD-1 expression level was related to cell proliferation status.

Note: The CCR7, CD45RA and CD45RO surface proteins were used to identify cell subsets [78]

CHAPTER 5

PROCESS ENGINEERING OF CELLULOSIC N-BUTANOL PRODUCTION FROM  
CORN-BASED BIOMASS USING *CLOSTRIDIUM CELLULOVORANS*

by

JIANFA OU, NINGNING XU, PATRICK ERNST, CHAO MA, MEREDITH BUSH,  
KAHYONG GOH, JINGBO ZHAO, LUFANG ZHOU, SHANG-TIAN YANG,  
XIAOGUANG (MARGARET) LIU

Process Biochemistry, 62, 144-150

Copyright

2017

by

ELSEVIEW

Used by permission

Format adapted for dissertation

## **Abstract**

The cellulolytic *Clostridium cellulovorans* has been engineered to produce n-butanol from low-value lignocellulosic biomass by consolidated bioprocessing (CBP). The objective of this study was to establish a robust cellulosic biobutanol production process using a metabolically engineered *C. cellulovorans*. Firstly, various methods for the pretreatment of four different corn-based residues, including corn cob, corn husk, corn fiber, and corn bran, were investigated. The results showed that better cell growth and higher concentration of n-butanol were produced from the corn cob pretreated with sodium hydroxide. Secondly, the effects of different carbon sources (glucose, cellulose and corn cob), basal media and culture pH values on butanol production were evaluated in the fermentations performed in 2-L bioreactors to identify the optimal CBP conditions. Finally, the engineered *C. cellulovorans* produced butanol with  $>3$  g/L, yield  $>0.14$  g/g, and selectivity  $>3$  g/g from pretreated corn cob at pH 6.5 in CBP. This study showed that the fermentation process engineering enabled a high butanol production directly from agricultural residues.

**Keywords:** *Clostridium cellulovorans*; butanol fermentation; consolidated bioprocessing; corn residues

## 1. Introduction

n-Butanol is a potential substitute for gasoline, a raw material to generate bio-jet fuel and biodiesel, and an important industrial chemical [1]. The butanol produced from conventional acetone-butanol-ethanol (ABE) fermentation is uneconomical in fuel market, mainly attributed to the high expense of starchy feedstock [2].

Compared to the starch-based fermentation, the production cost of butanol from lignocellulosic biomass, such as agricultural residues of corn, rice, wheat and soybean, grass, and wood, can be significantly reduced [3, 4]. The lignocellulose is typically composed of cellulose, hemicellulose, and lignin. The pectinolytic enzymes and lignin degrading enzymes can loose the cell wall and allow the access to cellulose and hemicellulose. The fermentable sugars, such as glucose, xylose, arabinose, galactose, mannose and rhamnose, can be converted from cellulose and hemicellulose by cellulase and hemicellulase, respectively [5, 6].

Tremendous progress has been made to produce n-butanol from cellulosic biomass. For instance, the cellulosic hydrolysate has been fermented by solventogenic strains [7-11], but cellulose hydrolysis has significantly increased the operation cost. Alternatively, butanol can be produced directly from biomass by consolidated bioprocessing (CBP) that combines cellulase and hemicellulase production, cellulose and hemicellulose hydrolysis, and hexose and pentose sugars fermentation. For example, mini cellulosome has been synthesized in solventogenic clostridia [12-14] for cellulosic butanol production in CBP, but the expression of heterologous cellulosome is unstable. The co-fermentations of

cellulolytic and solventogenic strains, such as *C. thermocellum* & *C. acetobutylicum* and *C. cellulovorans* & *C. beijerinckii*, have been used to generate cellulosic butanol [15-17], but it's hard to engineer the co-fermentation of clostridia due to the complicated cellular interaction.

Alternatively, the cellulolytic clostridia that express highly active cellulase and hemicellulase, such as *C. thermocellum* and *C. cellulovorans* [18], could be metabolically engineered to produce n-butanol. For instance, the heterologous bifunctional acetaldehyde/alcohol dehydrogenase (*adhE2*) catalyzing butyryl-CoA to butanol has been introduced into acidogenic *C. cellulovorans* (Figure. 1), producing 1.6 g/L of n-butanol from cellulose [19]. The cellulosome in *C. cellulovorans* has been well investigated [20-23], but the production of n-butanol from agricultural residues by CBP has not been fully explored.

The objective of this study was to develop a robust CBP that contains biomass pretreatment and cellulosic n-butanol production using the metabolically engineered *C. cellulovorans-adhE2*. Chemical pretreatment of four different corn-based biomass was investigated. The n-butanol fermentation process was optimized by evaluating the effects of carbon sources, basal media and culture pH. A higher level of butanol was produced from corn cob in CBP by applying the optimized conditions, which could offer an economical bioprocess for cellulosic n-butanol production.

## 2. Materials and Methods

### 2.1 Strain and culture media

A mutant strain of *C. cellulovorans* ATCC 743B with overexpressed heterologous *adhE2* gene, which produced n-butanol from cellulose [24], was used in this study. The seed culture was anaerobically maintained in the modified DSMZ 520 medium supplemented with 30 µg/mL of thiamphenicol (Tm, Alfa Aesar, Ward Hill, MA) and 20 g/L of glucose at 37 °C. Both modified DSMZ 520 and ATCC 1345 media were used as reported previously [25, 26] and evaluated by comparing the cell growth and n-butanol production. Different carbon sources, including glucose, cellulose (microcrystalline, Alfa Aesar), corn cob (Northern Tool, Burnsville, MI), corn husk (collected from fresh corn and dried at 100 °C), corn fiber (Cargill, Wayzata, MN), and corn bran (Honeyville, Brigham City, UT), were tested. All chemical reagents were purchased from Thermo Fisher Scientific (Waltham, MA), unless otherwise specified.

### 2.2 Pretreatment (delignification) of corn residues

The size of corn cob was 0.29-0.38 mm, the corn bran was purchased in the form of fine powder, and the fiber and husk were ground with a Cuisinart DBM-8 Supreme Grind Automatic Burr Mill. The pretreatment of biomass was carried out in 200-mL screwed cap media bottles to evaluate the delignification efficiency. Each bottle containing 10 g of biomass and 100 mL of 0.5% H<sub>2</sub>SO<sub>4</sub>, 0.2 M Ca(OH)<sub>2</sub> or 0.4 M NaOH, respectively, was autoclaved at 121 °C for 2 h. During pretreatment, the lignin structure of the biomass

was disrupted and the hemicellulose substrates were extracted and solubilized. After cooling down, the treated biomass was neutralized and washed with tap water by filtering through Whatman Grade 1 qualitative filter paper, and dried at 80 °C for 2 days. The pretreated biomass samples that mainly contain cellulose were stored in sealed plastic bags at 4 °C before usage.

### *2.3 Cellulosic butanol fermentation*

The cellulosic butanol fermentations of *C. cellulovorans-adhE2* were performed in 2-L stirred-tank bioreactors (FS-01-A; Major science, Saratoga, CA). The bioreactors containing basal medium and carbon source, i.e. delignified biomass, cellulose or glucose (control), were autoclaved at 121 °C for 60 min and sparged with nitrogen at 10 mL/min for 3 h to reach anaerobiosis. Fresh seed culture with optical density at 600 nm (OD<sub>600</sub>) of 1.0 was used to inoculate the fermentation medium to reach seeding density of OD<sub>600</sub> of ~0.05. All fermentations were operated at Temperature 37 °C, agitation 100 rpm, and various pHs (6.5, 7.0 and 7.5) controlled with 5 N NaOH. The bioreactors were sampled at regular intervals (once or twice a day) to monitor cell growth and titrate the substrate and products. The seed cultures of bioreactors and mini butanol fermentations were performed in static 100-mL serum bottles by manually adjusting the pH to 7.0 twice a day using 5 N NaOH. All fermentations were carried out in duplicate and data were presented as the average of replicates with standard deviation.

## 2.4 Analytical methods

In this study, the composition of cellulose, hemicellulose and lignin in the corn cob was analyzed using the previously developed RI method [27]. The cell density was estimated by measuring the OD<sub>600</sub> of cell suspension using a spectrophotometer (Biomate; Thermo Fisher Scientific, Waltham, MA). The concentrations of fermentation products, including butanol, butyrate, acetate and ethanol, were analyzed using high performance liquid chromatography system (HPLC, Shimadzu, Columbia, MD) equipped with Rezex RHM-Monosaccharide H<sup>+</sup> column (Phenomenex, Torrance, CA) and a refractive index detector (Shimadzu RID-10A) [28].

## 3. Results and Discussion

### 3.1 Effect of basal media

Two basal media were tested for n-butanol production by *C. cellulovorans-adhE2* in bioreactors at pH 7.0, including ATCC 1345 and DSMZ 520. As shown in Figure. 2, faster cell growth and higher cell density could be reached in DSMZ 520 medium, with maximum OD<sub>600</sub> of 1.11 in ATCC 1345 (Figure. 2A) and 2.02 in DSMZ 520 (Figure. 2B) after 50 h in fermentation. Both media produced similar levels of n-butanol, butyrate and acetate with final concentrations of 1.6-1.8 g/L, 0-0.73 g/L, and 1.26-1.85 g/L. However, ATCC 1345 produced significantly lower concentration of ethanol than DSMZ 520, 0.92 g/L vs. 3.32 g/L. In addition, the fermentation time using DSMZ 520 was much shorter than that using ATCC 1345, 53 h vs. 66 h. These fermentation data showed that DSMZ

basal medium was more efficient in butanol production. In previous studies, the basal medium ATCC 1345 was originally used to grow *C. cellulovorans* for cellulosome study [29] and the DSMZ 520 medium was originally designed to cultivate *C. cellulolyticum* [30]. As compared to ATCC 1345, the DSMZ 520 medium contained the added 4 g/L of tryptone and the increased yeast extract from 1 g/L to 2 g/L, which improved the cell growth and shortened the fermentation of *C. cellulovorans-adhE2* [31].

### 3.2 Effect of pretreatment of corn-based biomass

Various pretreatment strategies were developed to delignify the cellulosic biomass, including physical, physicochemical, chemical, biological, electrical, or a combination of these methods [32]. For instance, steam was widely used to partially remove lignin; acid was used to pretreat a wide range of feedstocks such as corn stover [33]; alkaline was demonstrated as an effective pretreatment reagent due to the high efficiency of delignification and the less degradation of sugars [34, 35].

In this study, four corn-based agriculture residues, including corn husk, corn fiber, corn bran and corn cob, were used to evaluate the pretreatments using 0.5 % H<sub>2</sub>SO<sub>4</sub>, 0.2 M Ca(OH)<sub>2</sub>, and 0.4 M NaOH. The cell growth data of *C. cellulovorans-adhE2* on these substrates with various pretreatments in 100-mL serum bottles is shown in Figure. 3. The *C. cellulovorans-adhE2* mutant cells using NaOH pretreated biomass as carbon sources had obvious cell growth, OD<sub>600</sub> of 2.49 for corn fiber, 2.24 for corn husk, 1.88 for corn cob, and 1.71 for corn bran (Figure. 3C). However, the mutant cells grown on the H<sub>2</sub>SO<sub>4</sub>

or Ca(OH)<sub>2</sub> pretreated biomass had no obvious cell growth (Figure. 3A and 3B). Previous study showed that the lignin content of the NaOH pretreated biomass substrates was much lower than the pretreated substrates using H<sub>2</sub>SO<sub>4</sub> or Ca(OH)<sub>2</sub> [34, 35]. Lignin is not fermentable and also decreases the accessibility of cellulose by the cellulolytic microorganism. Therefore, it was easier for *C. cellulovorans* to consume the NaOH pretreated biomass to support the cell growth.

In addition to cell growth, the cellulosic butanol production by *C. cellulovorans-adhE2* was also tested in 100-mL serum bottles to further evaluate the NaOH pretreated four corn residues. As presented in Table 1, the pretreated corn cob produced higher n-butanol than other biomass, with butanol concentration of 2.13 g/L vs. 1.34-1.93 g/L. The relatively higher butanol production indicated that corn cob is a good carbon source in CBP for n-butanol production. In this experiment, the commercial cellulose was used as control substrate and produced 1.25 g/L of butanol, which was slightly lower than that produced by the NaOH pretreated biomass. The better cell growth and butanol production could be attributed to the effective delignification of biomass using NaOH solution [36, 37]. Additionally, corn cob is a lower value biomass as compared to corn fiber and corn bran that can be used as food additives or animal feed supplements. The corn cob used in this study was comprised of 30.9-36.3% of cellulose and 27.8-31.6% of hemicellulose, and 13.1-17.1% of lignin. The lignin content of the corn cob is higher than corn fiber (7.8%) and corn bran (0.7-1%) [38]. Therefore, the low-value corn cob pretreated with NaOH was identified as a good candidate carbon source in CBP.

### 3.3 Effect of carbon sources

To further evaluate the effects of carbon source on butanol production, glucose (control), cellulose and NaOH pretreated corn cob were used in the n-butanol fermentation in stirred-tank bioreactors at pH 6.5 by *C. cellulovorans-adhE2*. The n-butanol concentration and selectivity (g-butanol/g-total products) were compared among these three substrates (Figure. 4). The butanol selectivity was 0.35 g/g, 0.30 g/g and 0.28 g/g, the ethanol selectivity was 0.22 g/g, 0.08 g/g and 0.08 g/g, and butyrate selectivity was 0.09 g/g, 0.25 g/g and 0.24 g/g by glucose, cellulose and corn cob, respectively. The corn cob produced 3.37 g/L of butanol, higher than that produced by glucose (3.08 g/L) and cellulose (2.31 g/L). As compared to glucose fermentation, similar butanol selectivity, significantly lower ethanol selectivity and higher butyrate selectivity were obtained in the fermentations of corn cob or cellulose. The selectivity of C4 products (butanol and butyrate) of the fermentations using glucose, cellulose and pretreated corn cob as carbon source was 0.44 g/g, 0.55 g/g and 0.52 g/g, respectively. These data showed that the conversion from C2 to C4 was more effective during the fermentation of cellulose and pretreated corn cob than glucose. In the fermentation of pretreated corn cob, the production of C2 byproduct ethanol was low (0.98 g/L) while the production of C4 byproduct butyrate was much higher (2.83 g/L). This result indicated that the n-butanol production could be further improved by down-regulating the metabolic pathway that produces butyrate from butyryl-CoA.

In previous studies, the *C. cellulovorans* produced similar butanol yield from cellulose and glucose [31]. The ethanol yield from glucose and NaOH pretreated cotton

was similar but higher than that from cellulose by *Saccharomyces cerevisiae* [39]. The selectivity of ethanol from the pretreated poplar was higher than that from Avicel in CBP fermentation by *Caldicellulosiruptor sp.* [40]. Another study of mixed fermentation from lignocellulosic biomass by cellulolytic strains showed that different type of carbon substrates and their concentrations changed the yield of ethanol [41]. These previous studies showed that carbon source could change the solvent production in CBP fermentation, which is consistent with the results in this study.

In our study, the commercial microcrystalline cellulose was obtained at an industrial scale through the hydrolysis of wood and cotton biomass using dilute mineral acids, while the corn cob was pretreated using alkaline. The pretreatment method identified in this study could soften the biomass and make the cellulose component more accessible to cellulose by *C. cellulovorans* in CBP process. To check the structure of fermentation substrate, we observed the cellulose and the pretreated corn cob that were collected from the log-phase fermentation using a scanning electron microscope (SEM, Figure. 5). Compared to cellulose, the NaOH pretreated corn cob had a loose, croissant-like structure that allows *cellulovorans-adhE2* to access easily, which could explain its higher butanol production than cellulose.

### 3.4 Effect of fermentation pH

The pH of 7.0 was used in the cultivation and cellulosic fermentation of *C. cellulovorans* in previous studies [25, 31]. We tested fermentation pHs of 6.5, 7.0 and 7.5.

As described in Figure. 6, the butanol concentration was 3.07 g/L, 1.82 g/L and 1.33 g/L and the selectivity was 0.34 g/g, 0.24 g/g and 0.27 g/g at pH of 6.5, 7.0 and 7.5, respectively. It is clear that pH 6.5 is a much better fermentation pH value for cellulosic butanol production by *C. cellulovorans-adhE2*. Very interestingly, the butyrate production was zero but ethanol production was increased at pHs of 7.0 and 7.5. In addition, the C4/C2 ratio was 0.214 and 0.149 mol/mol at pH 7.0 and 7.5, much lower than the C4/C2 ratio of 0.536 at pH 6.5.

The synthesized AdhE2 enzyme in *C. cellulovorans-adhE2* could catalyze the formation of ethanol and butanol. The enzymatic activity of AdhE2 was greatly affected by culture pH in the range of pH 6-8 [42], so pH was an important process parameter in butanol production using CBP. In ABE fermentation by *C. acetobutylicum*, the change of pH during fermentation could initiate the switch from acidogenesis to solventogenesis. It was found that the lower fermentation pH shifted the metabolic flux to the production of acetone and butanol because of the higher level of mRNA of *adhE2* [43], and the lower pH could reduce the activity of the enzymes that catalyze acids formation [44]. Our study showed that the cell growth of *C. cellulovorans* stopped when the culture pH dropped below 5.5 (data not shown), but high fermentation pH could reduce the production and selectivity of butanol. Therefore, the pH of 6.5 was identified as the optimal cellulosic fermentation pH in CBP using *C. cellulovorans*.

### 3.5 Cellulosic butanol production in optimized CBP

Both acid and alkaline pretreatments combined with enzymatic saccharification have been successfully used for alcohol production. For example, 19 g/L of solvents were produced from the corn cob that was pretreated with NaOH followed by cellulase hydrolysis in ABE fermentation [45]; and 69 g/L of ethanol was produced from the sulfuric acid-sodium hydroxide pretreated corn cob in the fed-batch simultaneous saccharification and fermentation [46]. However, none of these studies investigated the effect of different pretreatments of multiple corn-based biomass on n-butanol production in CBP.

In this study, the cellulosic butanol production was performed using the optimal CBP parameters, i.e. DSMZ as basal medium, NaOH pretreated corn cob as substrate and fermentation pH 6.5. The cellulose was used as control substrate. The fermentation kinetics results are described in Figure. 7 and the cell growth, fermentation products concentration, yield and productivity data are summarized in Table 2.

As shown in Figure. 7, the *C. cellulovorans-adhE2* cell grew immediately after inoculation and reached maximum cell density at 40-60 h. The high inoculation OD for the fermentation using cellulose as substrate was due to the interference of cellulose particle. The fermentations were stopped when the production of the main C4 products stopped or the substrates were no longer consumed. The total fermentation timeline was about 120 h. The cell growth rates were 0.014 h<sup>-1</sup> and 0.187 h<sup>-1</sup> and the biomass yields were 0.08 g/g and 0.15 g/g for cellulose fermentation and corn cob fermentation, respectively (Table 2). As presented in Figure. 7, the added cellulose with initial concentration of 20 g/L and

pretreated corn cob with initial concentration of 30 g/L provided enough carbon. A certain level of glucose (~2.2 g/L) was carried over in the fermentation broth through inoculation but it was consumed after the acids and solvents products had obvious accumulation at time of 10 h. The concentrations of acids and solvents were continuously increased over the whole fermentation process.

As summarized in Table 2, the butanol production from corn cob was higher than that from cellulose, with average concentration of 3.37 g/L vs. 2.31 g/L, yield of 0.15 g/g-glucose vs. 0.13 g/g-glucose, and productivity of 0.046 g/L/h vs. 0.019 g/L/h. High butanol/ethanol molar ratio was observed, 2.27 from corn cob and 2.12 from cellulose. This result confirmed that the heterologous butanol pathway by overexpressing *adhE2* gene in the acidogenic *C. cellulovorans* is efficient for butanol production by cellulolytic clostridia. However, the low molar ratio between C4 products and C2 products, 0.88 from cellulose and 0.78 from corn cob, revealed that the *C. cellulovorans-adhE2* could be further engineered to re-distribute the carbon from C2 to C4 in order to improve butanol production. In addition, the zero accumulation of sugars in butanol fermentation broth indicated that the activity and/or expression of cellulosome needs to be improved by either cell engineering or process engineering in order to improve the efficiency of cellulolysis and the productivity of butanol. With high butanol production, we concluded that the pretreatment of corn-based biomass and the optimal butanol fermentation conditions developed in this study benefited the cellulosic butanol production in CBP by the engineered *C. cellulovorans-adhE2*.

The cell growth with maximum OD<sub>600</sub> of 3.9 was relatively low in this study, which could be improved by using the immobilized-cell fermentation in a fibrous-bed bioreactor (FBB). The FBB has been used to produce various biofuels and biochemicals [47-51], achieving a 10-fold higher cell density than that in free-cell fermentation, with a maximum density of  $3 \times 10^8$  cells/cm<sup>3</sup> packed bed. The FBB fermentation enables higher butanol production and tolerance to end products and toxic inhibitors due to gradual adaptation, so the pretreated low-value biomass without detoxification could be used in immobilized-cell fermentation. It is expected to produce higher level of n-butanol using immobilized-cell fermentation, which will be tested in our future study.

In conventional biofuel or biochemical production using biomass as carbon source, the biomass pretreatment, hydrolysis and fermentation are performed sequentially. For example, the effect of citrate buffer on the enzymatic hydrolysis of corn stover and acetone-butanol-ethanol fermentation integrated with vapor stripping-vapor permeation (VSVP) has been investigated [52], which demonstrated that higher concentration (>30 mM) of citrate buffer had a deleterious effect on cell growth, cellular metabolism and butanol production. As compared to the conventional butanol fermentations, the butanol production cost (raw material cost, operation cost and capital investment) using CBP could be reduced significantly although the cell growth and butanol concentration could be lower. In addition, the market price of cellulosic butanol production from CBP could be more competitive than that produced from the other process [53].

In addition, advanced technologies have been developed to enhance the butanol concentration in current butanol biorefinery. Multi-Omics technologies can be used to develop a comprehensive understanding of the host cell regulation and also identify the limiting step and its host cell regulators. The systems-level understanding of the intracellular metabolism of *C. cellulovorans* can guide the rational design of the metabolic cell engineering strategies via regulating carbon, redox and energy for cellulosic butanol production. The metabolic process engineering also plays an important role in improving butanol production. For example, the addition of methyl viologen into fermentation broth increased the availability of reducing power (NADH), altered the flux distribution and fermentation kinetics, and enhanced the butanol production [50]. The immobilized-cell fermentation in FBB has the potential to achieve a high cell density, high butanol production and high end-product tolerance [49]. The in situ butanol recovery technology has shown the benefits on reducing the end-product inhibition and increasing the butanol productivity [53]. A robust process that integrated in situ gas stripping with FBB achieved 30-fold higher butanol production comparing to simple batch culture [54]. All these technologies can be used to improve the cellulosic butanol production in CBP.

## **5. Conclusions**

A consolidated bioprocess was developed and optimized to produce n-butanol by an engineered *C. cellulovorans* mutant from low-value corn-based agricultural residues. Among them, corn cob pretreated with NaOH was the best carbon source for cellulosic n-

butanol production. The robust CBP process established with the optimization of basal medium, pretreatment, and fermentation pH gave high butanol concentration, yield and productivity, demonstrating the feasibility of cellulosic n-butanol production from corn-based biomass by cellulolytic *C. cellulovorans*.

### **Acknowledgements**

This work was supported by the Department of Energy - Office of Energy Efficiency and Renewable Energy (grant number DE-EE 0007005, 2015). The authors would like to acknowledge Dr. Kim Lackey from the Department of Biological Sciences at the University of Alabama for the SEM analysis, and Dr. Edward J. Wolfrum from the National Renewable Energy Laboratory for the substrate compositional analysis.

## References

- [1] C. Xue, M. Liu, X. Guo, E. Hudson, L. Chen, F. Bai, F. Liu, S.T. Yang. Bridging chemical-and bio-catalysis: high-value liquid transportation fuel production from renewable agricultural residues, *Green Chemistry* 19 (2017) 660-669.
- [2] C. Xue, J. Zhao, L. Chen, S.T. Yang, F. Bai. Recent advances and state-of-the-art strategies in strain and process engineering for biobutanol production by *Clostridium acetobutylicum*, *Biotechnol Adv* 35(2) (2017) 310-322.
- [3] K. Matsui, J. Bae, K. Esaka, H. Morisaka, K. Kuroda, M. Ueda, Exoproteome profiles of *Clostridium cellulovorans* grown on various carbon sources, *Appl Environ Microbiol* 79(21) (2013) 6576-6584.
- [4] C. Lu, C. Ma, X.M. Liu, High-productivity and low-cost biobutanol production by integrated process development, *Intl J Innov Res Sci Eng.* 2(3) (2014) ISSN 2347-3207.
- [5] P. Abdesahian, M.D. Dashti, M.S. Kalil, W.M.W. Yusoff, Production of biofuel using biomass as a sustainable biological resource, *Asian Network for Scientific Information* 9(3) (2010) 274-282.
- [6] J.H. Van Vleet, T.W. Jeffries. Yeast metabolic engineering for hemicellulosic ethanol production, *Curr Opin Biotechnol* 20(3) (2009) 300-306.
- [7] J. Wang, X. Yang, C. Chen, S. Yang, Engineering clostridia for butanol production from biorenewable resources: from cells to process integration, *Curr Opin Chem Eng* 6 (2014) 43-54.

- [8] M. Galbe, G. Zacchi, Pretreatment of lignocellulosic materials for efficient bioethanol production, *Adv Biochem Eng Biotechnol* 108 (2007) 41-65.
- [9] F. Raganati, G. Olivieri, P. Gotz, A. Marzocchella, P. Salatino, Butanol production from hexoses and pentoses by fermentation of *Clostridium acetobutylicum*, *Anaerobe* 34 (2015) 146-155.
- [10] S.M. Gaida, A. Liedtke, A.H. Jentges, B. Engels, S. Jennewein, Metabolic engineering of *Clostridium cellulolyticum* for the production of n-butanol from crystalline cellulose, *Microb Cell Fact* 15 (2016) 6-11.
- [11] G.C. Xu, J.C. Ding, R.Z. Han, J.J. Dong, Y. Ni, Enhancing cellulose accessibility of corn stover by deep eutectic solvent pretreatment for butanol fermentation, *Bioresour Technol* 203 (2016) 364-369.
- [12] L.R. Lynd, W.H. van Zyl, J.E. McBride, M. Laser, Consolidated bioprocessing of cellulosic biomass: an update, *Curr Opin Biotechnol* 16(5) (2005) 577-583.
- [13] F. Salimi, R. Mahadevan, Characterizing metabolic interactions in a clostridial co-culture for consolidated bioprocessing, *BMC Biotechnol* 13 (2013) 95-103.
- [14] F. Salimi, K. Zhuang, R. Mahadevan, Genome-scale metabolic modeling of a clostridial co-culture for consolidated bioprocessing, *Biotechnol J* 5(7) (2010) 726-738.
- [15] E.K.C. Yu, M.H. Chan, S. Saddler, Butanol production from cellulosic substrates by sequential co-culture of *Clostridium thermocellum* and *C. acetobutylicum*, *Biotechnol Lett* 7 (1985) 509-514.

- [16] S. Nakayama, K. Kiyoshi, T. Kadokura, A. Nakazato, Butanol production from crystalline cellulose by cocultured *Clostridium thermocellum* and *Clostridium saccharoperbutylacetonicum* N1-4, *Appl Environ Microbiol* 77(18) (2011) 6470-6475.
- [17] Z. Wen, M. Wu, Y. Lin, L. Yang, J. Lin, P. Cen, Artificial symbiosis for acetone-butanol-ethanol (ABE) fermentation from alkali extracted deshelled corn cobs by co-culture of *Clostridium beijerinckii* and *Clostridium cellulovorans*, *Microb Cell Fact* 13(1) (2014) 92-102.
- [18] R.B. Karin Öhgren, J. Saddler, G. Zacchi, Effect of hemicellulose and lignin removal on enzymatic hydrolysis of steam pretreated corn stover, *Bioresour Technol* 98(13) (2007) 2503-2510.
- [19] X. Yang, Metabolic engineering of cellulolytic *Clostridium cellulovorans* PhD dissertation, Ohio State University, Columbus, OH (2014).
- [20] J. Ou, C. Ma, N. Xu, Y. Du, X. Liu, High butanol production by regulating carbon, redox and energy in Clostridia, *Front Chem Sci Eng* 9(3) (2015) 317-323.
- [21] C.M. Fontes, H.J. Gilbert, Cellulosomes: highly efficient nanomachines designed to deconstruct plant cell wall complex carbohydrates, *Annu Rev Biochem* 79 (2010) 655-681.
- [22] Y. Tamaru, H. Miyake, K. Kuroda, A. Nakanishi, C. Matsushima, R.H. Doi, M. Ueda, Comparison of the mesophilic cellulosome-producing *Clostridium cellulovorans* genome with other cellulosome-related clostridial genomes, *Microb Biotechnol* 4(1) (2011) 64-73.

- [23] H. Morisaka, K. Matsui, Y. Tatsukami, K. Kuroda, H. Miyake, Y. Tamaru, M. Ueda, Profile of native cellulosomal proteins of *Clostridium cellulovorans* adapted to various carbon sources, *AMB Express* 2(1) (2012) 37-41.
- [24] T. Inamori, S. Aburaya, H. Morisaka, K. Kuroda, M. Ueda. Characteristic strategy of assimilation of various saccharides by *Clostridium cellulovorans*. *AMB Express* 6(1) (2016) 64-69.
- [25] X. Yang, M. Xu, S.T. Yang, Restriction modification system analysis and development of in vivo methylation for the transformation of *Clostridium cellulovorans*, *Appl Microbiol Biotechnol* 100(5) (2016) 2289-2299.
- [26] G.T. Attwood, H.P. Blaschek, B.A. White, Transcriptional analysis of the *Clostridium cellulovorans* endoglucanase gene, *engB*, *FEMS Microbiol Lett* 124(3) (1994) 277-284.
- [27] E.J. Wolfrum, A.D. Sluiter, Improved multivariate calibration models for corn stover feedstock and dilute-acid pretreated corn stover, *Cellulose* 16(4) (2009) 567-576.
- [28] C. Ma, J. Ou, M. Miller, S. McFann, X. Liu, High production of butyric acid by *Clostridium tyrobutyricum* mutant, *Front Chem Sci Eng* 9(3) (2015) 369-375.
- [29] S.O. Han, H. Yukawa, M. Inui, R.H. Doi, Transcription of *Clostridium cellulovorans* cellulosomal cellulase and hemicellulase genes, *J Bacteriol* 185(8) (2003) 2520-2527.
- [30] X. Peng, R.A. Borner, I.A. Nges, J. Liu, Impact of bioaugmentation on biochemical methane potential for wheat straw with addition of *Clostridium cellulolyticum*, *Bioresour Technol* 152 (2014) 567-571.

- [31] X. Yang, M. Xu, S.T. Yang, Metabolic and process engineering of *Clostridium cellulovorans* for biofuel production from cellulose, *Metab Eng* 32 (2015) 39-48.
- [32] P. Kumar, D.M. Barrett, M.J. Delwiche, P. Stroeve, Methods for pretreatment of lignocellulosic biomass for efficient hydrolysis and biofuel production, *Ind Eng Chem Res* 48(8) (2009) 3713-3729.
- [33] C.I. Ishizawa, M.F. Davis, D.F. Schell, D.K. Johnson, Porosity and its effect on the digestibility of dilute sulfuric acid pretreated corn stover, *J Agric Food Chem* 55(7) (2007) 2575-2581.
- [34] Z. Wang, R. Li, J. Xu, J.M. Marita, R.D. Hatfield, R. Qu, J.J. Cheng, Sodium hydroxide pretreatment of genetically modified switchgrass for improved enzymatic release of sugars, *Bioresour Technol* 110 (2012) 364-370.
- [35] J. Xu, J.J. Cheng, Pretreatment of switchgrass for sugar production with the combination of sodium hydroxide and lime, *Bioresour Technol* 102(4) (2011) 3861-3868.
- [36] M.A. Millett, A.J. Baker, L.D. Satter, Physical and chemical pretreatments for enhancing cellulose saccharification, *Biotechnol Bioeng Symp (United States)*, Dept. of Agriculture, Madison, WI, 1976.
- [37] V.B. Agbor, N. Cicek, R. Sparling, A. Berlin, D.B. Levin, Biomass pretreatment: fundamentals toward application, *Biotechnol Adv* 29(6) (2011) 675-685.
- [38] D.J. Rose, G.E. Inglett, S.X. Liu. Utilisation of corn (*Zea mays*) bran and corn fiber in the production of food components. *J Sci Food Agric* 90(6) (2010) 915-924.

- [39] A. Jeihanipour, M.J. Taherzadeh, Ethanol production from cotton-based waste textiles, *Bioresour Technol* 100(2) (2009) 1007-1010.
- [40] V.A. Svetlitchnyi, O. Kensch, D.A. Falkenhan, S.G. Korseska, N. Lippert, M. Prinz, J. Sassi, A. Schickor, S. Curvers, Single-step ethanol production from lignocellulose using novel extremely thermophilic bacteria, *Biotechnol Biofuel* 6(1) (2013) 31-45.
- [41] C.H. Zhou, X. Xia, C.X. Lin, D.S. Tong, J. Beltramini, Catalytic conversion of lignocellulosic biomass to fine chemicals and fuels, *Chem Soc Rev* 40(11) (2011) 5588-5617.
- [42] J.S. Chen, Alcohol dehydrogenase: multiplicity and relatedness in the solvent-producing clostridia, *FEMS Microbiol Rev* 17(3) (1995) 263-273.
- [43] D. Honicke, T. Lutke-Eversloh, Z. Liu, D. Lehmann, W. Liebl, A. Ehrenreich, Chemostat cultivation and transcriptional analyses of *Clostridium acetobutylicum* mutants with defects in the acid and acetone biosynthetic pathways, *App Microbiol Biotechnol* 98(23) (2014) 9777-9794.
- [44] Y. Zhu, S.T. Yang, Effect of pH on metabolic pathway shift in fermentation of xylose by *Clostridium tyrobutyricum*, *J Biotechnol* 110(2) (2004) 143-157.
- [45] K. Gao, Y. Li, S. Tian, X. Yang, Screening and characteristics of a butanol-tolerant strain and butanol production from enzymatic hydrolysate of NaOH-pretreated corn stover, *World J Microbiol Biotechnol* 28(10) (2012) 2963-2971.

- [46] M. Zhang, F. Wang, R. Su, W. Qi, Z. He, Ethanol production from high dry matter corncob using fed-batch simultaneous saccharification and fermentation after combined pretreatment, *Bioresour Technol* 101(13) (2010) 4959-4964.
- [47] L. Jiang, J. Wang, S. Liang, X. Wang, P. Cen, Z. Xu, Butyric acid fermentation in a fibrous bed bioreactor with immobilized *Clostridium tyrobutyricum* from cane molasses, *Bioresour Technol* 100(13) (2009) 3403-3409.
- [48] L. Jiang, J. Wang, S. Liang, X. Wang, P. Cen, Z. Xu, Production of butyric acid from glucose and xylose with immobilized cells of *Clostridium tyrobutyricum* in a fibrous-bed bioreactor, *App Biochem Biotechnol* 160(2) (2010) 350-359.
- [49] D. Wei, X. Liu, S.T. Yang, Butyric acid production from sugarcane bagasse hydrolysate by *Clostridium tyrobutyricum* immobilized in a fibrous-bed bioreactor, *Bioresour Technol* 129 (2013) 553-560.
- [50] Y. Du, W. Jiang, M. Yu, I.C. Tang, S.T. Yang, Metabolic process engineering of *Clostridium tyrobutyricum* *Deltaack-adhE2* for enhanced n-butanol production from glucose: effects of methyl viologen on NADH availability, flux distribution, and fermentation kinetics, *Biotechnol Bioeng* 112(4) (2015) 705-715.
- [51] A.M. Jaros, U. Rova, K.A. Berglund, Acetate adaptation of *Clostridium tyrobutyricum* for improved fermentation production of butyrate, *SpringerPlus* 2(1) (2013) 1-8.
- [52] C. Xue, Z. Wang, S. Wang, X. Zhang, L. Chen Y. Mu, F. Bai. The vital role of citrate buffer in acetone-butanol-ethanol (ABE) fermentation using corn stover and high-efficient

product recovery by vapor stripping-vapor permeation (VSVP) process, *Biotechnol Biofuels* 9 (2016) 146-164.

[53] D.G. Olson, J.E. McBride, A.J. Shaw, L.R. Lynd. Recent progress in consolidated bioprocessing, *Curr Opin Biotechnol* 23(3) (2012): 396-405.

[54] C. Xue, J. Zhao, C. Lu, S.T. Yang, F. Bai, I.C. Tang. High-titer n-butanol production by *clostridium acetobutylicum* JB200 in fed-batch fermentation with intermittent gas stripping, *Biotechnol Bioeng* 109 (11) (2012) 2746-2756.

[55] C. Xue, F. Liu, M. Xu, J. Zhao, L. Chen, J. Ren, F. Bai, S.T. Yang. A novel in situ gas stripping-pervaporation process integrated with acetone-butanol-ethanol fermentation for hyper n-butanol production, *Biotechnol Bioeng* 113 (1) (2016) 120-129.

**Table 1** Effect of the pretreatment of biomass on butanol production by *C. cellulovorans-adhE2*

Pretreatment <sup>a</sup>	Cob	Husk	Fiber	Bran	Cellulose <sup>a</sup>
Control <sup>b</sup>	0.00±0.00	0.58±0.03	0.36±0.01	0.19±0.01	1.25±0.04
H <sub>2</sub> SO <sub>4</sub>	0.00±0.00	0.00±0.00	0.26±0.04	0.00±0.00	N/A <sup>a</sup>
Ca(OH) <sub>2</sub>	0.00±0.00	0.00±0.00	0.00±0.00	0.19±0.01	N/A <sup>a</sup>
NaOH	2.13±0.04	1.87±0.01	1.93±0.01	1.34±0.03	N/A <sup>a</sup>

<sup>a</sup> Butanol fermentation was carried out in serum bottles. The unit of butanol concentration is g/L.

<sup>b</sup> Control means no pretreatment.

<sup>c</sup> N/A: Not applied.

**Table 2** Effect of carbon sources on butanol production of *C. cellulovorans*

Substrates <sup>a</sup>	Cellulose	Corncob
Cell growth (h <sup>-1</sup> )	0.014±0.003	0.187±0.043
Biomass yield (g/g) <sup>b</sup>	0.140±0.061	0.146±0.014
Concentration (g/L)		
Butanol	2.306±0.179	3.366±0.204
Butyrate	1.883±0.337	2.834±0.181
Ethanol	0.631±0.470	0.984±0.059
Acetate	2.749±0.303	4.660±0.390
Yield (g/g-glucose)		
Butanol	0.134±0.001	0.147±0.003
Butyrate	0.210±0.035	0.172±0.040
Ethanol	0.042±0.046	0.072±0.029
Acetate	0.155±0.019	0.179±0.045
Productivity (g/L/h)		
Butanol	0.019±0.002	0.046±0.011
Butyrate	0.015±0.009	0.039±0.028
Ethanol	0.006±0.005	0.020±0.005
Acetate	0.023±0.005	0.065±0.002
C4/C2(mol/mol)	0.882	0.783

<sup>a</sup> The n-butanol fermentations were carried out in 2-L stirred-tank bioreactors at pH 6.5.

<sup>b</sup> The biomass amount is estimated as 1 OD<sub>600</sub> = 0.38 g/L [49].

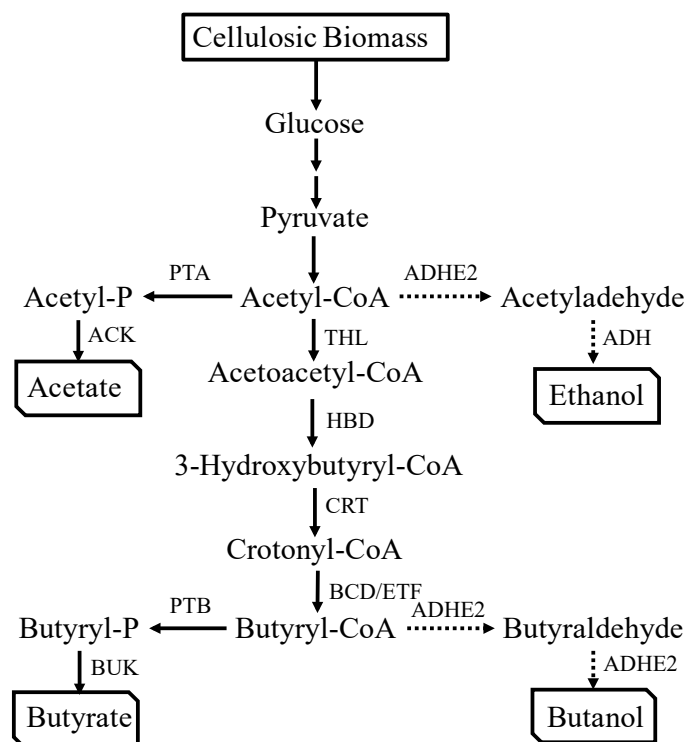


**Figure. 1** Metabolic pathway in *C. cellulovorans-adhE2*. Abbreviations: THL, thiolase; HBD, beta-hydroxybutyryl-CoA dehydrogenase; CRT, 3-hydroxybutyryl-CoA dehydratase; BCD, butyryl-CoA dehydrogenase; ETF, electron transfer flavoprotein; PTA, phosphotransacetylase; ACK, acetate kinase; PTB, phosphotransbutyrylase; BUK, butyrate kinase; ADH, alcohol dehydrogenase; ADHE2, bifunctional acetaldehyde/alcohol dehydrogenase.

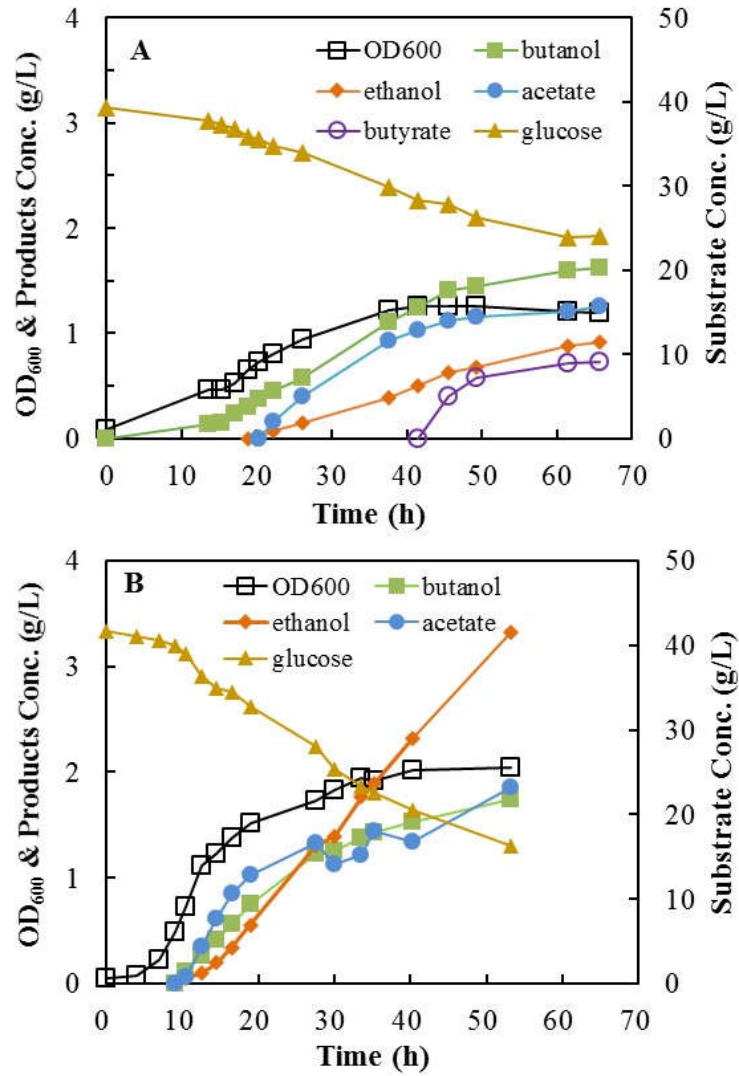


**Figure. 2** Fermentation kinetics of *C. cellulovorans-adhE2* using glucose as substrate in ATCC 1345 medium (A) and DSMZ 520 medium (B) in 2-L bioreactor at pH 7.0, temperature 37 °C, and agitation 100 rpm. □: OD<sub>600</sub>, ▲: glucose, ○: butyrate, ●: acetate, ■: butanol, ◆: ethanol.

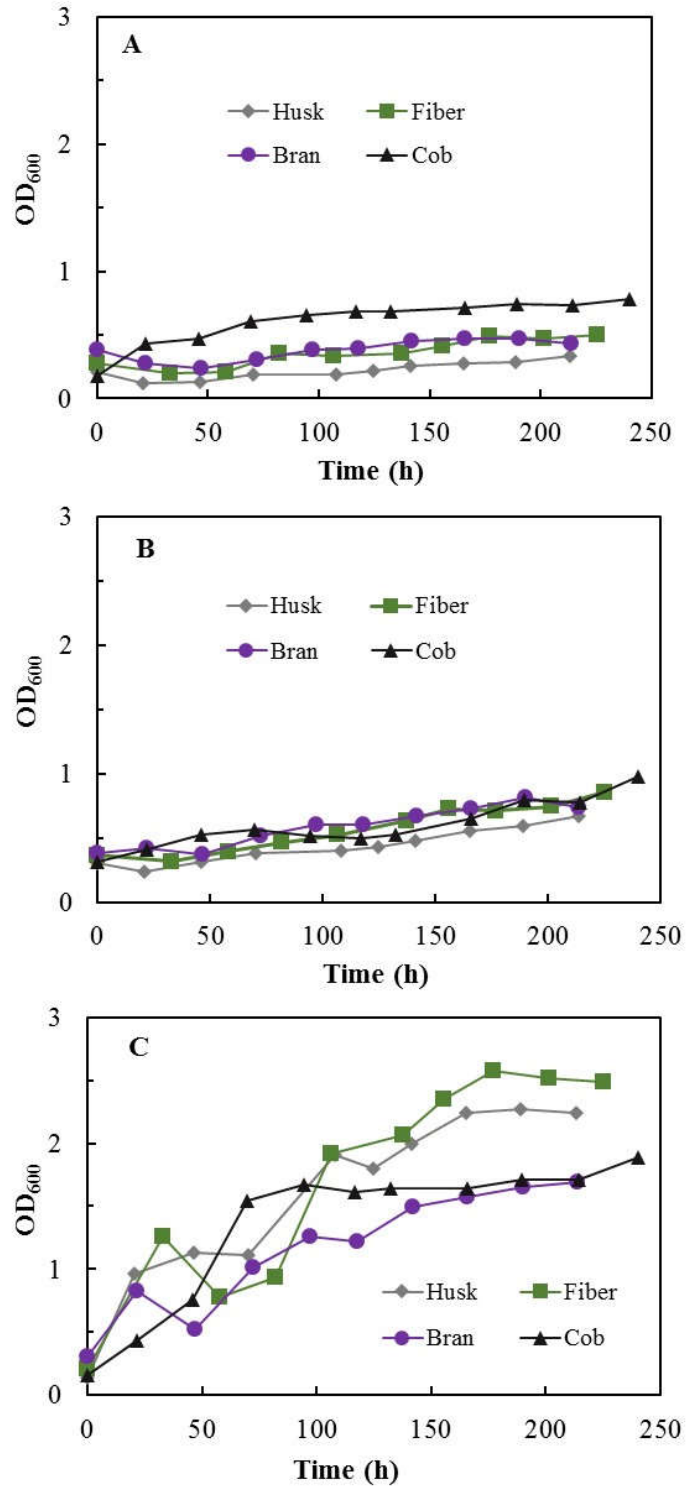


**Figure. 3** Effect of pretreatment of corn-based biomass on the cell growth of *C. cellulovorans-adhE2*. A) Pretreatment with  $H_2SO_4$ , B) Pretreatment with  $Ca(OH)_2$ , C) Pretreatment with  $NaOH$ .  $\blacklozenge$ : Corn husk,  $\blacksquare$ : Corn fiber,  $\bullet$ : Corn bran, and  $\blacktriangle$ : Corn cob.

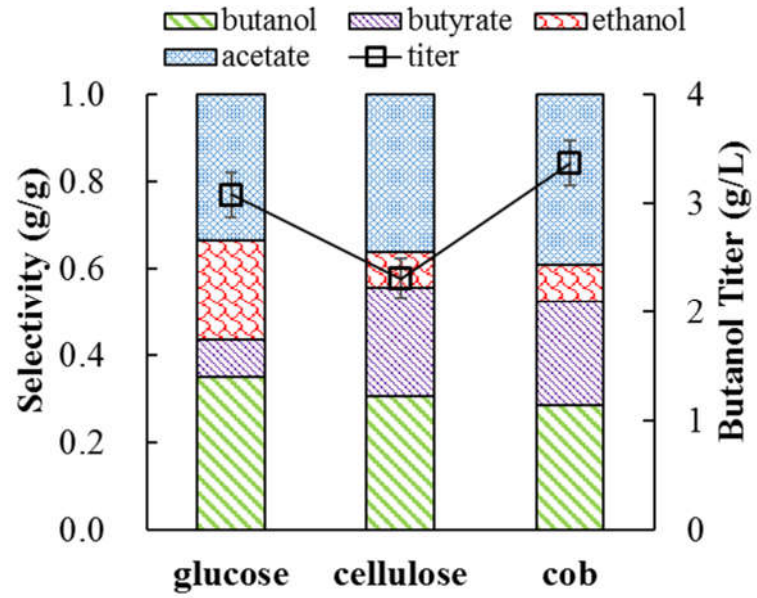


**Figure. 4** Butanol selectivity (g-butanol/g-total products) and concentration as affected by various carbon substrates at pH 6.5. □: Concentration.

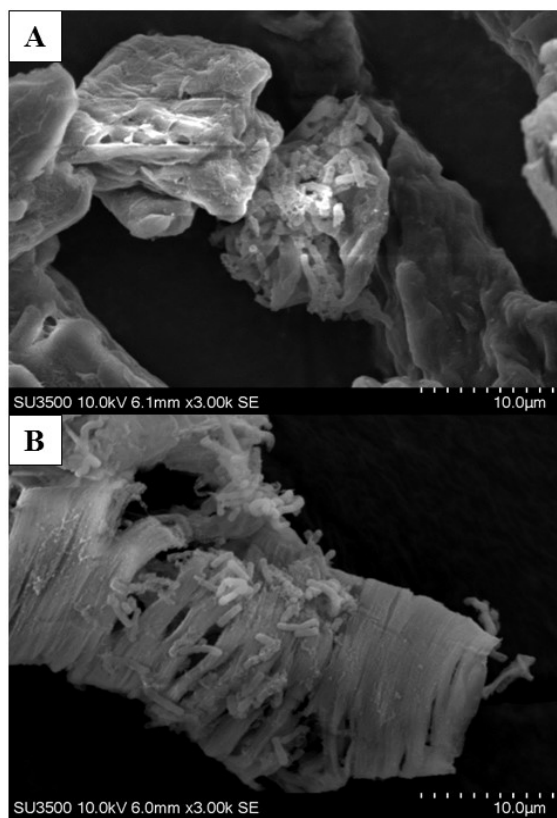


**Figure. 5** SEM analysis for *C. cellulovorans-adhE2* cells grown on A) cellulose and B) NaOH pretreated cob.

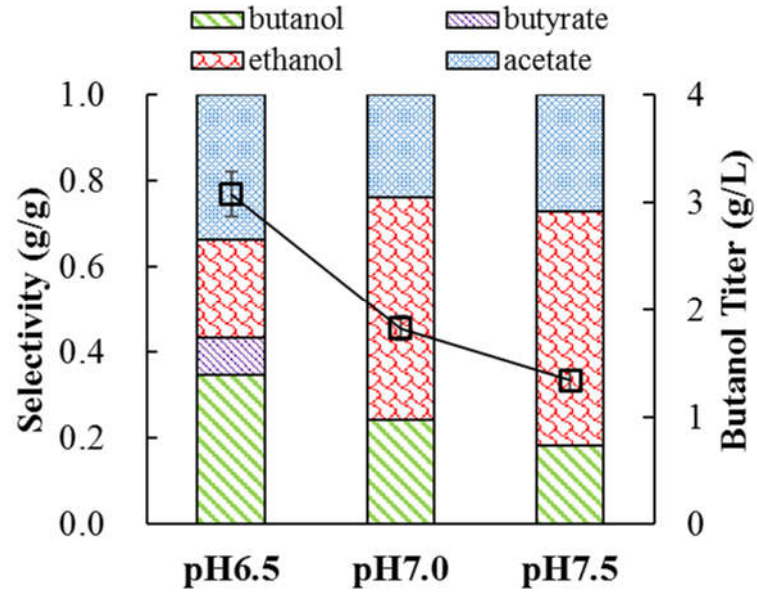


**Figure. 6** Effects of fermentation pH value on butanol selectivity and product concentration using glucose as substrate. □: Concentration.

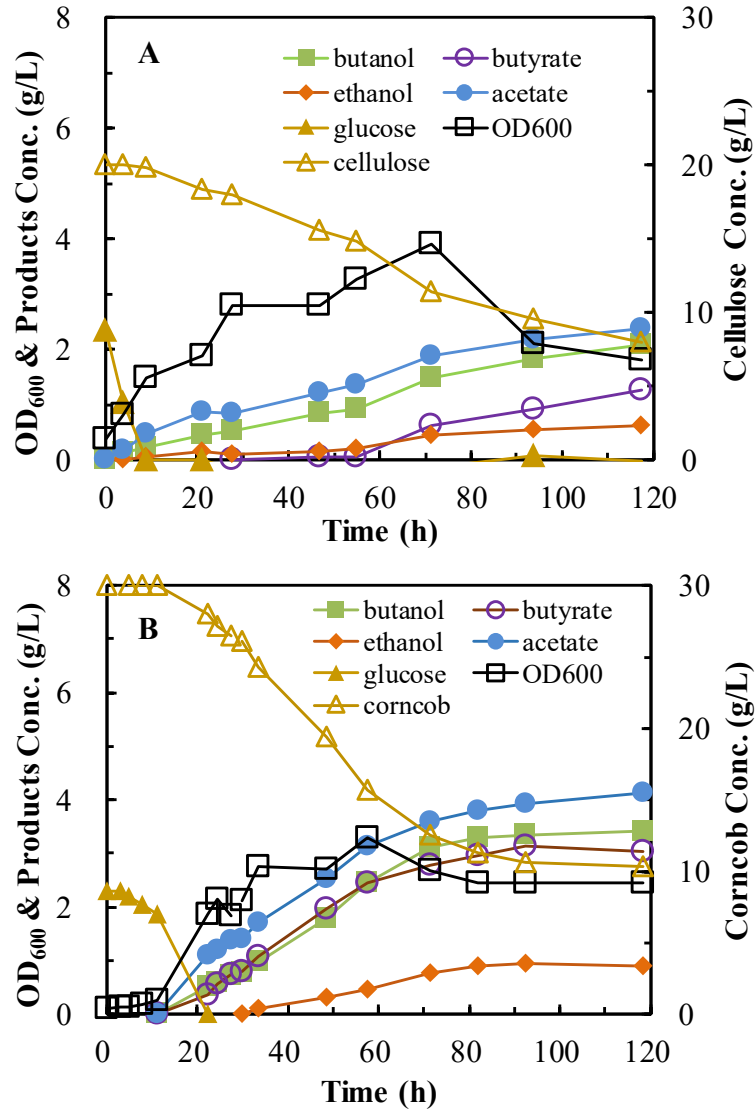


**Figure. 7** Fermentation kinetics for cellulosic n-butanol production from A) cellulose and B) pretreated corncob by *C. cellulovorans-adhE2* in 2-L bioreactor at pH 6.5, temperature 37 °C, and agitation 100 rpm. □: OD<sub>600</sub>, ▲: glucose, △: cellulose/corncob, ○: butyrate, ●: acetate, ■: butanol, ◆: ethanol.

CHAPTER 6

INTRACELLULAR METABOLISM ANALYSIS OF *CLOSTRIDIUM*  
*CELLULOVORANS* VIA MODELING INTEGRATING PROTEOMICS,  
METABOLOMICS AND FERMENTATION

by

JIANFA OU, XIAOGUANG (MARGARET) LIU

In preparation

Format adapted for dissertation

## Abstract

A consolidated bioprocessing has been developed to produce n-butanol from cellulosic biomass using an engineered cellulolytic *Clostridium cellulovorans*, but the butanol production was low. This study aimed to develop a comprehensive understanding of cellular metabolism of *C. cellulovorans* using a novel dynamic mathematic model, for the first time, to integrate our proteomics, metabolomics and fermentation data collected from the wild type and n-butanol producing mutant strains. Total 1,820 host cell proteins were detected in the comparative proteomics study and total 474 primary and secondary intracellular metabolites were titrated in metabolomics study. The expression of most cellulases were up-regulated, but phosphofructokinase (Pfk1), fructose-1,6-bisphosphate aldolase (Aldo) and phosphoglycerate kinase (Pgk) in glycolysis and thiolase (Thl), crotonase (Crt) and electron transfer flavoprotein A/B (EtfA/B) in the central metabolic pathway were down-regulated by the synthesized butanol pathway. The maximal reaction rate (cRmax), which was calculated using the intracellular metabolite data, showed strong correlation with the expression level of the corresponding catalytic enzyme. Metabolic control analysis ranked the important impact factors that could contribute to butanol production improvement, including assimilation of substrates (cellulose and glucose), formation of byproducts (ethanol, acetate and butyrate) and four key enzymes (Thl, Hbd, Crt and EtfA/B). Several strategies to rationally engineer *C. cellulovorans* and cellulosic fermentation were proposed as the output of modeling and validated by up-regulating the identified host cell regulators (Thl and Hbd). Finally, the cellulosic n-butanol production (i.e. final concentration and yield) was greatly improved by the new-generation, rationally engineered strain.

**Keywords:** *C. cellulovorans*; cellulosic n-butanol fermentation; proteomics; metabolomics; dynamic model; metabolic engineering

## 1. Introduction

As an important industrial chemical and potential substitute for gasoline, n-butanol can be sustainably produced from lignocellulosic biomass. Our previous study has developed a consolidated bioprocessing (CBP) to convert biomass to n-butanol by a metabolically engineered cellulolytic *Clostridium cellulovorans* [1, 2]. However, the final butanol concentration and productivity were low. To improve butanol production, it is very important to develop a full understanding of cellular metabolism and its interaction with process parameters and create a platform to rationally engineer *C. cellulovorans* and/or CBP.

The advances in Omics technologies, such as genomics, proteomics and metabolomics, have enabled the systematic characterization of microorganisms. In genomics study, the genome sequencing of cellulolytic *C. cellulovorans* 743B [3], *C. cellulolyticum* H10 [4], and *C. thermocellum* [5] has been completed. All these clostridia are acetate or butyrate-producing strains that could be engineered to produce ethanol or butanol. Proteomics has been performed in *C. acetobutylicum*, *C. thermocellum* and *Clostridium* sp. to analyze the expression of intracellular proteins and identify the key enzymes involved in cell growth, carbohydrate metabolism, and/or solvent tolerance [6-10]. Metabolomics is capable of investigating the regulatory mechanism of metabolism via directly analyzing the global extracellular and intracellular metabolites. The public databases provide metabolic maps of clostridia, such as MetaCyc, Kyoto Encyclopedia of Genes and Genomes, Pathway Interaction Database, Reactome and WikiPathway [11]. Several proteomics or metabolomics studies have studied carbon flux [10], substrate transportation [12], growth phase transition [13], substrate [14] and product inhibition [15].

However, none of these studies focused on identifying host cell regulators at enzyme level or investigating process regulators at metabolite level. Moreover, neither proteomics nor metabolomics has been performed in *C. cellulovorans*.

Several genome-scale models, including iCAC490 for *C. acetobutylicum* [16]; [17], iCM925 for *C. beijerinckii* [18], iHN637 for *C. ljungdahlii* [19], iSR432 for *C. thermocellum* [20], and iFS431 for co-cultivated *C. acetobutylicum* and *C. cellulolyticum* [21], have been developed to study solvent selectivity, butanol and ethanol production, cellulose metabolism, and/or cell growth. These models can provide valuable insights into the cellular responses to genetic perturbation or a single process factor, but the lack of experimental, global metabolomics data has limited the accurate output of the modeling [22-24]. A mathematic model that integrates experimental proteomics, metabolomics and cellulosic fermentation data is highly needed.

The objective of this study was to develop a comprehensive understanding how gene manipulation and cellulosic fermentation parameters affect the intracellular metabolism of *C. cellulovorans*. Comparative proteomics of wild type and engineered strain was performed to investigate the key host enzymes, and metabolomics was applied to analyze the intracellular metabolite profiling under different fermentation conditions. A dynamic mathematic model was developed by integrating proteomics, metabolomics and fermentation data, which revealed the regulating enzymes or metabolisms. The key regulators with high impact factor was defined from a further metabolic control analysis. We proposed several strategies to rationally engineer *C. cellulovorans* and cellulosic fermentation, validated two metabolic engineering strategies, and finally significantly improved n-butanol production.

## 2. Materials and methods

### 2.1 Fermentation and samples collection

The wild type *C. cellulovorans* ATCC 743B and mutant *C. cellulovorans adhE2* overexpressing heterologous *adhE2* gene [2] were used to collect Omics and cellulosic fermentation data following our previously published procedures [1]. Unless otherwise noted, the cellulosic butanol fermentations were performed in 2-L stirred-tank bioreactors (FS-01-A; Major science, Saratoga, CA). The bioreactors containing basal medium and carbon source were sterilized at 121°C for 60 min and sparged with nitrogen at 10 mL/min for 3 h for anaerobiosis. The log-phase fresh seed culture in serum bottle was used to inoculate bioreactors with targeted OD<sub>600</sub> of ~0.05. All fermentations were carried out in duplication at Temp 37 °C, agitation 100 rpm, and pH 6.5 controlled with 5 N NaOH. Pretreated cellulose and glucose (control) were used as carbon sources. The bioreactors were sampled at least once a day to monitor cell growth and analyze substrate and products. Cell density was estimated by measuring the OD<sub>600</sub> using a spectrophotometer (Biomate; Thermo Fisher Scientific, Waltham, MA), and the end products, including butanol, butyrate, acetate and ethanol, were titrated using high performance liquid chromatography system (HPLC, Shimadzu, Columbia, MD) equipped with a Rezex RHM-Monosaccharide H<sup>+</sup> column (Phenomenex, Torrance, CA) and a refractive index detector (Shimadzu).

### 2.2 Proteomics

Omics samples were taken at late log phase under all conditions, i.e. at ~18 h for glucose fermentation and ~40 h for cellulose fermentation, and samples were harvested, fresh frozen, and immediately stored at -80 °C. The detailed procedure of protein extraction

and digestion was described in previous publications [10, 25]. Specifically, host cell proteins were extracted using B-PER, denatured using lithium dodecyl sulfate buffer, run into a 10% SDS-PAGE. The entire protein band was excised, equilibrated in 100 mM ammonium bicarbonate, reduced, carbidomethylated, dehydrated and digested with Trypsin Gold (Promega, Madison, WI). The digested peptides were concentrated under vacuum and resolubilized in 0.1% formic acid prior to 1D reverse phase nLC-ESI-MS analysis. A 1260 Infinity nHPLC stack (Agilent, Santa Clara, CA) equipped with a Jupiter C-18 column (300 Å, 5 µm, 75 µm I.D. × 15 cm, Phenomenex) was used to separate the digested peptides. The peptides were eluted using 0%-30% acetonitrile in D.I. H<sub>2</sub>O containing 0.1% formic acid with a flow rate of 0.3 µL/min, and sprayed into a hybrid mass spectrometer (MS, Thermo Orbitrap Velos Pro) equipped with a nano-electrospray source to collect proteomics data in collision-induced dissociation mode. The collected XCalibur RAW files were centroided and converted to MzXML format using ReAdW and converted to mgf files using MzXML2Search. The data were searched with SEQUEST against UniProt-derived proteome databases, the identified proteins were described using UniRef100 ID, and their expression levels were depicted using the normalized spectra count abundance between samples.

### *2.3 Metabolomics*

The metabolomics samples were prepared using the automated MicroLab STAR® system (Hamilton, Reno, NV) [26]. To remove protein, dissociate small molecules bound to protein or trapped in the precipitated protein matrix and recover chemically diverse metabolites, proteins were precipitated with methanol under vigorous shaking for 2 min

followed by centrifugation. The resulting extract was divided and analyzed by two separated reverse phase (RP)/UPLC-MS/MS methods with positive ion mode electrospray ionization (ESI), RP/UPLC-MS/MS with negative ion mode ESI, HILIC/UPLC-MS/MS with negative ion mode ESI. These methods utilized an ACQUITY ultra-performance liquid chromatography (UPLC, Waters, Milford, MA) and a Q-Exactive high resolution/accurate mass spectrometer (Thermo Fisher Scientific, Waltham, MA). Samples were placed briefly on a TurboVap® (Zymark, Midland, ON, Canada) to remove the organic solvent. The sample extracts were stored overnight under nitrogen before preparation for analysis. Raw data was extracted, peak-identified and QC processed using Metabolon's hardware and web-service software utilizing Microsoft's .NET technologies. Compounds were identified by comparison to the library entries of purified standards or recurrent unknown entities. Peaks were quantified using area-under-the-curve. Statistical analyses were performed in ArrayStudio, and programs R or JMP.

#### *2.4 Dynamic model development*

The biochemical reactions in the central metabolic pathway from substrate to end fermentation products were used to develop the dynamic mathematic model, and both intracellular and extracellular metabolites data were used as input for calculation. The following general ordinary differential equation (ODE, Eq 1) was used in this model. The detailed ODEs and representative parameters were summarized in [Supplementary Table S1](#) and [Table S2](#). The K values were collected from other clostridia strains including *C. acetobutylicum* and *C. saccharoperbutylacetonicum* [27]. The Gibb's Free Energy that quantifies the thermodynamic favorability of the listed reactions was also summarized in

[Supplementary Table S2](#). The ODE equations were solved using the software MATLAB R2016a built-in stiff ODE solver, ODE15s.

$$\frac{dM}{dt} = S * R + b \quad (\text{Eq 1})$$

where  $dM/dt$  represents the vector of metabolite concentration time derivatives,  $S$  is the stoichiometric matrix,  $b$  encompasses rate-independent terms such as product transport, and  $R$  is the vector containing all enzyme catalyzed reaction rates, excluding the  $R_{max}$  values which are to be optimized.  $R$  is described using the Michaelis-Menten kinetics (Eq 2).

$$R = \frac{R_{max}[S]}{K+[S]} \quad (\text{Eq 2})$$

where  $R_{max}$  is the maximal reaction rate,  $[S]$  is a metabolite concentration, and  $K$  is the Michaelis constant. The  $R_{max}$  values were generated by linear optimization using the simplex algorithm with MATLAB linear programming function “linprog.” The optimization was constrained by mass, energy, and redox balance ([Supplementary Table S3](#)).

### 2.5 Metabolic control analysis

Metabolic control analysis offers quantitative insight into the control of a metabolic pathway. In this study, control refers to the effect of a change or regulation in one step of the metabolic pathway on a given metabolic flux. The flux control coefficients were calculated using the following equation (Eq 3) as reported [28].

$$C_p^J = \frac{\partial J}{\partial p} * \frac{p}{J} \quad (\text{Eq 3})$$

where  $J$  is the metabolic flux being controlled and  $p$  is the parameter whose control  $J$  is being calculated.

## 2.6 Traditional static model

The traditional model, also known as metabolic flux analysis, was adopted from previous studies using the reactions listed in [Supplementary Table S3 \[29, 30\]](#). It was assumed that there was no net accumulation of intermediates (such as pyruvate and acetyl-CoA), and the energy and redox in these reactions were balanced. The production data of the end fermentation products were used as input to calculate the molar carbon fluxes in the metabolic pathway.

## 2.7 Validation of model analysis

Metabolic cell engineering was performed to validate the modeling output by regulating two of the identified key host cell regulators. Specifically, the plasmids pMTL83151d2-*thl-adhE2* and pMTL83151d2-*hbd-adhE2* were constructed to up-regulate the expression of Thl and Hbd, respectively. The thiolase (*thl*) gene was cloned from *C. acetobutylicum* ATCC 824 and hydroxybutyryl-CoA dehydrogenase (*hbd*) gene was cloned from *C. tyrobutyricum* ATCC 25755. The thiolase promoter ( $P_{thl}$ ) cloned from *C. tyrobutyricum* was used for heterologous genes overexpression. The plasmid pMTL83151d2-*adhE2* was used as a backbone to construct the Thl and Hbd overexpressing plasmids using the In-Fusion HD Cloning Kit (TaKaRa Clontech, Japan). The restriction sites of *C. cellulovorans* Cce743I/II (GACGC and CCAGG) were completely removed from the plasmids by synonymous mutations (unpublished method). The strains, plasmids, and primers are summarized in [Supplementary Table S4](#). The pMTL83151d2-*thl-adhE2* and pMTL83151d2-*hbd-adhE2* plasmids were transformed into

*C. cellulovorans* as previously described [2], which generated *C. cellulovorans thl-adhE2* and *C. cellulovorans hbd-adhE2* mutants. Fermentations with these two mutants were then studied to validate model predictions. All strains were maintained in DSMZ 520 medium supplemented with glucose or cellulose (microcrystalline, Alfa Aesar), and the same medium was used to run cellulosic fermentation.

### 3. Results

#### 3.1 Fermentation products

In this study, the cellulosic fermentations by wild type (control) and the previously engineered mutant of *C. cellulovorans adhE2* were carried out in 2-L stirred-tank bioreactors at pH 6.5 and Temp 37 °C. The fermentation using glucose as carbon source was also performed as control to study the effect of substrate on cellular metabolism. The fermentation kinetic profiles are described in [Figure 1](#), and the summarized fermentation data, including cell growth, end products concentration, yield and productivity, are presented in [Table 1](#).

As expected, the wild type strain produced 4.51 g/L butyrate and 1.37 g/L acetate but no butanol and ethanol from cellulose. The mutant *C. cellulovorans adhE2* produced 1.55 g/L butanol, 0.16 g/L butyrate, 0.85 g/L ethanol and 3.65 g/L acetate from cellulose, and 3.07 g/L butanol, 0.73 g/L butyrate, 1.99 g/L ethanol and 2.65 g/L acetate from glucose. As compared to glucose, cellulose shifted more carbon flux to acetate, inhibited butyrate production with lower concentration, yield and selectivity, and reduced the final concentration and productivity of ethanol by around 50%. The C<sub>4</sub>/C<sub>2</sub> ratio in the fermentation using glucose and cellulose by mutant *C. cellulovorans adhE2* was 0.534 and

0.344, respectively. The C4/C2 ratio in the cellulosic fermentation by wild type was 1.567. The synthesis of *adhE2* gene not only generated n-butanol, but also produced ethanol, so more carbon flux was shifted from C4 to C2 in the mutant. It was also found that the fermentation time was extended from 60 h using glucose as substrate to 120 h using cellulose as substrate.

### 3.2 Global host cell protein expression map and intracellular metabolite profiling

To understand how metabolic engineering and fermentation conditions change host cell protein expression and regulate intracellular metabolism, we ran proteomics and metabolomics analysis using cell samples collected from CBP fermentation. We analyzed both global profiling and central metabolism to identify key regulators for high n-butanol production. The complete datasets of the detected 1,820 proteins in *C. cellulovorans*, including raw MS data, summarized data, search parameters, and reference database with statistical analysis, were deposited in the public repository PeptideAtlas (<http://www.peptideatlas.org/>, accession no. PASS01153).

The global proteomics and pairwise analysis results are described in [Figure 2](#). In this proteomics study, total 624 proteins with  $\leq 1\%$  False Discovery Rate (FDR) were quantitated. These proteins were functionally classified into three gene ontologies through Software Tool for Rapid Annotation of Proteins (STRAP) which was developed by Cardiovascular Proteomics Center of Boston University School of Medicine (Boston, MA) for automatic protein annotation [31]. Of all the detected proteins, there were 493 proteins involved in biological process, 324 proteins belonging to cellular components, and 792 proteins responding to molecular function. Around 49% of the molecular function proteins

played important roles in catalysis. The same protein could involve in multiple functions. Pairwise analysis was performed to understand how gene manipulation and fermentation substrates changed the expression of intracellular proteins. The results showed that the expression of 42 proteins and 85 proteins were changed significantly (i.e. >50%) by the synthesized butanol pathway and fermentation substrates, respectively. The majority of the changes was observed in the proteins that were functional in cellular process (16 in Pair 1 and 37 in Pair 2), localization (6 and 10), cytoplasm (8 and 15), binding (16 and 46), and catalytic activity (24 and 44). The Pair 1 was defined as mutant strain vs wild type (baseline) and Pair 2 was defined as cellulose vs. glucose (baseline). Generally, the substrate showed high impact on host cell proteins expression than the synthesis of butanol pathway.

The results of global metabolomics and pairwise analysis are summarized in [Figure 3](#). We detected and quantitated total 474 intracellular primary and secondary metabolites in *C. cellulovorans*. These metabolites were grouped into seven classes, where amino acid, carbohydrate and lipid counted for >70%. The pairwise analysis revealed that only 16 metabolites were significantly up- or down-regulated by butanol pathway synthesis, but 246 metabolites were significantly regulated by cellulose. Interestingly, the concentration of several metabolites increased by >1,000 folds by cellulose, including imidazole propionate involved in histidine metabolism and butanol tolerance [[32](#)], formiminoglutamate involved in histidine metabolism, tyramine involved in tyrosine pyruvate metabolism, and trans-urocanate derived from histidine [[33](#)]. The level of some metabolite decreased by >10 folds by cellulose, such as glutamate facilitating Clostridial colonization [[34](#)], gamma-glutamylglutamine as an intermediate in protein catabolism and cell signaling, diaminopimelate as a cell wall component, and gamma-glutamylcysteine

involved in glutamate metabolism. The intracellular level of diaminopimelate increased by 102 folds and N-acetyl-cadaverine (unclear function) increased by 17 folds in the mutant *C. cellulovorans adhE2* compared to wild type.

### 3.3 Key enzymes in cellulosome, glycolysis, and central pathway

In addition to global analysis, we investigated all the enzymes metabolites involved in the metabolism from cellulose to end fermentation products. Cellulosic degradation requires the interaction of multiple cellulosome [35], and the expression of 34 cellulases were grouped in the [Supplementary Table S5](#) based on sequence similarity [36]. It is found that most of the detected cellulases were significantly up-regulated in the cellulosic fermentation. The glycoside hydrolase, glucanase,  $\beta$ -xylanase and cellulosome docking enzymes were significantly up-regulated by butanol production and cellulose substrate ([Table 2](#)). These results suggested that we could improve cellulose metabolism efficiency by overexpressing 6-P- $\beta$ -glucosidase (Bgl) and Endoglucanase B (EngB) via metabolic engineering. We also noticed that most cellulases had no expression in glucose fermentation except a few enzymes, such as glycoside hydrolase and glucanase, and their expression was very low, which is consistent with previous publication [3].

The expression of enzymes catalyzing glycolysis and central metabolism from pyruvate to end fermentation products are reported in [Table 3](#). The butanol formation reduced the expression of ATP-dependent phosphofructokinase (Pfk1), fructose-1,6-bisphosphate aldolase (Aldo), and ADP-dependent phosphoglycerate kinase (Pgk). These data indicated that the up-regulation of these three proteins could improve the glycolytic efficiency. In the central pathway to form n-butanol, the expression level of thiolase (Thl)

that catalyzes “Acetyl-CoA  $\rightarrow$  Acetoacetyl-CoA”, crotonase (Crt) catalyzing “3-Hydroxybutyryl-CoA  $\rightarrow$  Crotonyl-CoA” and the electron transfer flavoprotein A/B (EtfA/B) converting “Crotonyl-CoA  $\rightarrow$  Butyryl-CoA” in the cellulosic fermentation by mutant *C. cellulovorans* adhE2 were lower than the cellulosic fermentation by wild type and the glucose fermentation by mutant. These proteomics data explained the reduced C4/C2 ratio, yield and selectivity of butanol by AdhE2 synthesis and substrate change. However, we could improve cellulosic n-butanol production by up-regulating the expression of Thl and Crt. In addition, the hydrogenase (Hyd) involved in the hydrogen production and NADH production showed the lowest expression (MS of 0.26) in cellulosic fermentation by mutant *C. cellulovorans* adhE2 as compared to the cellulosic fermentation by wild type (MS of 3.03) and the glucose fermentation by mutant (MS of 5.87).

In the ethanol formation pathway, wild type *C. cellulovorans* expressed native NAD(P)H-dependent aldehyde-alcohol dehydrogenase (Adh) at high level (MS of up to 32), so the synthesis of AdhE2 with high expression (MS of up to 295) in *C. cellulovorans* adhE2 mutant formed a complete and effective pathway “Acetyl-CoA  $\rightarrow$  Acetylaldehyde  $\rightarrow$  Ethanol”, which explained the high production of ethanol in fermentation (Fig. 1). In the butanol production pathway, the homogenous NAD(P)H-dependent butanol dehydrogenase (Bdh) was not detected in all the proteomic samples. The genome database of *C. cellulovorans* (GenBank: CP002160.1) also shows that *bdh* gene is missed. Although AdhE2 enzyme can catalyze the reaction “Butyryl-CoA  $\rightarrow$  Butanol”, the lack of Bdh repressed butanol production as compared to ethanol. The wild type *C. cellulovorans* had no *adhE2* gene, so the solvent production was zero in fermentation.

### 3.4 Model integrating proteomics, metabolomics and fermentation data

Proteomics enabled us to identify the enzymes that could be the potential candidates for gene manipulation. To further evaluate the catalytic efficiency of these enzymes and understand their roles in regulating the central metabolic pathway to generate n-butanol, this study, for the first time, integrated the experimental data from proteomics, metabolomics and cellulosic fermentation using *C. cellulovorans*.

The titration data of fermentation end products and intracellular metabolites (Supplementary Table S6) were used to analyze the reaction rates of the bioreactions in central pathway. As shown in Table 4, the calculated maximal reaction rates (cRmax) showed strong correlation with the expression level of their catalytic enzymes in four bioreactions, including “Pyruvate  $\rightarrow$  Acetyl-CoA”, “Acetyl-CoA  $\rightarrow$  Acetoacetyl-CoA”, “3-hydroxyacyl-CoA  $\rightleftharpoons$  Crotonyl-CoA”, and “Crotonyl-CoA  $\rightarrow$  Butyryl-CoA”. The enzymes Thl, Crt and EtfA/B showing reduced expression in cellulosic butanol fermentation by mutant *C. cellulovorans* also had lower cRmax. The expression of Hbd catalyzing “Acetoacetyl-CoA  $\rightarrow$  3-Hydroxybutyryl-CoA”, one key bioreaction to drive carbon flux from C2 to C4, was not available. The metabolomics data showed that the ratio of intracellular acetyl-CoA was 7:34:1 among cellulosic fermentation by wild type, cellulosic fermentation by mutant and glucose fermentation by mutant, while the ratio of intracellular pyruvate was 0.8:0.6:1. Very interestingly, the concentration of some amino acids, such as glutamate, was significantly reduced in cellulosic fermentation by the mutant, indicating that feeding amino acids could improve the efficiency of cellular metabolism.

Our model also revealed the reaction rates of acids production and assimilation in the reversible reactions “Acetyl-CoA  $\rightleftharpoons$  Acetate” and “Butyryl-CoA  $\rightleftharpoons$  Butyrate”. In cellulose fermentation, the higher ratio of acetate formation rate/assimilation rate, i.e. 8.85 by mutant vs. 0.41 by wild type, explained the higher acetate production, i.e. 3.65 g/L by mutant vs. 1.37 g/L by wild type. The lower ratio of butyrate formation rate/assimilation rate caused lower butyrate production. In glucose fermentation by mutant, the cRmax values in acids formation pathways were not consistent with acids production. The root cause could be the inaccurate titration of acetyl-CoA and butyryl-CoA that were unstable and very sensitive to the sample handling conditions. The lower expression of Thl and Crt in mutant *C. cellulovorans adhE2* reduced the carbon distribution from C2 to C4, so the ratio of C2 products/C4 products was higher, i.e. 2.63 vs. 1.22.

### 3.5 Host cell regulators identification

Metabolic control analysis could offer quantitative insight into the regulation in metabolic pathway. In this case, the control referred to the effect of one-step change in the metabolic pathway on a specific target. The dynamic model developed in this study was used to perform metabolic control analysis to evaluate the possible regulators identified in proteomics and metabolomics, including the substrate assimilation, formation of byproducts (ethanol, acetate and butyrate), and four key enzymes (Thl, Hbd, Crt and EtfA/B). The goal is to narrow down the host cell regulators for metabolic engineering. [Figure 4](#) shows the quantitative analysis how these regulators affect butanol production. In glucose fermentation, the four enzymes had relatively high impact with value of 0.17 (Thl), 0.26 (Hbd), 0.15 (Crt) and 0.19 (EtfA/B). In cellulosic fermentation, Thl and substrate

assimilation showed the highest impact factors of 0.58 and 0.44, and the ethanol production, acetate production, acetate assimilation, and Hbd had impact factors of -0.18, -0.22, 0.13 and 0.08. The positive impact factor indicated upregulation, negative impact factor indicated downregulation, and manipulating the high-impact regulators could achieve higher cellulosic n-butanol production.

### 3.6 Comparison between dynamic and static models

The dynamic model developed in this study integrated the intracellular proteomics, metabolomics and fermentation data. The traditional static model used the end fermentation products with the assumption that there was no accumulation of intermediates [24, 29, 37]. The equations in central metabolic pathway were summarized in [Supplementary Table S3](#). The metabolic flux was calculated using both static and dynamic models and presented in [Fig. 5](#).

In dynamic modeling, we observed higher flux in most pathways in the glucose fermentation by mutant *C. cellulovorans adhE2* except butyrate production, and the flux data were consistent with the final concentrations of fermentation products. The reaction “Acetoacetyl-CoA  $\rightarrow$  3-hydroxybutyryl-CoA” showed a high flux in the cellulosic fermentation by the mutant *C. cellulovorans adhE2*, indicating the upregulation of Hbd. The static modeling showed that the flux distribution in most reactions was similar for the cellulosic and glucose fermentations by mutant. As compared to traditional model, the metabolic flux calculated using our dynamic model was more accurate due to the facts that: 1) both intracellular and extracellular metabolites were used in calculation; 2) the effect of enzyme expression on reaction rate was considered; 3) the acids assimilation was

integrated into the model; 4) the redox balance was adjusted by proportioning hydrogen production with substrate assumption and the calculated reaction rate in “Pyruvate  $\rightarrow$  Acetyl-CoA + H<sub>2</sub> + CO<sub>2</sub>” was consistent with the intracellular hydrogenase expression (Table 3).

### 3.7 Model validation via rationally metabolic engineering

The metabolically engineered new-generation mutants, i.e. *C. cellulovorans thl-adhE2* and *C. cellulovorans hbd-adhE2*, were generated and characterized in CBP fermentation in order to validate the output of our dynamic modeling and metabolic control analysis. The kinetic profiles of cellulosic fermentation are described in Fig. 6A-6D. It is showed that the butanol production was significantly improved by *C. cellulovorans thl-adhE2* and *C. cellulovorans hbd-adhE2* with final concentration of 2.10 g/L and 1.98 g/L, respectively, as compared to the first-generation mutant *C. cellulovorans adhE2* with final concentration of 1.55 g/L. The C<sub>4</sub>/C<sub>2</sub> ratios were significantly increased: the values were 1.01 and 0.78 in glucose and cellulose fermentation by mutant *C. cellulovorans thl-adhE2*, and 0.85 and 0.62 by mutant *C. cellulovorans hbd-adhE2*. Fig. 6E and 6F reveal the change of butanol yield, where *C. cellulovorans adhE2* < *C. cellulovorans thl-adhE2* < *C. cellulovorans hbd-adhE2* in glucose fermentation, and *C. cellulovorans adhE2* < *C. cellulovorans hbd-adhE2* < *C. cellulovorans thl-adhE2* in cellulose fermentation. The result was consistent with the impact factor prediction described in Section 3.5.

## 4. Discussion

### 4.1 Solvent production and substrate played important role

This study, for the first time, applied the mathematic model integrating multi-Omics data to develop an in-depth understanding of intracellular metabolism in *C. cellulovorans*. Previous study reported that solvent production affected the expression of cellulosome components [15] and inhibited the cellulase expression [38]. As an intermediate of cellulose hydrolysis, cellobiose was found to inhibit the expression of cellobiohydrolases and induce the expression of glucosidase [39, 40]. Previous studies also showed that alcohol inhibited the glycolysis in consolidating fermentation, but the inhibition was alleviated when using glucose as substrate [10, 15]. All these studies showed that solvent products and substrate could significantly change the metabolism of clostridia, so this study investigated the effect of synthesized butanol pathway and cellulose substrate on the host cell proteins, intracellular metabolism and cellulosic fermentation.

### 4.2 Effect of carbon source on metabolic control coefficient

In this study, both cellulose and glucose were used as substrate in the cellulosic n-butanol fermentation by mutant *C. cellulovorans adhE2*. These two substrates showed different fermentation production of acids and solvents, expression of intracellular enzymes, level of intracellular metabolites, and thereby metabolic flux control coefficient. Differently from glucose fermentation, the high impact of cellulose assimilation indicated the important role of cellulase in the conversion from cellulose to glucose that is easy to ferment. The ethanol production that consumed NAD(P)H, an important cofactor in the production of butanol, showed negative impact on butanol production. The lower

expression of NAD<sup>+</sup>-dependent triosephosphate isomerase (Tpi) and hydrogenase (Hyd) in cellulosic fermentation caused unbalanced redox and resulted in the low production of solvents (ethanol and butanol). Acetate had little impact on n-butanol production, but the acetate production had negative impact and acetate assimilation showed positive impact on cellulosic n-butanol production. We also found the increased expression of ATP-dependent Pfk1 and decreased expression of ADP-dependent Pgc, acetate kinase (Ack) and butyrate kinase (Buk). All these results indicated a high need for easy to ferment carbon sources in cellulose fermentation, and more ATP is needed to rebalance the energy. In glucose fermentation, Thl, Hbd, Crt and EtfA/B had similar range of impact while Thl showed significantly higher impact on butanol production. The high impact of Thl could be caused by the significant higher acetate assimilation and lower acetate production in cellulose fermentation.

#### *4.3 Novel modeling integrating experimental multi-Omics and fermentation data*

This study developed the first mathematic model to integrate the experimental proteomics data, metabolomics data and fermentation data of *C. cellulovorans*. Different from previous modeling [24, 27, 41, 42], we used the experimental data to simulate and identify the potential cell and process regulators, and also performed metabolic control analysis to define the most important regulators. In addition, our dynamic modeling filled the gaps in proteomics and metabolomics due to the limitation of available LC/MS technologies and databases. The capability to calculate metabolic reaction rates, metabolic flux and the impact factors of key enzymes or reactions enabled the dynamic model to

guide the rational metabolic engineering. Moreover, we could expand this dynamic model to analyze the genome-scale metabolic network in future.

#### 4.4 Strategies of rational metabolic engineering

As compared to single Omics, the integration of proteomics or metabolomics via the dynamic model offered us a powerful approach to quantitatively analyze the intracellular metabolism in *C. cellulovorans*. The capability to identify key host cell regulators and bioprocessing regulators by the integrated modeling could guide us to rationally design metabolic engineering strategies.

Firstly, the proteomics data showed that the expression of Thl, Crt and EtfA/B was significantly down-regulated in the cellulosic fermentation by mutant *C. cellulovorans*. The dynamic modeling demonstrated that the reactions catalyzed by these three enzymes and Hbd had low reaction rates. The metabolomics data also showed a significant higher accumulation of acetyl-CoA and reduced C4/C2 in the cellulosic fermentation by mutant, indicating the low catalyzing efficiency of Thl in the conversion from C2 to C4. More importantly, the metabolic control analysis showed that Thl had the highest effect on butanol production. Therefore, we proposed to overexpress Thl (and Hbd) to shift the carbon from C2 to C4.

Secondly, *C. cellulovorans* expressed a certain level of Adh but no expression of Bdh, the complete ethanol pathway (Adh-AdhE2) in mutant strain produced a significant amount of ethanol. The metabolic control analysis demonstrated that ethanol production had a high negative impact factor. To reduce ethanol production, we proposed to synthesize a new heterologous pathway as a substitution of AdhE2, i.e. *ald-bdh* (aldehyde

dehydrogenase-butanol dehydrogenase) pathway that catalyzes the reaction “Butyryl-CoA → Butyraldehyde → Butanol” with higher selectivity.

Thirdly, the cellulosic fermentation by mutant produced a high level of acetate and the modeling indicated a high reaction rate in acetate production. Therefore, we proposed to down-regulate the *pta-ack* pathway to reduce acetate production. Because ATP was produced in the acetate formation pathway, we would not suggest knocking out the *pta* or *ack* gene completely. In addition, the metabolic control analysis indicated that acetate assimilation had important impact on butanol production, so we proposed to engineer the consolidated bioprocessing by adding acetate supplement in the basal fermentation medium.

Fourthly, the low expression of Pfk, Aldo and Pgk suggested that the glycolytic efficiency could be up-regulated to benefit fermentation production. The cellulosic efficiency could also be improved by overexpressing 6-P- $\beta$ -glucosidase and Endoglucanase B via metabolic cell engineering.

Finally, amino acids involved in the regulation of cellular metabolism and cell growth, so feeding amino acids supplement could improve n-butanol production. Butanol production consumes reducing power NAD(P)H, so we could hypothesize that the higher production of cellulosic butanol needs additional reducing power supply in basal medium, such as methyl viologen hydrate [43, 44].

#### 4.5. Rational metabolic engineering

With the guidance of our dynamic model, we identified Thl and Hbd as the most important butanol production regulators for cellulose and glucose fermentation and

validated it by constructing two mutants, *C. cellulovorans thl-adhE2* and *C. cellulovorans hbd-adhE2*. As expected, these two rationally engineered mutants significantly improved butanol concentration and their yields as compared to the previous mutant *C. cellulovorans adhE2*. It is clear that that our multi-Omics-based dynamic model accurately predicted the key host cell regulators and successfully guided the rational metabolic engineering to boost n-butanol production.

It is noted that both *C. cellulovorans thl-adhE2* and *C. cellulovorans hbd-adhE2* produced higher level of butyrate because the carbon flux was shifted from acetyl-CoA to butyryl-CoA by the upregulation of Thl and Hbd. To further increase the butanol production, we can re-distribute the carbon flux from butyrate to butanol by down-regulating the pathway of “Butyryl-CoA → Butyrate” and/or boost the reducing power via optimizing the fermentation process, for example, with supplement of an artificial electron carrier methyl viologen hydrate [29].

In addition, the newly engineered mutants in this study had reduced productivity, which may be caused by the burden of high protein expression or inhibition of high n-butanol production. We could overcome it via cell adaptation to gradually increased end-product or the application of semi-continuous CBP with immobilized cells [45] or cell recycling [46].

## 5. Conclusions

This study, for the first time, developed a comprehensive understanding of the interaction between cellular metabolism in *C. cellulovorans* and CBP parameters in cellulosic n-butanol production. This was also the first time to collect the global proteomics

data and metabolomics data of the cellulosic *C. cellulovorans* under different fermentation conditions. Another novelty of this study was to develop and validate a dynamic mathematic model that integrates the proteomics, metabolomics and fermentation data, which enabled identifying the CBP regulators at both cellular and processing levels. The proposed rationally metabolic engineering strategies will benefit future cellulosic n-butanol production from biomass.

### **Acknowledgements**

The proteomic analysis was conducted at the UAB Comprehensive Cancer Center Mass Spectrometry/Proteomics (MSP) Shared Facility. The metabolomic analysis was conducted at Metabolon, Inc. The authors would like to acknowledge Dr. Edward J. Wolfrum from the National Renewable Energy Laboratory for the substrate compositional analysis.

### **Funding**

This work was supported by the Department of Energy - Office of Energy Efficiency and Renewable Energy (grant number DE-EE 0007005, 2015).

## References

1. Ou, J., et al., *Process engineering of cellulosic n -butanol production from corn-based biomass using Clostridium cellulovorans*. *Process Biochemistry*, 2017. **62**: p. 144-150.
2. Yang, X., M. Xu, and S.T. Yang, *Restriction modification system analysis and development of in vivo methylation for the transformation of Clostridium cellulovorans*. *Appl Microbiol Biotechnol*, 2015.
3. Tamaru, Y., et al., *Genome sequence of the cellulosome-producing mesophilic organism Clostridium cellulovorans 743B*. *J Bacteriol*, 2010. **192**(3): p. 901-2.
4. Tamaru, Y., et al., *Comparative genomics of the mesophilic cellulosome-producing Clostridium cellulovorans and its application to biofuel production via consolidated bioprocessing*. *Environ Technol*, 2010. **31**(8-9): p. 889-903.
5. Feinberg, L., et al., *Complete genome sequence of the cellulolytic thermophile Clostridium thermocellum DSM1313*. *J Bacteriol*, 2011. **193**(11): p. 2906-7.
6. Janssen, H., et al., *A proteomic and transcriptional view of acidogenic and solventogenic steady-state cells of Clostridium acetobutylicum in a chemostat culture*. *Appl Microbiol Biotechnol*, 2010. **87**(6): p. 2209-26.
7. Sivagnanam, K., et al., *Shotgun proteomic monitoring of Clostridium acetobutylicum during stationary phase of butanol fermentation using xylose and comparison with the exponential phase*. *J Ind Microbiol Biotechnol*, 2012. **39**(6): p. 949-55.
8. Burton, E. and V.J. Martin, *Proteomic analysis of Clostridium thermocellum ATCC 27405 reveals the upregulation of an alternative transhydrogenase-malate*

- pathway and nitrogen assimilation in cells grown on cellulose. Can J Microbiol*, 2012. **58**(12): p. 1378-88.
9. Comba Gonzalez, N., et al., *Protein identification in two phases of 1,3-propanediol production by proteomic analysis. J Proteomics*, 2013. **89**: p. 255-64.
  10. Ma, C., et al., *Comparative proteomics analysis of high n-butanol producing metabolically engineered Clostridium tyrobutyricum. Journal of Biotechnology*, 2015. **193**: p. 108-119.
  11. Buchel, F., et al., *Path2Models: large-scale generation of computational models from biochemical pathway maps. BMC Syst Biol*, 2013. **7**: p. 116.
  12. Mao, S., et al., *Comparative analysis on the membrane proteome of Clostridium acetobutylicum wild type strain and its butanol-tolerant mutant. Mol Biosyst*, 2011. **7**(5): p. 1660-77.
  13. Rydzak, T., et al., *Growth phase-dependant enzyme profile of pyruvate catabolism and end-product formation in Clostridium thermocellum ATCC 27405. J Biotechnol*, 2009. **140**(3-4): p. 169-75.
  14. Raut, M.P., et al., *Quantitative proteomic analysis of the influence of lignin on biofuel production by Clostridium acetobutylicum ATCC 824. Biotechnol Biofuels*, 2016. **9**: p. 113.
  15. Yang, S., et al., *Clostridium thermocellum ATCC27405 transcriptomic, metabolomic and proteomic profiles after ethanol stress. BMC Genomics*, 2012. **13**: p. 336.

16. McAnulty, M.J., et al., *Genome-scale modeling using flux ratio constraints to enable metabolic engineering of clostridial metabolism in silico*. BMC Syst Biol, 2012. **6**: p. 42.
17. Dash, S., C.Y. Ng, and C.D. Maranas, *Metabolic modeling of clostridia: current developments and applications*. FEMS Microbiol Lett, 2016. **363**(4).
18. Milne, C.B., et al., *Metabolic network reconstruction and genome-scale model of butanol-producing strain Clostridium beijerinckii NCIMB 8052*. BMC Syst Biol, 2011. **5**: p. 130.
19. Nagarajan, H., et al., *Characterizing acetogenic metabolism using a genome-scale metabolic reconstruction of Clostridium ljungdahlii*. Microb Cell Fact, 2013. **12**: p. 118.
20. Roberts, S.B., et al., *Genome-scale metabolic analysis of Clostridium thermocellum for bioethanol production*. BMC Syst Biol, 2010. **4**: p. 31.
21. Ma, C., et al., *Comparative proteomics analysis of high n-butanol producing metabolically engineered Clostridium tyrobutyricum*. J Biotechnol, 2015. **193**: p. 108-19.
22. Kim, W.J., H.U. Kim, and S.Y. Lee, *Current state and applications of microbial genome-scale metabolic models*. Current Opinion in Systems Biology, 2017. **2**: p. 10-18.
23. Martien, J.I. and D. Amador-Noguez, *Recent applications of metabolomics to advance microbial biofuel production*. Curr Opin Biotechnol, 2017. **43**: p. 118-126.

24. Millat, T. and K. Winzer, *Mathematical modelling of clostridial acetone-butanol-ethanol fermentation*. Appl Microbiol Biotechnol, 2017. **101**(6): p. 2251-2271.
25. Xu, N., et al., *Comparative proteomic analysis of three Chinese hamster ovary (CHO) host cells*. Biochemical Engineering Journal, 2017. **124**: p. 122-129.
26. Bridgewater Br, E.A.M., *High Resolution Mass Spectrometry Improves Data Quantity and Quality as Compared to Unit Mass Resolution Mass Spectrometry in High-Throughput Profiling Metabolomics*. Journal of Postgenomics Drug & Biomarker Development, 2014. **04**(02).
27. Shinto, H., et al., *Kinetic modeling and sensitivity analysis of acetone-butanol-ethanol production*. J Biotechnol, 2007. **131**(1): p. 45-56.
28. Cortassa, S., et al., *Control and regulation of mitochondrial energetics in an integrated model of cardiomyocyte function*. Biophys J, 2009. **96**(6): p. 2466-78.
29. Du, Y., et al., *Metabolic process engineering of Clostridium tyrobutyricum Deltaack-adhE2 for enhanced n-butanol production from glucose: effects of methyl viologen on NADH availability, flux distribution, and fermentation kinetics*. Biotechnol Bioeng, 2015. **112**(4): p. 705-15.
30. Ma, C., et al., *High production of butyric acid by Clostridium tyrobutyricum mutant*. Frontiers of Chemical Science and Engineering, 2015. **9**(3): p. 369-375.
31. Bhatia, V.N., et al., *Software tool for researching annotations of proteins: open-source protein annotation software with data visualization*. Anal Chem, 2009. **81**(23): p. 9819-23.

32. Xu, M., et al., *Engineering Clostridium acetobutylicum with a histidine kinase knockout for enhanced n-butanol tolerance and production*. Appl Microbiol Biotechnol, 2015. **99**(2): p. 1011-22.
33. H.Hug, D., D. D.Dunkerson, and J. K.Hunter, *The degradation of l-histidine and trans and cis-urocanic acid by bacteria from skin and the role of bacterial cis-urocanic acid isomerase*. Journal of Photochemistry and Photobiology B: Biology, 1999. **50**(1): p. 66-73.
34. Girinathan, B.P., et al., *Importance of Glutamate Dehydrogenase (GDH) in Clostridium difficile Colonization In Vivo*. PLOS ONE, 2016. **11**(7): p. e0160107.
35. Kumar, R., S. Singh, and O.V. Singh, *Bioconversion of lignocellulosic biomass: biochemical and molecular perspectives*. J Ind Microbiol Biotechnol, 2008. **35**(5): p. 377-391.
36. Lombard, V., et al., *The carbohydrate-active enzymes database (CAZy) in 2013*. Nucleic Acids Res, 2014. **42**(Database issue): p. D490-5.
37. Song, H., et al., *Modeling of batch experimental kinetics and application to fed-batch fermentation of Clostridium tyrobutyricum for enhanced butyric acid production*. Biochemical Engineering Journal, 2010. **53**(1): p. 71-76.
38. Ghosh, P., N.B. Pamment, and W.R.B. Martin, *Simultaneous saccharification and fermentation of cellulose: effect of  $\beta$ -d-glucosidase activity and ethanol inhibition of cellulases*. Enzyme and Microbial Technology, 1982. **4**(6): p. 425-430.
39. Adav, S.S., A. Ravindran, and S.K. Sze, *Quantitative proteomic analysis of lignocellulolytic enzymes by Phanerochaete chrysosporium on different lignocellulosic biomass*. J Proteomics, 2012. **75**(5): p. 1493-504.

40. Xiao, Z., et al., *Effects of Sugar Inhibition on Cellulases and  $\beta$ -Glucosidase During Enzymatic Hydrolysis of Softwood Substrates*, in *Proceedings of the Twenty-Fifth Symposium on Biotechnology for Fuels and Chemicals Held May 4–7, 2003, in Breckenridge, CO*, M. Finkelstein, et al., Editors. 2004, Humana Press: Totowa, NJ. p. 1115-1126.
41. Millat, T., et al., *Integrative modelling of pH-dependent enzyme activity and transcriptomic regulation of the acetone-butanol-ethanol fermentation of *Clostridium acetobutylicum* in continuous culture*. *Microb Biotechnol*, 2013. **6**(5): p. 526-39.
42. Thorn, G.J. and J.R. King, *Modelling the role of CtfA/B in reverse shift continuous culture experiments of *Clostridium acetobutylicum**. *Mathematical Biosciences*, 2016. **276**: p. 101-113.
43. Wang, Y., K.-Y. San, and G.N. Bennett, *Cofactor engineering for advancing chemical biotechnology*. *Current Opinion in Biotechnology*, 2013. **24**(6): p. 994-999.
44. Ou, J., et al., *High butanol production by regulating carbon, redox and energy in *Clostridia**. *Frontiers of Chemical Science and Engineering*, 2015. **9**(3): p. 317-323.
45. Lu, C., et al., *Fed-batch fermentation for n-butanol production from cassava bagasse hydrolysate in a fibrous bed bioreactor with continuous gas stripping*. *Bioresour Technol*, 2012. **104**: p. 380-7.
46. Zheng, J., et al., *Continuous butanol fermentation from xylose with high cell density by cell recycling system*. *Bioresour Technol*, 2013. **129**: p. 360-5.

**Table 1.** Summary of cellulosic n-butanol fermentation by wide type and mutant of *C. cellulovorans*.

Parameters	Wild type	Mutant	
	Cellulose	Cellulose	Glucose
<b>Concentration (g/L)</b>			
Butanol	0.00±0.00	1.55±0.06	3.07±0.23
Butyrate	4.51±0.39	0.39±0.34	0.73±0.13
Ethanol	0.00±0.00	0.85±0.06	1.99±0.20
Acetate	1.37±0.11	3.65±0.02	2.65±0.38
<b>Yield (g/g-glucose)</b>			
Butanol	0.00±0.00	0.11±0.05	0.12±0.01
Butyrate	0.35±0.02	0.07±0.03	0.03±0.001
Ethanol	0.00±0.00	0.08±0.001	0.08±0.01
Acetate	0.12±0.01	0.24±0.02	0.10±0.01
<b>Productivity (g/l/h)</b>			
Butanol	0.000±0.000	0.019±0.002	0.105±0.009
Butyrate	0.048±0.004	0.015±0.009	0.007±0.001
Ethanol	0.000±0.000	0.017±0.005	0.050±0.007
Acetate	0.017±0.004	0.039±0.005	0.158±0.014
<b>Selectivity (g/g-total product)</b>			
Butanol	0.00±0.00	0.26±0.03	0.35±0.03
Butyrate	0.70±0.04	0.05±0.04	0.09±0.01
Ethanol	0.00±0.00	0.13±0.04	0.23±0.04
Acetate	0.30±0.04	0.56±0.03	0.34±0.00

**Table 2.** The cellulolytic enzymes with significant expression identified in proteomics.

Accession #	Enzymes		Spectral Count (Expression)		
	Name	Gene	WT cellulose	Mutant cellulose	Mutant glucose
D9SV64	Cellulase	<i>cel</i>	7.70±0.89	52.22±15.66	0.00±0.00
D9SRM3	Glycoside hydrolase 5	<i>gh5</i>	9.47±3.78	18.19±6.55	0.00±0.00
D9SQT2	Glycoside hydrolase 9	<i>gh9</i>	13.41±13.54	42.69±17.05	0.00±0.00
D9SMN8	Glycoside hydrolase 31	<i>gh31</i>	0.00±0.00	2.12±1.56	0.00±0.00
D9SS72	Glycoside hydrolase 48	<i>gh48</i>	47.23±9.64	81.71±17.06	4.01±1.66
D9SSR5	6-P-β-glucosidase	<i>bgl</i>	8.81±1.66	16.02±3.04	0.00±0.00
P28621	Endoglucanase B	<i>engB</i>	3.48±3.30	19.20±6.81	0.00±0.00
D9SS70	Glycoside hydrolase 9*	<i>gh9</i>	40.02±19.00	112.90±26.98	5.22±4.24
D9SS71	Glucanase	<i>glu</i>	31.01±10.04	46.76±7.43	0.00±0.00
D9SST3	β-xylanase	<i>xyn</i>	30.52±15.53	119.00±26.14	0.24±0.41
D9SUC4	Dockerin type 1 ( <i>dk1</i> )*	Clocel_3193	4.51±7.82	27.17±13.32	0.00±0.00
D9SWN8	Dockerin type 1 ( <i>dk1</i> )*	Clocel_3650	2.06±1.80	12.96±1.89	0.00±0.00
D9SQT1	Dockerin type 1 ( <i>dk1</i> )*	Clocel_2575	0.97±1.68	5.92±4.06	0.00±0.00

**Note:**

\*: The proteins were predicted under the same cluster. They have similar functions but different sequences.

1) The proteomics cell samples were collected from the triplicated fermentation.

2) Only representative enzymes that showed significant change in expression level, i.e. MS count ratio of mutant cellulose/WT cellulose > 2 (p<0.05), were presented.

3) A complete proteomics data of the cellulolytic enzymes, enzymes in glycolysis and enzymes in central metabolic pathway from pyruvate to end products are shown in supplemental Tables.

4) All raw MS data, search parameters, search database and summarized data with statistic analysis were deposited to a public repository PeptideAtlas (<http://www.peptideatlas.org/>, accession no. PASS01153).

**Table 3.** Expression of enzymes involved in glycolysis and central metabolic pathways.

Function	Protein			Spectral Count		
	Accession #	Name	Gene	WT cellulose	Mutant cellulose	Mutant glucose
<b>Carbon: glycolysis</b>	D9SVJ3	Glucose-6-phosphate isomerase	<i>pgi</i>	19.56±7.91	17.92±3.56	14.12±1.99
	D9SST4	Phosphofructokinase (ATP)	<i>pfkl</i>	9.23±5.31	2.14±1.96	0.23±0.40
	D9SR38	Fructose-1,6-bisphosphate aldolase, class II	<i>aldo</i>	35.92±7.21	21.08±6.29	45.57±6.53
	D9SRX5	Triosephosphate isomerase (NAD <sup>+</sup> )	<i>tpi</i>	35.24±7.11	33.27±4.63	50.82±3.46
	D9SRX3	Glyceraldehyde-3-phosphate dehydrogenase	<i>gapdh</i>	89.85±30.22	89.47±7.79	90.01±20.83
	D9SRX4	Phosphoglycerate kinase (ADP)	<i>pgk</i>	70.89±10.64	22.54±18.63	77.55±8.33
	D9SRX6	2,3-phosphoglycerate-independent phosphoglycerate mutase	<i>pgm</i>	7.25±5.32	10.57±8.00	12.90±4.55
	D9SRY4	Enolase	<i>eno</i>	2.96±2.81	5.96±10.33	0.00±0.00
	D9SQA2	Pyruvate kinase (ADP)	<i>pyk</i>	12.60±11.19	15.01±3.18	19.55±4.88
	D9SVF1	Malate dehydrogenase ( <i>mdh</i> )	<i>mdh</i>	12.38±1.09	6.03±1.46	9.18±0.82
<b>Carbon: core pathway and products formation pathways</b>	D9SKD2	Pyruvate:ferredoxin (flavodoxin) oxidoreductase	<i>pfor</i>	81.48±37.59	79.55±22.51	119.18±5.03
	D9STL4	Acetyl-CoA acetyltransferase	<i>thl</i>	75.71±5.05	36.21±3.01	67.67±7.91
	D9ST02	3-hydroxyacyl-CoA dehydrogenase NAD-binding	<i>crt</i>	34.46±17.25	25.73±7.16	49.33±6.90
	D9ST03	Electron transfer flavoprotein alpha/beta-subunit	<i>etfA/B</i>	24.27±18.48	20.20±7.90	32.24±3.24
	D9ST04	Electron transfer flavoprotein alpha/beta-subunit	<i>etfA/B</i>	14.50±13.64	10.34±13.10	25.84±3.14
	D9SLC0	Acetate kinase (ADP)	<i>ack</i>	2.29±2.48	1.37±1.29	18.58±1.79
	D9SWR2	Probable butyrate kinase (ADP)	<i>buk</i>	24.15±12.34	6.92±6.58	27.96±2.87
	Q7DFN2	Aldehyde-alcohol dehydrogenase (NAD(P)H)	<i>adhE2</i>	0.00±0.00	295.38±98.30	157.96±36.87
	A0A084J995	Aldehyde-alcohol dehydrogenase (NAD(P)H)	<i>adh</i>	5.22±7.65	4.63±4.41	0.00±0.00
	D9SKR5	Iron-containing alcohol dehydrogenase (NAD(P)H)	<i>adh</i>	32.20±1.33	15.69±6.65	3.52±0.66
D9SMA3	Hydrogenase, Fe-only (NAD <sup>+</sup> )	<i>hyd</i>	3.03±2.91	0.26±0.44	5.87±1.00	

**Table 4.** Correlate proteomics with metabolomics *via* dynamic mathematic modeling.

Reaction	Enzymes		Spectral Count (Expression)			Calculated Max. Reaction Rate in Modeling		
	Accession #	Name	WT cellulose	Mutant cellulose	Mutant glucose	WT cellulose	Mutant cellulose	Mutant glucose
Pyruvate → Acetyl-CoA	D9SQA2	Pyruvate kinase ( <i>pk</i> )	12.60±11.19	15.01±3.18	19.55±4.88	2.32	2.51	17.46
Acetyl-CoA → Acetoacetyl-CoA	D9STL4	Acetyl-CoA acetyltransferase ( <i>thl</i> )	75.71±5.05	36.21±3.01	67.67±7.91	0.99	0.67	4.27
Acetoacetyl-CoA → 3-Hydroxybutyryl-CoA	-	beta-hydroxybutyryl-CoA dehydrogenase ( <i>hbd</i> )	-	-	-	0.98	0.67	3.5
3-hydroxyacyl-CoA → Crotonyl-CoA	D9ST02	3-hydroxyacyl-CoA dehydrogenase ( <i>crt</i> )	34.46±17.25	25.73±7.16	49.33±6.90	0.97	0.66	3.19
Crotonyl-CoA → Butyryl-CoA	D9ST03	Electron transfer flavoprotein A/B ( <i>etfA/B</i> )	24.27±18.48	20.20±7.90	32.24±3.24	0.95	0.65	2.72
	D9ST04	Electron transfer flavoprotein A/B ( <i>etfA/B</i> )	14.50±13.64	10.34±13.10	25.84±3.14	-	-	-
Acetyl-CoA → Acetate	D9SLC0	Acetate kinase ( <i>ack</i> )	2.29±2.48	1.37±1.29	18.58±1.79	54.21	131.84	10.58
Acetate → Acetyl-CoA						131.91	14.89	103.75
Butyryl-CoA → Butyrate	D9SWR 2	Butyrate kinase ( <i>buk</i> )	24.15±12.34	6.92±6.58	27.96±2.87	84.39	35.65	0.09
Butyrate → Butyryl-CoA						117	133.31	0
Butyryl-CoA → Butanol	Q7DFN2	Aldehyde-alcohol dehydrogenase ( <i>adhE2</i> )	0.00±0.00	295.38±98.30	157.96±36.8 7	0	12.74	22.63
Acetyl-CoA → Ethanol						0	19.27	4.84
Pyruvate → Acetyl-CoA + H <sub>2</sub> + CO <sub>2</sub>	D9SMA 3	Hydrogenase, Fe-only ( <i>hyd</i> )	3.03±2.91	0.26±0.44	5.87±1.00	1.52	1.76	9.94

**Note:** The concentrations of intracellular metabolites and the yield of the extracellular end products were used to calculate the Max. reaction rate and metabolic flux in the dynamic modeling. The productivity data of end fermentation products were used to define the transportation rate of the dynamic model.

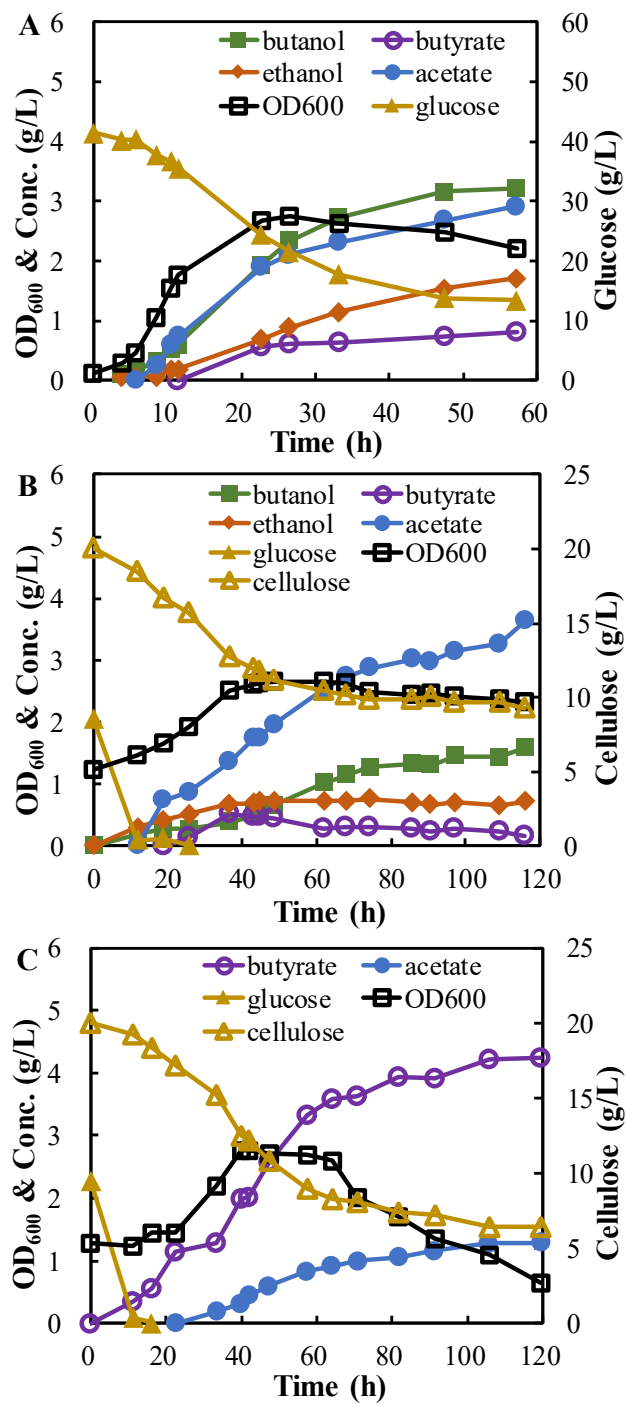
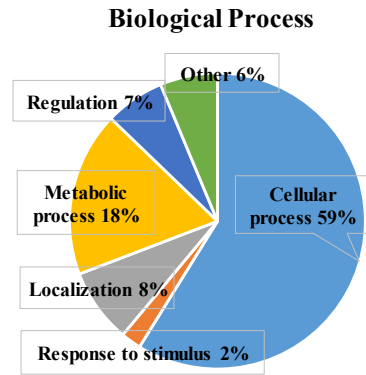
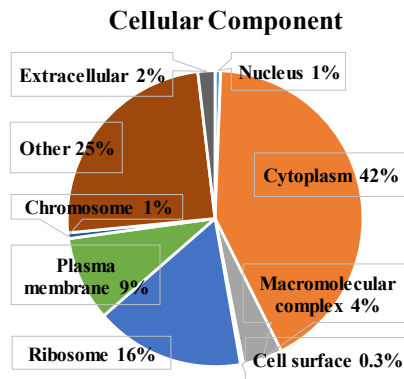


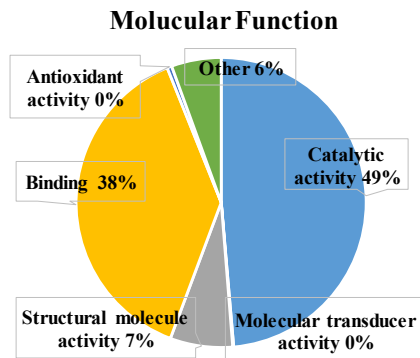
**Fig. 1.** Fermentation kinetics for cellulolic n-butanol production by A) mutant strain *C. cellulovorans adhE2* using glucose as substrate, B) *C. cellulovorans adhE2* using cellulose as substrate, and C) wild type strain (WT) using cellulose as substrate. □: OD<sub>600</sub>, ▲: glucose, △: cellulose, ○: butyrate, ●: acetate, ■: butanol, ◆: ethanol.



Ontology Term	Pair1	Pair2
Cellular process	↑8 ↓8	↑8 ↓29
Localization	↑1 ↓5	↑6 ↓4
Metabolic process	↑6 ↓2	↑4 ↓5
Regulation	↑0 ↓1	↑0 ↓2
Response to stimulus	↑0 ↓0	↑1 ↓0
Other	↑0 ↓2	↑2 ↓5

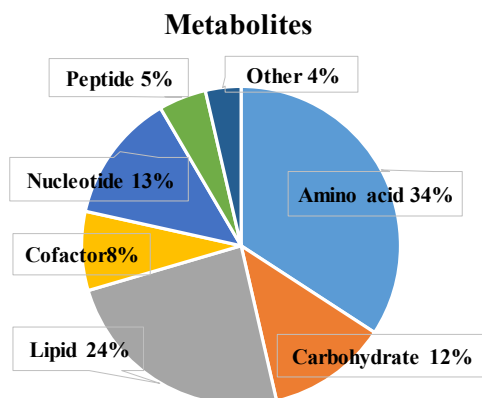


Ontology Term	Pair1	Pair2
Chromosome	↑0 ↓0	↑0 ↓1
Cytoplasm	↑1 ↓7	↑2 ↓13
Macromolecular complex	↑0 ↓2	↑0 ↓1
Nucleus	↑0 ↓1	↑0 ↓0
Plasma membrane	↑1 ↓4	↑5 ↓1
Ribosome	↑3 ↓0	↑0 ↓13
Other	↑0 ↓6	↑9 ↓1



Ontology Term	Pair1	Pair2
Binding	↑7 ↓9	↑11 ↓35
Catalytic Activity	↑12 ↓12	↑14 ↓30
Molecular transducer activity	↑0 ↓1	↑1 ↓0
Structural molecule activity	↑3 ↓0	↑0 ↓12
Other	↑0 ↓4	↑5 ↓3

**Fig. 2.** Global and pairwise analysis of protein expression in *C. cellulovorans*. Total 624 host cell proteins with <1% False Discovery Rate were quantitated in global analysis. Only the proteins with significant expression change (>50%) were presented in the pairwise analysis. Pair 1: wild type strain vs. mutant strain using cellulose. Pair 2: cellulose vs. glucose fermented by the mutant strain.



Metabolites	Pair1	Pair2
Amino acid	↑4 ↓1	↑82 ↓21
Carbohydrate	↑0 ↓1	↑21 ↓11
Lipids	↑1 ↓1	↑20 ↓29
Cofactors	↑0 ↓2	↑8 ↓11
Nucleotide	↑0 ↓5	↑16 ↓12
Peptide	↑0 ↓1	↑1 ↓6
Others	↑0 ↓0	↑8 ↓0

**Fig. 3.** Global and pairwise analysis of the function of metabolites in *C. cellulovorans*. Total 474 metabolites were extracted and identified from the metabolomics study, and the global metabolites were grouped into seven classes based on their function. Only the intracellular metabolites with significant expression change (>50%) were presented in the pairwise analysis. Pair 1: wild type strain vs. mutant strain using cellulose. Pair 2: glucose vs. cellulose fermented by the mutant strain.

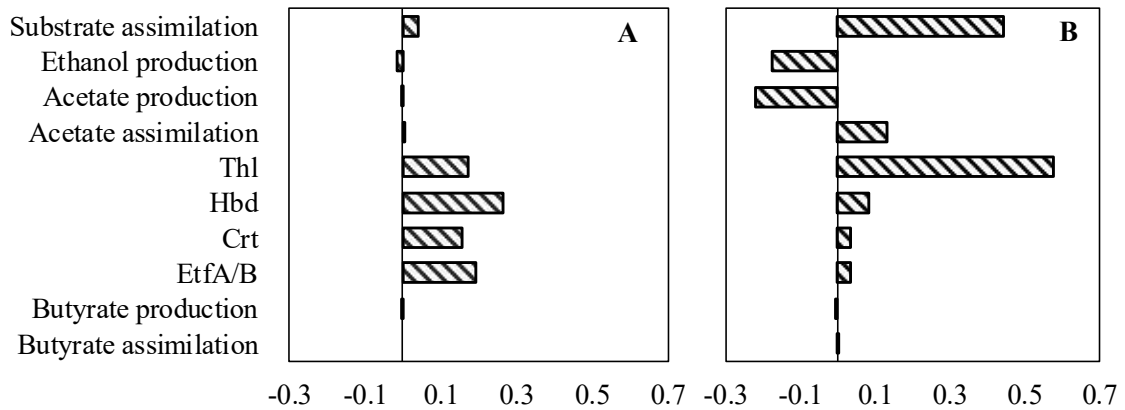


**Fig. 4.** The metabolic flux control coefficient in cellulosic n-butanol production by the mutant of *C. cellulovorans* using A) glucose and B) cellulose. Higher control efficiency indicated higher impact. Thl: acetyl-CoA acetyltransferase; Hbd: beta-hydroxybutyryl-CoA dehydrogenase; Crt: 3-hydroxyacyl-CoA dehydrogenase; EtfA/B: electron transfer flavoprotein A/B-subunit.

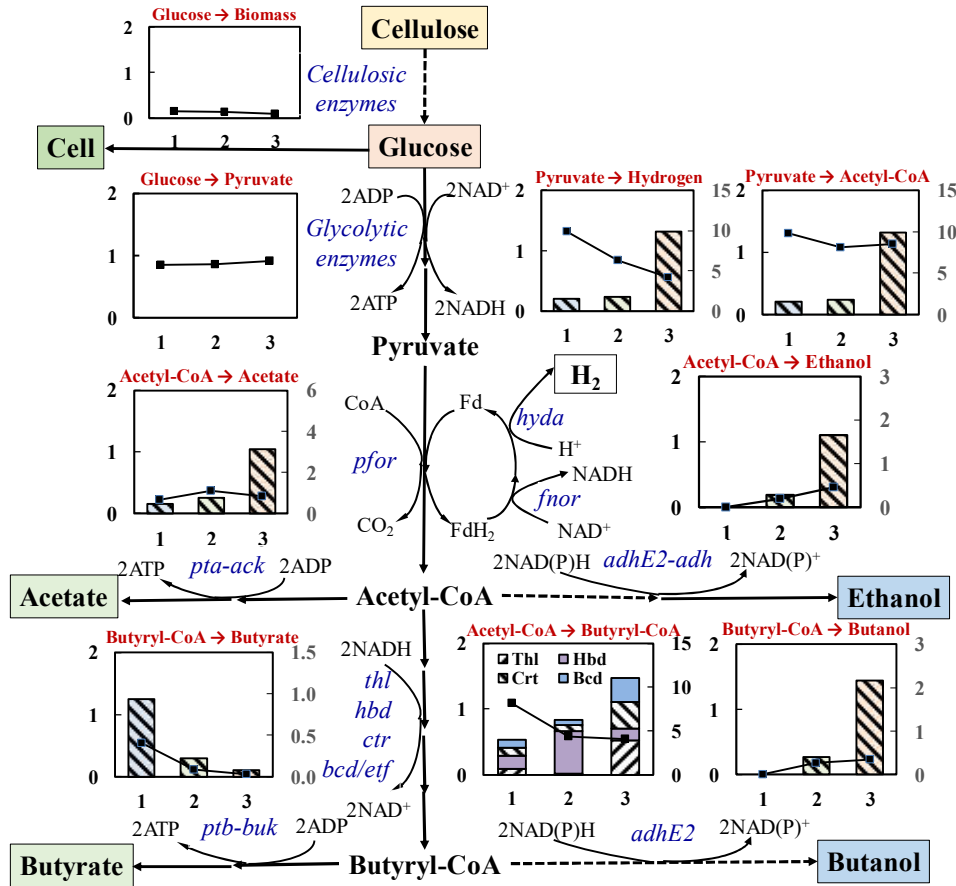


**Fig. 5.** Metabolic flux analysis of *C. cellulovorans* using the novel dynamic model developed in this study (column, secondary Y-axis) and the traditional static model (dot line, primary Y-axis). 1: wild type using cellulose, 2: mutant strain using cellulose, and 3: mutant stain using glucose. Abbreviations: *pta*, phosphotransacetylase; *ack*, acetate kinase; *ptb*, phosphotransbutyrylase; *buk*, butyrate kinase; *thl*, thiolase; *hbd*, beta-hydroxybutyryl-CoA dehydrogenase; *pfor*, pyruvate: ferredoxin oxidoreductase; *hyda*, hydrogenase; *ctf A/B*, CoA transferase; *adhe2*, bifunctional acetaldehyde/alcohol dehydrogenase; *crt*, 3-hydroxybutyryl-CoA dehydratase; *bcd*, butyryl-CoA dehydrogenase; *etf*, electron transfer flavoprotein. The production of the end products in fermentation were used to calculate the metabolic flux in the static model. The concentrations of intracellular metabolites and the extracellular end products were used to calculate the metabolic flux in the dynamic model.

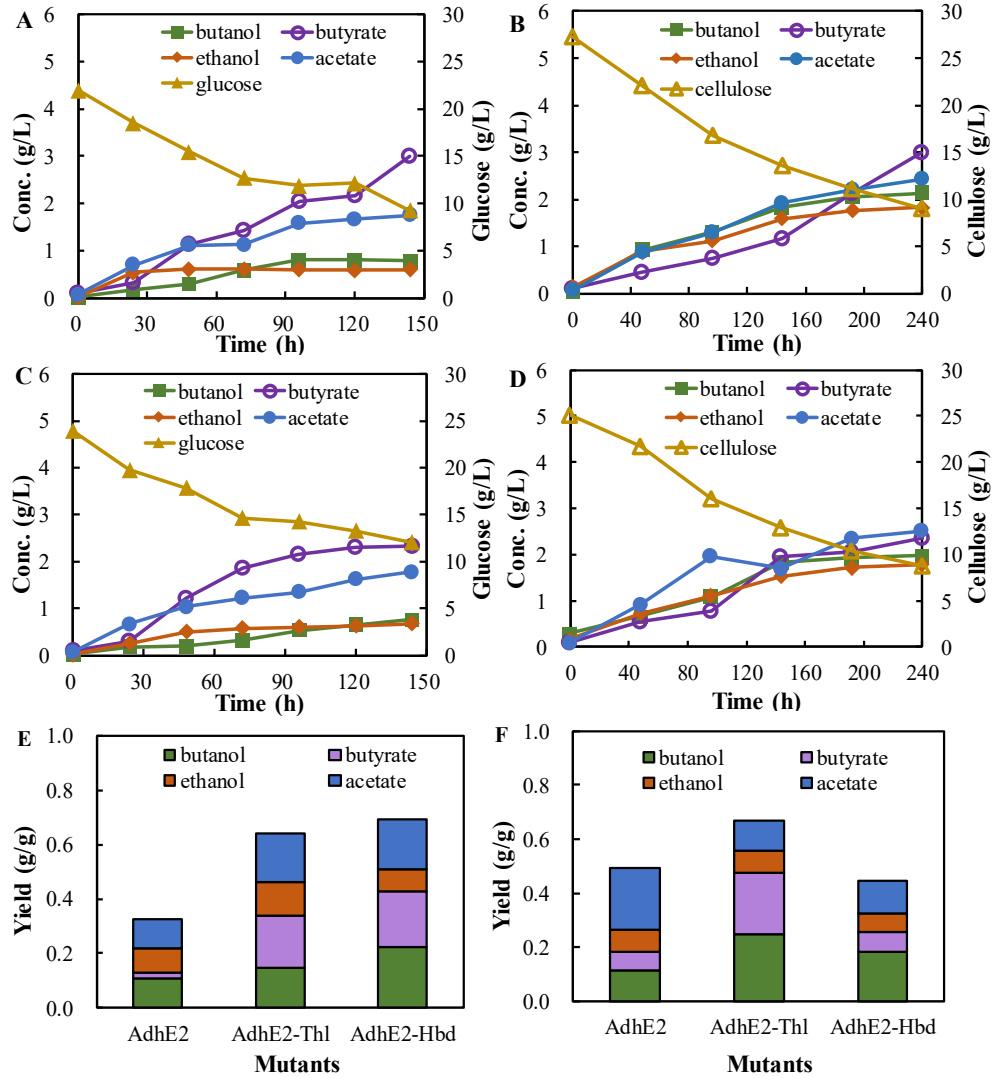


**Fig. 6.** Fermentation kinetics of new-generation metabolically engineered mutants. A) mutant *C. cellulovorans thl-adhE2* using glucose, B) mutant *C. cellulovorans thl-adhE2* using cellulose, C) mutant *C. cellulovorans hbd-adhE2* using glucose, D) mutant *C. cellulovorans hbd-adhE2* using cellulose. E) yield of glucose fermentation by three mutants, F) yield of cellulose fermentation by three mutants. □: OD<sub>600</sub>, ▲: glucose, △: cellulose, ○: butyrate, ●: acetate, ■: butanol, ◆: ethanol.

## SUMMARY AND CONCLUSION

This dissertation has presented the bioprocess/biomanufacturing development of several novel anti-cancer therapies and a high value biochemical, including 1) novel mAb development for PanNET treatment, 2) optimized ADC preparation for improved biological quality and anti-cancer toxicity, 3) high quality and efficient T cell manufacturing for adoptive therapy, 4) establishment of the first consolidated bioprocessing of butanol production from biomass, and 5) model-guided rational design. New discoveries on the bioprocess will contribute to the novel anti-cancer therapy and high value biochemical development.

In Chapter 2, a novel mAb targeting SSTR was developed using hybridoma technology. Its binding affinity was significantly increased (6 fold) compared to the commercial antibody. The efficacy of cancer treatment was improved by ADC strategy, where in house anti-SSTR mAb was conjugated to MMAE. In Chapter 3, a CHO cell fed-batch culture platform was developed and produced >2 g/L of anti-HER2 mAb. As the therapeutic effect of ADC is significantly affected by its bioproduction process, key parameters, including linker selection, ratio of drug and mAb, and conjugation approach, were investigated to improve the ADC conjugation yield and product quality. A robust ADC production process was established. Over the studies, the quality of our antibodies

were evaluated via SDS-PAGE, live-cell confocal microscopy imaging, and flow cytometry analysis. The ADC efficacy was confirmed via *in vitro* and *in vivo* experiments.

In Chapter 4, a robust protocol was established to grow T cells in a stirred tank bioreactor with control of pH, temperature, and dissolved oxygen. A large scaled culture was established in a 2-L stirred tank bioreactor. The process generated high density ( $8.33 \times 10^6$  cells/mL) cell culture in a short period of time (4 days) with strong robustness, where proliferation >132-fold expansion was achieved among five donors, and >500,000-fold expansion was achieved in the best case after combining the first two stimulations. High cell quality was ensured by flow cytometry analysis on cell type, activation signal, inhibitory signal, memory type, and cytokine production.

In Chapter 5, a robust cellulosic biobutanol conversion process was established using a metabolically engineered *C. cellulovorans*, which produced butanol with >3 g/L, yield >0.14 g/g, and selectivity >3 g/g from pretreated corn cob at pH 6.5 in CBP. The optimized fermentation process engineering enabled a high butanol production directly from agricultural residues. Further, Chapter 6 developed a comprehensive understanding of cellular metabolism of *C. cellulovorans* using a novel dynamic mathematic model, for the first time, to integrate our proteomics, metabolomics and fermentation data collected from the wild type and n-butanol producing mutant strains. Important impact factors were ranked for their possible contribution to butanol production improvement. Several strategies for rationally engineering were proposed and validated. The cellulosic n-butanol production was greatly improved by the new-generation, rationally engineered strain.

## GENERAL REFERENCE

1. Ferlay, J., et al., *Cancer incidence and mortality worldwide: Sources, methods and major patterns in GLOBOCAN 2012*. International Journal of Cancer, 2015. **136**(5): p. E359-E386.
2. Zugazagoitia, J., et al., *Current challenges in cancer treatment*. Clinical therapeutics, 2016. **38**(7): p. 1551-1566.
3. Rao, W. and Z.-S. Deng, *A review of hyperthermia combined with radiotherapy/chemotherapy on malignant tumors*. Critical Reviews™ in Biomedical Engineering, 2010. **38**(1).
4. Barton, M.B., et al., *Estimating the demand for radiotherapy from the evidence: a review of changes from 2003 to 2012*. Radiotherapy and oncology, 2014. **112**(1): p. 140-144.
5. Morrison, R., et al., *Targeting the mechanisms of resistance to chemotherapy and radiotherapy with the cancer stem cell hypothesis*. Journal of oncology, 2011. **2011**.
6. Sawyers, C., *Targeted cancer therapy*. Nature, 2004. **432**: p. 294.
7. Huang, M., et al., *Molecularly targeted cancer therapy: some lessons from the past decade*. Trends in pharmacological sciences, 2014. **35**(1): p. 41-50.
8. Holohan, C., et al., *Cancer drug resistance: an evolving paradigm*. Nature Reviews Cancer, 2013. **13**(10): p. 714.
9. Griner, L.A.M., et al., *High-throughput combinatorial screening identifies drugs that cooperate with ibrutinib to kill activated B-cell–like diffuse large B-cell*

- lymphoma cells*. Proceedings of the National Academy of Sciences, 2014. **111**(6): p. 2349-2354.
10. Sharma, S.V., D.A. Haber, and J. Settleman, *Cell line-based platforms to evaluate the therapeutic efficacy of candidate anticancer agents*. Nature reviews cancer, 2010. **10**(4): p. 241.
  11. Ouyang, L., et al., *Programmed cell death pathways in cancer: a review of apoptosis, autophagy and programmed necrosis*. Cell proliferation, 2012. **45**(6): p. 487-498.
  12. Anastas, J.N. and R.T. Moon, *WNT signalling pathways as therapeutic targets in cancer*. Nature Reviews Cancer, 2013. **13**(1): p. 11.
  13. Liu, X., C. Ma, and L. Zhou, *Targeted cancer therapy*. Pharmaceutical Bioprocessing, 2017. **5**(2): p. 025-207.
  14. Zhou, L., et al., *Targeted biopharmaceuticals for cancer treatment*. Cancer Letters, 2014. **352**(2): p. 145-151.
  15. Christofk, H.R., et al., *The M2 splice isoform of pyruvate kinase is important for cancer metabolism and tumour growth*. Nature, 2008. **452**(7184): p. 230.
  16. Clarke, M.F. and A.T. Hass, *Cancer stem cells*. Reviews in Cell Biology and Molecular Medicine, 2006.
  17. Reya, T., et al., *Stem cells, cancer, and cancer stem cells*. nature, 2001. **414**(6859): p. 105.
  18. Sato, Y., et al., *Cancer cells expressing toll-like receptors and the tumor microenvironment*. Cancer microenvironment, 2009. **2**(1): p. 205-214.

19. Wise, D.R. and C.B. Thompson, *Glutamine addiction: a new therapeutic target in cancer*. Trends in Biochemical Sciences, 2010. **35**(8): p. 427-433.
20. Hoelder, S., P.A. Clarke, and P. Workman, *Discovery of small molecule cancer drugs: Successes, challenges and opportunities*. Molecular Oncology, 2012. **6**(2): p. 155-176.
21. Adams, D.J., *The Valley of Death in anticancer drug development: a reassessment*. Trends in Pharmacological Sciences, 2012. **33**(4): p. 173-180.
22. Jackman, D., et al., *Clinical definition of acquired resistance to epidermal growth factor receptor tyrosine kinase inhibitors in non-small-cell lung cancer*. Journal of clinical oncology, 2010. **28**(2): p. 357.
23. Ryan, C.J., et al., *Abiraterone in metastatic prostate cancer without previous chemotherapy*. New England Journal of Medicine, 2013. **368**(2): p. 138-148.
24. Crews, C.M., *Targeting the undruggable proteome: the small molecules of my dreams*. Chemistry & biology, 2010. **17**(6): p. 551-555.
25. Xu, N., et al., *Achievements and perspectives in Chinese hamster ovary host cell engineering*. Pharmaceutical Bioprocessing, 2015. **3**(4): p. 285-292.
26. Beck, A., et al., *Strategies and challenges for the next generation of therapeutic antibodies*. Nature Reviews Immunology, 2010. **10**(5): p. 345.
27. Scott, A.M., J.P. Allison, and J.D. Wolchok, *Monoclonal antibodies in cancer therapy*. Cancer Immunity Archive, 2012. **12**(1).
28. Robbie, G.J., et al., *A novel investigational Fc modified humanized monoclonal antibody, Motavizumab-YTE, has an extended half-life in healthy adults: a*

- randomized study. Antimicrobial agents and chemotherapy*, 2013: p. AAC. 01285-13.
29. Xu, N., M. Liu, and M. Liu, *The Pharmacology, Pharmacokinetics, and Pharmacodynamics of Antibodies*, in *Biosimilars of Monoclonal Antibodies: A Practical Guide to Manufacturing, Preclinical, and Clinical Development*. 2016. p. 201-215.
  30. Chakraborty, C., et al., *The novel strategies for next-generation cancer treatment: miRNA combined with chemotherapeutic agents for the treatment of cancer. Oncotarget*, 2018. **9**(11): p. 10164-10174.
  31. Stump, B. and J. Steinmann, *Conjugation process development and scale-up*, in *Antibody-Drug Conjugates*. 2013, Springer. p. 235-248.
  32. Liu, X. and L. Zhou, *Mini review: the application of omics in targeted anticancer biopharmaceuticals development. Austin J. Biomed. Eng*, 2014. **1**(1): p. 1-8.
  33. Hughes, B., *Antibody–drug conjugates for cancer: poised to deliver?* 2010, Nature Publishing Group.
  34. Roh, K.H., R.M. Nerem, and K. Roy, *Biomanufacturing of Therapeutic Cells: State of the Art, Current Challenges, and Future Perspectives. Annu Rev Chem Biomol Eng*, 2016. **7**: p. 455-78.
  35. Bourin, P., et al., *Stromal cells from the adipose tissue-derived stromal vascular fraction and culture expanded adipose tissue-derived stromal/stem cells: a joint statement of the International Federation for Adipose Therapeutics and Science (IFATS) and the International Society for Cellular Therapy (ISCT). Cytotherapy*, 2013. **15**(6): p. 641-648.

36. Trounson, A., et al., *Clinical trials for stem cell therapies*. BMC medicine, 2011. **9**(1): p. 52.
37. Di Stasi, A., et al., *Inducible apoptosis as a safety switch for adoptive cell therapy*. New England Journal of Medicine, 2011. **365**(18): p. 1673-1683.
38. Lipsitz, Y.Y., N.E. Timmins, and P.W. Zandstra, *Quality cell therapy manufacturing by design*. Nature Biotechnology, 2016. **34**(4): p. 393.
39. Rowley, J., et al., *Meeting lot-size challenges of manufacturing adherent cells for therapy*. BioProcess Int, 2012. **10**(3): p. 7.
40. Sensebé, L., P. Bourin, and K. Tarte, *Good manufacturing practices production of mesenchymal stem/stromal cells*. Human gene therapy, 2010. **22**(1): p. 19-26.
41. Mazzei, D., et al., *A low shear stress modular bioreactor for connected cell culture under high flow rates*. Biotechnology and bioengineering, 2010. **106**(1): p. 127-137.
42. Li, F., et al., *Cell culture processes for monoclonal antibody production*. MAbs, 2010. **2**(5): p. 466-79.
43. Breslin, S. and L. O'Driscoll, *Three-dimensional cell culture: the missing link in drug discovery*. Drug discovery today, 2013. **18**(5-6): p. 240-249.
44. Van der Valk, J., et al., *Optimization of chemically defined cell culture media—replacing fetal bovine serum in mammalian in vitro methods*. Toxicology in vitro, 2010. **24**(4): p. 1053-1063.
45. Young, E.W. and D.J. Beebe, *Fundamentals of microfluidic cell culture in controlled microenvironments*. Chemical Society Reviews, 2010. **39**(3): p. 1036-1048.

46. Xu, N., et al., *High-level expression of recombinant IgG1 by CHO K1 platform*. *Frontiers of Chemical Science and Engineering*, 2015. **9**(3): p. 376-380.
47. De Jesus, M. and F.M. Wurm, *Manufacturing recombinant proteins in kg-ton quantities using animal cells in bioreactors*. *European Journal of Pharmaceutics and Biopharmaceutics*, 2011. **78**(2): p. 184-188.
48. Amanullah, A., et al., *Novel micro-bioreactor high throughput technology for cell culture process development: Reproducibility and scalability assessment of fed-batch CHO cultures*. *Biotechnology and bioengineering*, 2010. **106**(1): p. 57-67.
49. Chon, J.H. and G. Zarbis-Papastoitsis, *Advances in the production and downstream processing of antibodies*. *New biotechnology*, 2011. **28**(5): p. 458-463.
50. Liu, N., et al., *Characterization of novel mixed-mode protein adsorbents fabricated from benzoyl-modified polyethyleneimine-grafted Sepharose*. *Journal of Chromatography A*, 2014. **1372**: p. 157-165.
51. Kim, Y., et al., *High-throughput protein purification and quality assessment for crystallization*. *Methods*, 2011. **55**(1): p. 12-28.
52. Bhambure, R., K. Kumar, and A.S. Rathore, *High-throughput process development for biopharmaceutical drug substances*. *Trends in biotechnology*, 2011. **29**(3): p. 127-135.
53. Lenshof, A. and T. Laurell, *Continuous separation of cells and particles in microfluidic systems*. *Chemical Society Reviews*, 2010. **39**(3): p. 1203-1217.
54. Rajalahti, T. and O.M. Kvalheim, *Multivariate data analysis in pharmaceuticals: a tutorial review*. *International journal of pharmaceutics*, 2011. **417**(1-2): p. 280-290.

55. Read, E., et al., *Process analytical technology (PAT) for biopharmaceutical products: Part I. Concepts and applications*. Biotechnology and bioengineering, 2010. **105**(2): p. 276-284.
56. Yang, S.-T. and X. Liu, *Metabolic process engineering for biochemicals and biofuels production*, in *New Biotechnologies for Increased Energy Security: The Future of Fuel*. 2015. p. 179.
57. Kuhn, D., et al., *Systems biotechnology—Rational whole-cell biocatalyst and bioprocess design*. Engineering in Life Sciences, 2010. **10**(5): p. 384-397.
58. Altamirano, C., et al., *Strategies for fed-batch cultivation of t-PA producing CHO cells: substitution of glucose and glutamine and rational design of culture medium*. Journal of Biotechnology, 2004. **110**(2): p. 171-179.
59. Ma, C., et al., *Rebalancing redox to improve biobutanol production by Clostridium tyrobutyricum*. Bioengineering, 2015. **3**(1): p. 2.
60. Du, Y., et al., *Metabolic process engineering of Clostridium tyrobutyricum  $\Delta$ ack-*adhE2* for enhanced n-butanol production from glucose: Effects of methyl viologen on NADH availability, flux distribution, and fermentation kinetics*. Biotechnology and Bioengineering, 2015. **112**(4): p. 705-715.
61. Lan, T.-Q., et al., *Enhanced cellulase production by Trichoderma viride in a rotating fibrous bed bioreactor*. Bioresource Technology, 2013. **133**: p. 175-182.
62. Buyel, J., et al., *Rational design of a host cell protein heat precipitation step simplifies the subsequent purification of recombinant proteins from tobacco*. Biochemical engineering journal, 2014. **88**: p. 162-170.

63. Mandenius, C.-F. and A. Brundin, *Bioprocess optimization using design-of-experiments methodology*. Biotechnology Progress, 2008. **24**(6): p. 1191-1203.
64. Yang, R., et al., *Mitochondrial-Mediated Oxidative Ca<sup>2+</sup>/Calmodulin-Dependent Kinase II Activation Induces Early Afterdepolarizations in Guinea Pig Cardiomyocytes: An In Silico Study*. Journal of the American Heart Association, 2018. **7**(15): p. e008939.
65. Liu, X., S.-T. Yang, and L. Zhou, *The application of omics in pharmaceutical bioprocessing*. Pharmaceutical Bioprocessing, 2014. **2**(1): p. 1-4.
66. Yang, S.-T. and X. Liu, *Cell culture processes for biologics manufacturing: recent developments and trends*. Pharmaceutical Bioprocessing, 2013. **1**(2): p. 133-136.

APPENDIX A  
SUPPLEMENTAL MATERIALS

**Table S1.** Biochemical reaction rate equations in dynamic model.

Number	Equation
1	$\frac{d[Pyruvate]}{dt} = r_{pyr(trans)} - r_{pfor}$
2	$\frac{d[ACoA]}{dt} = r_{pfor} + r_{acep} - r_{acep} - r_{ethanol} - r_{thl} - r_{bio} - \mu[ACoA]$
3	$\frac{d[Acetate]}{dt} = r_{acep} - r_{acep} - \mu[Acetate] - r_{ace(trans)}$
4	$\frac{d[Ethanol]}{dt} = r_{ethanol} - \mu[Ethanol] - r_{eth(trans)}$
5	$\frac{d[AACoA]}{dt} = r_{thl} - r_{hbd} - \mu[AACoA]$
6	$\frac{d[3HC]}{dt} = r_{hbd} - r_{crt} - \mu[3HC]$
7	$\frac{d[CRC]}{dt} = r_{crt} - r_{bcd} - \mu[CRC]$
8	$\frac{d[BCoA]}{dt} = r_{bcd} + r_{buta} - r_{butp} - r_{butanol} - \mu[BCoA]$
9	$\frac{d[Butyrate]}{dt} = r_{butp} - r_{buta} - \mu[Butyrate] - r_{buty(trans)}$
10	$\frac{d[Butanol]}{dt} = r_{butanol} - \mu[Butanol] - r_{buta(trans)}$
11	$\frac{d[NADH]}{dt} = 4r_{pfor} - 2r_{ethanol} - 2r_{bcd} - 2r_{butanol} - 0.873\mu = 0$
12	$\frac{d[ATP]}{dt} = 2r_{acep} - 2r_{acep} + 2r_{butp} - 2r_{buta} - 14.85\mu = 0$

**Table S2.** Summary of the representative modeling parameters in the central metabolic pathway.

Reactions	Equations	Parameters	Reference	$\Delta G$ (kJ/mol)
1) Pyruvate $\rightarrow$ acetyl-CoA	$r_{pfor} = \frac{r_{pfor}^{max}[PYR]}{K_{pfor} + [PYR]}$	$K_{pfor}=0.8\text{mM}$	<i>C. pasteurianum</i> [1]	-6.5
2) Acetyl-CoA $\rightarrow$ Ethanol	$r_{ethanol} = \frac{r_{ethanol}^{max}[ACoA]}{K_{ethanol} + [ACoA]}$	$K_{ethanol}=5.33\text{mM}^*$	<i>C. acetobutylicum</i> [2, 3]	-0.7
3) Acetyl-CoA $\rightarrow$ Acetate	$r_{acep} = \frac{r_{acep}^{max}[ACoA]}{K_{acep} + [ACoA]}$	$K_{acep}=5\text{mM}$	<i>E. coli</i> [4]	1.0
4) Acetate $\rightarrow$ Acetyl-CoA	$r_{acea} = \frac{r_{acea}^{max}[Aacetate]}{K_{acea} + [Acetate]}$	$K_{acea}=285\text{mM}$	<i>C. thermocellum</i> [4]	-1.0
5) Acetyl-CoA $\rightarrow$ Acetoacetyl-CoA	$r_{thl} = \frac{r_{thl}^{max}[ACoA]}{K_{thl} + [ACoA]}$	$K_{thl}=0.27\text{mM}$	<i>C. acetobutylicum</i> [5]	5.3
6) Acetoacetyl-CoA $\rightarrow$ 3-Hydroxybutyryl-CoA	$r_{hbd} = \frac{r_{hbd}^{max}[AACoA]}{K_{hbd} + [AACoA]}$	$K_{hbd}=0.05\text{mM}$	<i>C. kluyveri</i> [6]	-5.4
7) 3-hydroxyacyl-CoA $\rightarrow$ Crotonyl-CoA	$r_{crt} = \frac{r_{crt}^{max}[3HC]}{K_{crt} + [3HC]}$	$K_{crt} = 0.03\text{mM}$	<i>C. acetobutylicum</i> [6]	0.5
8) Crotonyl-CoA $\rightarrow$ Butyryl-CoA	$r_{bcd} = \frac{r_{bcd}^{max}[CRC]}{K_{bcd} + [CRC]}$	$K_{bcd} = 0.004\text{mM}$	<i>C. acetobutylicum</i> [6]	-14.6
9) Butyryl-CoA $\rightarrow$ Butyrate	$r_{butp} = \frac{r_{butp}^{max}[BCoA]}{K_{butp} + [BCoA]}$	$K_{butp}=0.11\text{mM}$	<i>C. acetobutylicum</i> [7]	1.0
10) Butyrate $\rightarrow$ Butyryl-CoA	$r_{buta} = \frac{r_{buta}^{max}[Butyrate]}{K_{buta} + [Butyrate]}$	$K_{buta}=14\text{mM}$	<i>C. acetobutylicum</i> [8]	-1.0
11) Butyryl-CoA $\rightarrow$ Butanol	$r_{butanol} = \frac{r_{butanol}^{max}[BCoA]}{K_{butanol} + [BCoA]}$	$K_{butanol}=16\text{mM}$	<i>C. acetobutylicum</i> [2]	-0.7
12) Pyruvate $\rightarrow$ Acetyl-CoA + H <sub>2</sub> + CO <sub>2</sub>	$r_{H2} = \frac{r_{H2}^{max}[PYR]}{K_{H2} + [PYR]}$	$K_{H2} = 0.0033\text{mM}$	<i>C. acetobutylicum</i> [9]	-54.94

**Table S3.** Mass balance equations used in mathematic models.

Number	Function	Reaction
1	Biomass	Glucose + 0.873NADH + 14.85ATP → 6CH <sub>1.75</sub> O <sub>0.5</sub> N <sub>0.25</sub>
		2Acetyl-CoA + 0.873NADH + 14.85ATP → 6CH <sub>1.75</sub> O <sub>0.5</sub> N <sub>0.25</sub>
2	Pyruvate	Glucose + 2ADP + 2 NAD <sup>+</sup> → 2 Pyruvate + 2NADH + 2ATP
2	Acetyl-CoA	Pyruvate + CoA + Fd → Acetyl-CoA + CO <sub>2</sub> + FdH <sub>2</sub>
3	Ethanol	Acetyl-CoA + 2NADH → Ethanol + 2NAD <sup>+</sup>
4	Acetate production	Acetyl-CoA + 2ADP ↔ Acetate + 2ATP + CoA
5	Acetate assimilation	Acetate + 2ATP + CoA ↔ Acetyl-CoA + 2ADP (dynamic model <sup>a</sup> )
6	Acetoacetyl-CoA	2Acetyl-CoA → Acetoacetyl-CoA (dynamic model <sup>a</sup> )
7	3-Hydroxybutyryl-CoA	Acetoacetyl-CoA + 2NADH → 3-Hydroxybutyryl-CoA + 2NAD <sup>+</sup>
8	Crotonyl-CoA	3-Hydroxybutyryl-CoA → Crotonyl-CoA
9	Butyryl-CoA	Crotonyl-CoA → Butyryl-CoA (dynamic model <sup>a</sup> )
		2Acetyl-CoA + 2NADH → Butyryl-CoA + 2NAD <sup>+</sup> (static model <sup>b</sup> )
11	Butyrate production	Butyryl-CoA + 2ADP ↔ Butyrate + 2ATP + CoA
12	Butyrate assimilation	Butyrate + 2ATP + CoA ↔ Butyryl-CoA + 2ADP (dynamic model <sup>a</sup> )
13	Butanol	Butyryl-CoA + 2 NADH → Butanol + 2NAD <sup>+</sup>
14	NADH	FdH <sub>2</sub> + 2NAD <sup>+</sup> → Fd + 2NADH
15	Hydrogen	FdH <sub>2</sub> + 2H <sup>+</sup> → Fd + 2H <sub>2</sub>

**Note:**

a: These equations are used in dynamic model only.

b: These equations are used in static model only.

**Table S4.** Bacterial strains, plasmids, and primers used for the new generation metabolic engineering.

<b>Strain/Plasmid</b>	<b>Relevant Characteristics</b>	<b>Source</b>
<b><u>Strains</u></b>		
<i>E. coli</i> DH5 $\alpha$	Competent cells for transformation and amplification of plasmid recovered from <i>C. cellulovorans</i> transformant	NEB
<i>C. cellulovorans</i> 743B	DSM 3052	DSMZ
<i>C. cellulovorans thl-adhE2</i>	<i>C. cellulovorans</i> with plasmid pMTL8315183d2- <i>thl-adhE2</i>	This study
<i>C. cellulovorans hbd-adhE2</i>	<i>C. cellulovorans</i> with plasmid pMTL8315183d2- <i>hbd-adhE2</i>	This study
<i>C. tyrobutyricum</i> ATCC 25755	ATCC 25755	ATCC
<i>C. acetobutylicum</i> ATCC 824	ATCC 824	ATCC
<b><u>Plasmids</u></b>		
pMTL83151d2	From pMTL83151; <i>Cce</i> 743I/II restriction sites free	Unpublished
pMTL8315183d2- <i>adhE2-thl</i>	From p83151d2; P- <i>thl</i> , <i>adhE2</i> , <i>thl</i>	This study
pMTL8315183d2- <i>adhE2-hbd</i>	From p83151d2; P- <i>thl</i> , <i>adhE2</i> , <i>hbd</i>	This study
<b><u>Primers</u></b>		
C2-F2	5' GAATGGCGAATGGCGCTAGCATA 3'	
C2-R2	5' TGAAATTCCTCCTCATATAAATTTAAAATGATTTTATATAGATATC 3'	
thl-F1	5' ATTTATATGAGGAGGAATTTCAATGAAAGAAGTTGTAATAGCTAGTGCAGTAAG AACAG 3'	
thl-R1	5' GCTAGCGCCATTCGCCATTCCTAGCACTTTTCTAGCAATATTGCTGTTCCCTTG 3'	
hbd-F1	5' TTATATGAGGAGGAATTTCAATGAAAAAATATGTGTTCTTGGTGCAGGTAC 3'	
hbd-R1	5' ACCTCTACTGGATCCTTGCCTATGGCAATTGAACTTCTTTTACT 3'	
hbd-F2	5' GGCAAGGATCCAGTAGAGGTGGCAGAAGCTCCCGGATTT 3'	
hbd-R2	5' GCTAGCGCCATTCGCCATTCCTATTTTGAATAATCAAAGAATCCTTTTTT 3'	

**Table S5.** Expression of cellulosic enzymes.

Accession #	Protein		Spectral Count (Expression)		
	Name	Gene	WT cellulose	Mutant cellulose	Mutant glucose
D9SV64	Cellulase	Clocel_3359	7.70±0.89	52.22±15.66	0.00±0.00
D9STU6	Glycoside hydrolase family 1	Clocel_1020	0.00±0.00	0.43±0.74	5.65±1.89
D9STU4	Glycoside hydrolase family 1	Clocel_1018	0.00±0.00	0.00±0.00	2.12±1.23
D9SRM3	Glycoside hydrolase family 5	Clocel_0619	9.47±3.78	18.19±6.55	0.00±0.00
D9STR7	Glycoside hydrolase family 5	Clocel_3111	13.01±9.22	14.34±5.55	0.00±0.00
D9ST82	Glycoside hydrolase family 9	Clocel_0930	35.06±16.11	19.29±8.96	0.00±0.00
D9SQT2	Glycoside hydrolase family 9	Clocel_2576	13.41±13.54	42.69±17.05	0.00±0.00
D9SX09	Glycoside hydrolase family 9	Clocel_1624	13.99±12.18	34.11±14.60	0.00±0.00
D9SP57	Glycoside hydrolase family 11	Clocel_2295	1.79±1.56	8.92±9.33	0.00±0.00
D9SMN8	Glycoside hydrolase family 31	Clocel_0034	0.00±0.00	2.12±1.56	0.00±0.00
D9SS72	Glycoside hydrolase family 48	Clocel_2823	47.23±9.64	81.71±17.06	4.01±1.66
D9SNX7	Glycosyl transferase group 1	Clocel_2202	3.11±2.40	1.54±2.67	0.70±1.21
D9SSR5	6-phospho-beta-glucosidase	Clocel_2882	8.81±1.66	16.02±3.04	0.00±0.00
D9SLT8	6-phospho-beta-glucosidase	Clocel_4063	1.42±1.69	3.83±1.81	0.93±1.07
P28621	Endoglucanase B	<i>engB</i>	3.48±3.30	19.20±6.81	0.00±0.00
D9SS70	Glucanase	Clocel_2821	40.02±19.00	112.90±26.98	5.22±4.24
D9SS71	Glucanase	Clocel_2822	31.01±10.04	46.76±7.43	0.00±0.00
D9SRK9	Glucanase	Clocel_2741	22.41±8.90	19.48±9.93	0.00±0.00
D9SS68	Glucanase	Clocel_2819	12.54±13.09	12.84±5.92	0.00±0.00
D9SNX7	Glycosyl transferase group 1	Clocel_2202	3.11±2.40	1.54±2.67	0.70±1.21
D9SMN6	Glycosyltransferase 36	Clocel_0032	7.27±4.40	13.67±8.08	5.65±2.47
D9SQA4	Glycosyltransferase 36	Clocel_0391	2.33±4.04	4.74±0.78	2.82±1.39
D9SST3	Beta-xylanase	Clocel_2900	30.52±15.53	119.00±26.14	0.24±0.41
D9SUC9	Cellobiose 2-epimerase	Clocel_3198	5.47±5.01	6.23±5.47	0.00±0.00
D9SS73	Cellulosome anchoring protein cohesin region	Clocel_2824	32.65±8.01	35.59±15.15	4.00±2.14
D9SS69	Cellulosome anchoring protein cohesin region	Clocel_2820	6.64±2.60	3.24±2.82	5.40±0.33
D9SQV8	Dockerin type 1	Clocel_2607	10.87±2.58	14.70±7.24	0.71±0.70
D9SUC4	Dockerin type 1	Clocel_3193	4.51±7.82	27.17±13.32	0.00±0.00
D9SS67	Dockerin type 1	Clocel_2818	8.05±3.85	5.87±2.14	0.00±0.00
D9SWN8	Dockerin type 1	Clocel_3650	2.06±1.80	12.96±1.89	0.00±0.00
D9SQT1	Dockerin type 1	Clocel_2575	0.97±1.68	5.92±4.06	0.00±0.00
D9STT6	Dockerin type 1	Clocel_1010	0.00±0.00	3.34±5.78	0.00±0.00
D9SUM6	Dockerin type 1	Clocel_1175	0.00±0.00	1.28±2.22	0.00±0.00
D9SX08	Pectate lyase/Amb allergen	Clocel_1623	0.27±0.47	2.27±2.71	0.00±0.00

**Table S6.** Intracellular metabolite data used for modeling.

<b>Conc. (mM)</b>	<b>WT cellulose</b>	<b>Mutant cellulose</b>	<b>Mutant glucose</b>
Glucose	0.65	0.67	2.00
$\alpha$ -D-Glucose-6P	3.51	2.78	2.34
$\beta$ -D-Fructose-6P	3.51	2.78	2.34
$\beta$ -D-Fructose-1,6P	0.63	0.21	3.61
Glyceraldehyde-3P	1.51	2.45	1.76
Glycerate-1,3P	7.79	2.92	2.25
Phosphoenolpyruvate	1.46	47.93	1.68
Pyruvate	1.50	1.87	1.05
Acetyl CoA	0.58	0.08	2.75
Ethanol	0.00	10.35	1.45
Acetate	11.60	27.69	1.75
3-Hydroxybutyryl-CoA	0.94	0.94	1.09
Crotonyl-CoA	0.95	0.54	1.69
Butyryl-CoA	0.95	0.54	1.69
Butyrate	24.72	3.96	0.00
Butanol	0.00	11.14	2.71

**Table S7.** Summary of cellulosic n-butanol fermentation by new generation *C. cellulovorans* mutants.

Parameters	<i>C. cellulovorans thl-adhE2</i>		<i>C. cellulovorans hbd-adhE2</i>	
	Cellulose	Glucose	Cellulose	Glucose
<b>Concentration (g/L)</b>				
Butanol	2.10±0.03	0.85±0.04	1.98±0.03	0.77±0.02
Butyrate	3.04±0.07	2.85±0.10	2.18±0.02	2.43±0.13
Ethanol	1.84±0.01	0.64±0.03	1.80±0.04	0.69±0.02
Acetate	2.41±0.02	1.76±0.01	2.49±0.08	1.77±0.01
<b>Yield (g/g-glucose)</b>				
Butanol	0.25±0.02	0.14±0.02	0.18±0.04	0.22±0.03
Butyrate	0.23±0.01	0.19±0.03	0.07±0.03	0.20±0.02
Ethanol	0.08±0.00	0.12±0.02	0.07±0.01	0.08±0.03
Acetate	0.11±0.00	0.18±0.02	0.12±0.00	0.18±0.02
<b>Productivity (g/l/h)</b>				
Butanol	0.010±0.001	0.013±0.002	0.012±0.002	0.008±0.000
Butyrate	0.014±0.001	0.017±0.001	0.009±0.000	0.020±0.000
Ethanol	0.007±0.000	0.022±0.001	0.008±0.000	0.010±0.000
Acetate	0.010±0.000	0.023±0.002	0.011±0.000	0.012±0.001
<b>Selectivity (g/g-total product)</b>				
Butanol	0.22±0.00	0.14±0.01	0.23±0.00	0.14±0.01
Butyrate	0.32±0.00	0.47±0.01	0.26±0.03	0.43±0.02
Ethanol	0.20±0.00	0.11±0.00	0.21±0.01	0.12±0.00
Acetate	0.26±0.00	0.29±0.00	0.30±0.02	0.31±0.01

## References

1. Moulis, J., *Molecular mechanism of pyruvate-ferredoxin oxidoreductases based on data obtained with the Clostridium pasteurianum enzyme*. 1996.
2. W.Welch, R., *Purification and characterization of the NADH-dependent butanol dehydrogenase from Clostridium acetobutylicum (ATCC 824)*. 1989.
3. Ismaiel, A.A., et al., *Purification and characterization of a primary-secondary alcohol dehydrogenase from two strains of Clostridium beijerinckii*. J Bacteriol, 1993. **175**(16): p. 5097-105.
4. Knorr, R., M.A. Ehrmann, and R.F. Vogel, *Cloning, expression, and characterization of acetate kinase from Lactobacillus sanfranciscensis*. Microbiol Res, 2001. **156**(3): p. 267-77.
5. DENNIS P. WIESENBORN, *Thiolase from Clostridium acetobutylicum ATCC 824 and Its Role in the Synthesis of Acids and Solvents*. 1988.
6. Aboulnaga el, H., et al., *Effect of an oxygen-tolerant bifurcating butyryl coenzyme A dehydrogenase/electron-transferring flavoprotein complex from Clostridium difficile on butyrate production in Escherichia coli*. J Bacteriol, 2013. **195**(16): p. 3704-13.
7. Wiesenborn, D., *Phosphotransbutyrylase from Clostridium acetobutylicum ATCC 824 and its role in acidogenesis*. 1989.
8. Hartmanis, M., *Butyrate kinase from Clostridium acetobutylicum*. The Journal of biological chemistry, 1987. **262**(2): p. 617.
9. Demuez, M., et al., *Complete activity profile of Clostridium acetobutylicum [FeFe]-hydrogenase and kinetic parameters for endogenous redox partners*. FEMS Microbiol Lett, 2007. **275**(1): p. 113-21.
10. Metzler, D.E. *Biochemistry: the chemical reactions of living cells*. No. 574.876 M4. 1977.
11. Alberty, R. *Thermodynamics of the Nitrogenase Reactions* 1994.
12. Zheng, Y.N., Li, L.Z., Xian, M., Ma, Y. J., Yang, J.M., Xu, X., He, D.Z. *Problems with the microbial production of butanol*. 2009.

## APPENDIX B

### CELL THAWING AND CELL BANKING

### *Thawing Frozen Cells*

1. Many of the experiments need to begin from banking cells. To thaw a banking cell, medium needs to be warmed at 37°C for 1 h and transfer to BSC with other pipettes and cultural container previously.
2. When ready, take a tube of banking cell from liquid nitrogen (-196°C), thaw at 37°C water bath for about 1 min till there is still a small piece ice in the tube.
3. Transfer the tube into BSC, inoculate the fresh medium with all the cells as soon as possible (~1mL with cell density  $1.0 \times 10^6$  living cell / mL). For a 5 mL T-flask, add 4 mL fresh medium to the flask before inoculation.
4. Take about 0.3 mL cell mixture for cell counting. For the last example, cell density may be  $\sim 0.2 \times 10^6$  living cell / mL.
5. Transfer the cultural container to incubator (36.5°C, 5% CO<sub>2</sub>). T-flask is for static culture, while shaking flask is mostly set as 110 rpm (may vary according to cell using manual). Observe the cell condition every day and prepare for passaging every 2-3 days.

### *CHO Cells Banking*

1. Fill Mr. Frosty container with 100% isopropanol and store at 4 °C until use.
2. Prepare freezing medium containing 10% (v/v) DMSO by filter sterilization through a 0.22 um filter immediately before use.

3. Determine the viable cell density (VCD) and the cells viability by cell counting. For adherent cells, trypsin treatment followed by resuspension in pre-warmed medium is needed before cell counting.
4. Centrifuge cells at 400 g for 5 minutes at 4 °C to collect cell pellets. Aspirate the spent medium and resuspend cells in freezing medium for final VCD  $5-10 \times 10^6$  cells/mL.
5. Aliquot 1mL resuspend cells into one cryovial. Put the vials into Mr. Frosty. Then transfer Mr. Frosty to -80 °C as soon as possible.
6. After 24 hours, transfer frozen vials from Mr. Frosty to liquid nitrogen for long-term storage.

## APPENDIX C

### ANTIBODY TITRATION USING ELISA

## *Buffer and Reagent Preparation*

### 1. Coating buffer (50mM carbonate-bicarbonate buffer, pH 9.6)

- a. Dissolve 1.59 g of  $\text{Na}_2\text{CO}_3$  (106 g/mole) and 2.93 g  $\text{NaHCO}_3$  (84 g/mole) in 1 L of ddH<sub>2</sub>O.
- b. Mix thoroughly.
- c. Check pH and adjust pH as needed.
- d. Discard the buffer after use.

### 2. Wash buffer: PBS, pH 7.4 + 0.05% Tween 20

- a. Prepare sufficient quantity of wash buffer (for example, 2L) working as plate washer.
- b. Combine 200mL of PBS 10X with 1800mL of ddH<sub>2</sub>O.
- c. Add 2mL of 50% Tween 20.
- d. Mix thoroughly. Store at room temperature.

### 3. Blocking buffer 10X: 20% (w/v) BSA

- a. Weigh 20g of BSA.
- b. Dissolve BSA with 70mL of ddH<sub>2</sub>O completely.
- c. Adjust final volume with ddH<sub>2</sub>O to 100mL.
- d. Apportion 10mL into 15mL conical tubes and freeze at -20°C ~-30°C.
- e. Label the tubes with formulation and preparation date. BSA stock solution can be stored at -20°C to -30°C for 1 month.

### 4. Blocking buffer 1X: 2% (w/v) BSA.

- a. Thaw blocking buffer 10X stock in water bath at 37°C.

- b. Mix 10mL of blocking buffer 10X stock with 10mL of PBS 10X, pH 7.4 and 80mL of ddH<sub>2</sub>O.
- c. Blocking buffer 1X can be stored at 2~8°C for 1 week.

### *Plate Coating*

1. Dilute antibody sample in coating buffer to final concentration 2 µg/mL for Sandwich ELISA.
2. Mix the primary antibody solution by vortex or inverting tube at least 5 times.
3. Add 100 µL of the antigen sample solution to each well of 96-well plates. Cover the plates with sealing films.
4. Incubate at 2~8°C overnight without shaking.

### *Wash Plates*

1. Add 300 µL of wash buffer into each well, wait for 1 minute, then flip plate into sink to remove wash buffer and tap the plate invert onto paper towel to remove remained buffer.
2. Repeat washing step x3.

### *Plate Blocking*

1. Add 200 µL of blocking buffer to each well. Cover the plates with sealing films.
2. Incubate at 37°C for 1 hour without shaking. Or incubate at -2°C~8°C overnight without shaking.
3. Optional: After 1-hour incubation, the plates can be stored frozen at -20°C~ -30°C for 1 month. Label the plates with preparation date.

### *Standard Curve Preparation*

1. Dilution buffer can be culture medium, ELISA washing buffer (PBS, pH 7.4 + 0.05% Tween 20) or blocking buffer (2% BSA).
2. Prepare reference standard within 0-200 ng/ml range. For example, 0, 1.563, 3.125, 6.25, 12.5, 25, 50, 75, 100, 150, 200 ng/mL.
3. Prepare at least 350uL of each concentration for triplicate test.
4. Add 100  $\mu$ L of each concentration to each well.

### *Sample Preparation*

1. Dilute sample by suitable dilution factor.
2. Add 100  $\mu$ L of each sample for each well (x3). Incubate at 37°C for 1 hour.
3. Wash the plates 5 times with 300uL of buffer per well.

**Notes:** Sample must be stored frozen to avoid loss of bioactive mouse IgG1. If samples are to be run within 24 hours, they may be stored at 4°C. Otherwise, samples must be stored frozen at -70°C to avoid loss of bioactive mouse IgG1. Excessive freeze/thaw cycles should be avoided.

### *Secondary Antibody Incubation*

1. Dilute secondary antibody in blocking buffer. Final concentration is 50 ng/mL.
2. Add 100  $\mu$ L of diluted secondary antibody solution into each well.
3. Incubate at 37°C for 30 minutes without shaking.
4. Wash the plates 5 times with 300  $\mu$ L of buffer per well.

*Color Development and Reading*

1. Equilibrate TMB solution at room temperature.
2. Add 100uL of TMB solution into each well.
3. Read color development at 450nm every 5 minutes to determine if it is necessary to extend incubation. It mostly takes 30 minutes.
4. Stop the color development by adding 100uL of 1M H<sub>2</sub>SO<sub>4</sub>
5. Read color development at 450nm after shaking for 5 seconds.

APPENDIX D  
ANTIBODY PURIFICATION BY LC SYSTEM

### Column

Capture (affinity): UNOsphere SUPrA Cartridge, 5mL (Bio-Rad, Hercules, CA)

Intermediate and Polish (cation exchange): Nuvia S, 5mL (Bio-Rad, Hercules, CA)

### Procedures

(specific parameters are shown in Table 1 and Table 2)

1. Equilibrate system with buffer A1 for affinity purification or buffer A2 for cation exchange.
2. Prepare samples and load to purification column using the sample pump.
3. Wash column with buffer A1 or A2 until baseline is restored.
4. Elute antibody from column with buffer B1 or B2.

Table 1 Capture condition, UNOsphere SUPrA, affinity

Step	Buffer	Column Volume	Flow rate
Equilibrate	0.02M sodium phosphate, 0.02M sodium citrate, pH 7.5 (A1)	10-15	5mL/min (140 cm/hr)
Sample loading	diluted 1:10 into buffer A1; adjust to pH 7.5 with phosphoric acid or NaOH; clarified with 0.2um filter	-	5mL/min
Wash	A1	until absorbance returns to baseline	5mL/min
Elute*	Buffer B1 0.02M sodium citrate, 0.1M sodium chloride, pH 2.5	10	5mL/min

\*Elute fractions are collected.

Table 2 Intermediate condition, Foresight Nuvia S, cation exchange

Step	Buffer	Column Volume	Flow rate
Equilibrate	20mM CH <sub>3</sub> COONa, 20mM NaCl, pH 4.7 (Buffer A2)	15	2.5mL/min (297.5 cm/hr)
Sample loading	Eluted from capture, diluted 1:5 with dH <sub>2</sub> O, adjusted to pH 4.7 with 1M phosphoric acid.	-	2.5mL/min
Wash	Buffer A2	until absorbance returns to baseline	2.5mL/min
Elute*	Buffer B2 20mM sodium acetate, 200mM NaCl, pH 4.9.	15	2.5mL/min

\* Elute fractions are collected.

## APPENDIX E

### ANTIBODY BINDING EVALUATION BY FLOW CYTOMETRY

### *Flow Buffer*

Dissolve 0.5g BSA in 50mL 1x PBS. Filter sterilization. Keep ice cold.

### *Steps*

1. Collect cells by centrifuge at 400g for 5 minutes. Wash cells with flow buffer (1X PBS twice and resuspend as  $10 \times 10^6$  cells/mL.
2. Aliquot 100  $\mu$ L to each vial.
3. Add 0.1  $\mu$ g to 5  $\mu$ g conjugated antibodies to each vial. Mix well and incubate on ice/at 37 °C for 30 min in dark.
4. Add 1 mL flow buffer to each tube and centrifuge for 5 min at 400 g.
5. Repeat wash for once.
6. Resuspend cells to a final volume of 500  $\mu$ L per sample. Proceed with flow analysis in 5mL polystyrene round-bottom tubes.

APPENDIX F  
BIOCHEMICAL TITRATION BY HPLC

In this study, the concentrations of fermentation products, including glucose, butanol, butyrate, acetate and ethanol, were analyzed using high performance liquid chromatography system (HPLC)

*Equipment:* HPLC (Shimadzu, Columbia, MD) equipped with Rezex RHM-Monosaccharide H<sup>+</sup> column (Phenomenex, Torrance, CA) and a refractive index detector (Shimadzu RID-10A)

*Mobile Phase:* HPLC-grade H<sub>2</sub>O at a flow rate of 0.6 mL/min

*Column Temperature:* 78 °C

*Sample Injection Volume:* 10 µL

*Pressure:* <600psi

*Retention Time:* 40 min